Observing changes in lake level and glacial thickness on the Tibetan Plateau with the ICESat laser altimeter

Vu Hien Phan

Observing changes in lake level and glacial thickness on the Tibetan Plateau with the ICESat laser altimeter

Proefschrift

ter verkrijging van de graad van doctor
aan de Technische Universiteit Delft,
op gezag van de Rector Magnificus prof. ir. K.C.A.M. Luyben,
voorzitter van het College voor Promoties,
in het openbaar te verdedigen op Maandag 26 January 2015 om 15:00 uur

door

Vu Hien PHAN
Master of Engineering in Mapping, Remote Sensing and GIS
Ho Chi Minh City University of Technology, Vietnam

geboren te Sa Dec, Vietnam.

Dit proefschrift is goedgekeurd door de promoto: Prof. dr. M. Menenti

Copromotor: Dr. R.C. Lindenbergh

Samenstelling promotiecommissie:

Rector Magnificus,	voorzitter
Prof. dr. M. Menenti	Technische Universiteit Delft, promotor
Dr. R.C. Lindenbergh	Technische Universiteit Delft, copromotor
Prof. dr. M. Scaloni	Tongji University
Prof. dr. ir. Z. Su	Universiteit Twente
Prof. dr. ir. N.C. van de Giesen	Technische Universiteit Delft
Dr. J. Kropacek	Universität Tübingen
Dr. N. Gourmelen	The University of Edinburgh
Prof. dr. W.G.M. Bastiaanssen	Technische Universiteit Delft, reservelid

ISBN 978-94-6186-426-0

Author email: v.phanhien@tudelft.nl or phanhienvu@gmail.com

Preface

Many people contributed to the successful completion of this thesis in different ways. I wish to express my sincere gratitude to all of them.

Firstly, I am extremely grateful to my co-promoter **Dr. Roderik Lindenbergh.** You were always there to help and support me whenever I ran into a problem. I think your support and commitment during my study made other PhDs jealous in our section. In our weekly meetings, you always had excellent advice to give on my technical problems. I really appreciate your patience in correcting my English writing and the constructive feedback on how to write an effective article. Thank you for all your help and support to extend my knowledge and experiences in research.

Secondly, I would like to thank **Prof. Massimo Menenti,** for providing me with the opportunity to carry out my research and for your continuous support. With the extensive knowledge, you always gave me helpful ideas and provided me with clear and in-depth answers to my scientific and technical problems. Also, I would like to thank you for the constructive criticisms and relevant comments on the content of this dissertation.

I want to thank the Vietnam Ministry of Education and Training and the CEOP-AEGIS project on the Hydrology and Climatology of the Tibetan Plateau, project no. 212921 of the European Commission FP7 program for funding this research.

Furthermore, I wish to thank my friends at the OLRS section: Ali Mousivand, Hamid Reza Ghafarian Malamiri, and Seyed Enayat Hosseini Aria for sharing knowledge and experiences in studying and living in Delft and contributed to a nice and enjoyable life at TUDelft.

I am thankful to Lidwien De Jong, for all the support to process a lot of documents in regularization enthusiastically. I am also very grateful to Vietnamese students and all other colleagues here at TU Delft.

I am indebted to my mother in law for having taken care of my daughter in Vietnam, to my lovely wife for being sympathetic and encouraging to me, and to my beautiful daughter for still recognizing and loving me.

Last but not least, I wish to thank my lovely family and friends for their support and encouragement.

Table of content

Abbreviations

ASCII	American Standard Code for Information Interchange
CAREERI	Cold and Arid Regions Environmental and Engineering Research Institute
DEM	Digital Elevation Model
EMG96	Earth Gravitational Model 1996
EMG2008	Earth Gravitational Model 2008
FWHM	Full Width at Half Maximum pulse
GLAS	Geoscience Laser Altimeter System
GLIMS	Global Land Ice Measurements from Space
GRACE	Gravity Recovery And Climate Experiment
HDF	Hierarchical Data Format
HydroSHEDS	Hydrological data and maps based on SHuttle Elevation Derivatives at multiple Scales
ICESat	Ice, Cloud, and Land Elevation Satellite
MODIS	Moderate Resolution Imaging Spectroradiometer
NASA	National Aeronautics and Space Administration
NSIDC	National Snow and Ice Data Centre
SRTM	Shuttle Radar Topography Mission
TOPEX/Poseidon	Topography Experiment/Poseidon
UTC	Universal Coordinated Time
WGS84	World Geodetic System 1984

Summary

Observing changes in lake level and glacial thickness on the Tibetan Plateau with the ICESat laser altimeter

The Tibetan Plateau is a vast, elevated plateau in Central Asia. It occupies an area of ~2.5 million km^2 and has an average elevation of over 4,500 m. The Tibetan Plateau is not only the highest and largest plateau of the world, but also contains a large amount of glaciers. In addition, there are thousands of lakes in this region. Most of them supply fresh water for people, livestock and agriculture while some are salt water lakes. The Tibetan Plateau is also the origin of Asia's big rivers such as Brahmaputra, Ganges, Indus, Mekong, Salween, Yellow River, and Yangtze. Glacial melt water supplies large inflow for the rivers during the summer monsoon and is a primary water source in the dry season. It means that the Tibetan Plateau keeps the water resources under control for Southeast Asia, the most densely populated region on Earth. However, recent research reported that the glaciers have been retreating significantly in the last decades. That is expected to affect the water storage of this region. Therefore, understanding hydrologic processes and quantifying the water storage of the Tibetan Plateau is essential.

In general, the water storage of the Tibetan Plateau is determined by precipitation, surface runoff, evaporation and infiltration. Due to the vastness, high relief and the complicated climate, only a limited number of hydrometeorologic gauge measurements are available in this region. Thus it is difficult to quantify this water storage. However, the net annual water storage of a lake or river basin, considered as a simple water balance model, is one component of the total water storage of the Tibetan Plateau. Changes in water storage of open water bodies can be assessed by analyzing changes in their water levels. Moreover, one of the variables directly affecting water levels of lakes and rivers on the Tibetan Plateau is glacial melt water. Therefore, monitoring changes in glacial thickness and water level is a potential useful contribution to the understanding of the hydrologic processes and the water balance of the Tibetan Plateau.

In January 2003, the ICESat satellite was launched for measuring ice sheet mass balance, cloud and aerosol heights, as well as land topography and vegetation structure. The available ICESat/GLAS-derived land surface elevations have a vertical accuracy at the decimeter level over flat terrain and a horizontal accuracy in the order of meters. Each GLAS waveform was the result of the interaction of the emitted Gaussian pulse with the terrain surface within a ~70 m diameter footprint, much smaller than for example radar footprints. In addition, ICESat only obtained measurements along track with an along track distance between

consecutive footprints of 170 m. This small footprint makes the ICESat/GLAS laser altimeter more advantageous in monitoring changes in lake level and glacial thickness on the Tibetan Plateau than other remote sensing techniques.

The changes in lake level and glacial thickness can be converted to water volumes that can be used as input of water balance models. These contribute to improve the understanding of changes in the water storage of the Tibetan Plateau. That is why observing changes in lake level and glacial thickness on the Tibetan Plateau with the ICESat laser altimeter is reasonable. The research consists of three main parts: i) monitoring lake level changes, ii) monitoring glacial thickness changes and iii) assessing relationships between changes in lake level and glacial thickness.

Monitoring changes in lake levels: the ICESat GLA14 land surface elevation data in combination with the MODIS land-water mask was used to obtain water level variations of Tibetan lakes. The GLA14 elevations representing lake surface elevations were basically selected by using the lake outlines, derived from the MODIS land-water mask. For each ICESat sampled lake, anomalies in observed surface elevations due to e.g. clouds, saturation or surface characteristics, were removed using the RANSAC algorithm. Then the mean elevations corresponding to the ICESat acquisition times were determined. They were representative for lake levels during the observed period. Subsequently, a temporal lake level trend was estimated by linear regression. The results indicated that water level variations of 154 lakes spread all over the Tibetan Plateau between 2003 and 2009 could be obtained. Moreover, most of the lakes with a serious downwards trend are in the southern Tibetan Plateau and along the Himalaya mountain range and, vice versa, most of the lakes with a positive water level trend are in the inner Tibetan Plateau.

In addition, GLA14 elevations were grouped into three seasonal datasets following to the ICESat acquisition schedule: late dry season, wet season, and early dry season. Yearly trends were estimated using lake levels in the same season and different years. The results indicated that seasonal influences were more obvious in the South of the Tibetan Plateau than those in the Northwest. The seasonal influence on lake level gradually decreased from the Southeast to the Northwest of the Tibetan Plateau. These results correspond to trends in precipitation, temperature and humidity as documented in recent research on climate change at the Tibetan Plateau.

Monitoring changes in glacial thickness: the ICESat GLA14 land surface elevation data in combination with the SRTM DEM and the GLIMS glacier mask was used to obtain changes in glacial thickness. Here, the approach for estimating

glacial thickness was to estimate the difference between the GLA14 elevation and the reference SRTM DEM. By considering where ICESat sampled glaciers, ICESat-sampled nearby glaciers having similar orientation were grouped into observed glacial areas. Accordingly the GLA14 elevations on these glacial areas were selected. For each glacial area, uncertain GLAS elevations were removed, based on criteria that were also used for lakes, while in addition, also the terrain slope and roughness were considered. Subsequently, the mean elevation difference between the remaining GLA14 elevations and the SRTM DEM, corresponding to each ICESat acquisition time, was determined. Based on these mean differences, a temporal trend of glacier thinning or thickening between 2003 and 2009 was estimated. As a result trends in thickness change for 90 glacial areas on the whole Tibetan Plateau between 2003 and 2009 were obtained. Most of the observed glacial areas at the Tibetan Plateau experienced serious thinning, except the North-facing glaciers of the western Kunlun Mountains. Moreover, glacial thickness changes appeared to be strongly dependent on the relative position in a mountain range. Conversely most North-facing glaciers increased in thickness, although some decreased but in that case at a slower rate than its South-facing counterpart.

Assessing relationships between changes in glacial thickness and lake level: geometric links between glaciers and lakes on the Tibetan Plateau were determined by applying a surface flow network analysis in catchments with both a lake and a glacier. The surface flow network was based on the HydroSHEDS product which was derived from the SRTM DEM, but needed corrections at several locations. The results indicated that 25.3% of the glaciers release their melt water directly to 244 lakes. Moreover, the ratio between the total area of glaciers draining into a lake and the area of its catchment was introduced as a proxy for the dependency of a lake on glacial runoff. The results clearly listed which lakes are more or less dependent on glacial runoff and therefore indicate which lakes are expected to be strongly affected by the shrinkage of the glaciers on the Tibetan Plateau.

Because of its orbit constellation, ICESat only sparsely sampled glaciers and lakes on the Tibetan Plateau were observed. Change rates in glacial thickness and lake level between 2003 and 2009 on the Tibetan Plateau derived from the ICESat laser altimetry were computed. In addition, the geometric dependency of Tibetan lakes and glacial runoff represents levels of the dependency of a Tibetan lake on glacial runoff. An analysis of spatial patterns in water volume changes in glacial areas and lakes could be performed to determine a possible correlation. Results of such analysis would be a first additional step in the understanding of hydrological processes on the Tibetan Plateau.

Samenvatting

Het waarnemen met de ICESat laserhoogtemeter van veranderingen in waterniveaus van meren en diktes van gletsjers op het Tibetaanse Plateau

Het Tibetaans Plateau is een uitgestrekte hoogvlakte in Centraal-Azië. Het heeft een oppervlakte van ~2,5 miljoen km^2 en de gemiddelde hoogte is meer dan 4,500 meter. Het Tibetaanse Plateau is niet alleen de grootste en meest hooggelegen hoogvlakte van de wereld, maar bevat ook duizenden gletsjers en meren. De meeste meren zijn een bron van zoet water voor mensen, vee en landbouw, maar sommige meren zijn zout. Op het Tibetaanse Plateau ontspringen ook een aantal grote Aziatische rivieren, zoals de Brahmaputra, de Ganges, de Indus, de Mekong, de Salween, de Gele Rivier en de Yangtze. Smeltwater van de vele gletsjers stroomt massaal de rivieren in tijdens het zomermoesson en is de voornaamste bron van water in het droge seizoen. Op deze manier controleert het Tibetaanse Plateau de watervoorraden van Zuidoost-Azië, één van de meest dichtbevolkte gebieden op aarde. Recent onderzoek toont echter aan dat de gletsjers smelten, wat de waterhuishouding zal beïnvloeden. Om de verschillende hydrologische processen en hun mogelijke gevolgen te begrijpen, is het daarom essentiëël om mogelijke veranderingen in watervoorraden en watertransport op het Tibetaanse Plateau te kwantificeren.

De waterbalans van het Tibetaanse Plateau hangt af van neerslag, afvoer, verdamping en infiltratie. Door de hoogte, de ruwheid van het terrein en het barre klimaat zijn slechts beperkt metingen op locatie mogelijk. Daarom is het moeilijk om inzicht te krijgen in de totale waterbalans. Het oppervlaktewater, water in meren en rivieren, vormt echter een belangrijk onderdeel van de totale waterbalans. Veranderingen in de hoeveelheid oppervlaktewater kunnen worden afgeleid uit veranderingen in de waterstanden. Deze waterstanden worden ondermeer beinvloedt door de aanvoer van smeltwater van gletsjers. Daarom kan het monitoren van veranderingen in waterstanden en diktes van gletsjers bijdragen aan beter inzicht in de waterbalans van het Tibetaanse Plateau.

In januari 2003 werd de ICESat satelliet gelanceerd met als hoofddoel het meten aan de massabalans van de ijskappen. Daarnaast moest de satelliet ook bijdragen aan het bepalen van de hoogtes van wolken en het wereldwijd in kaart brengen van de structuur van onze vegetatie. Om deze metingen te kunnen uitvoeren gebruikte ICESat de GLAS laser hoogtemeter. ICESat was actief tussen 2003 en 2009. De ICESat/GLAS hoogtemetingen hebben een verticale nauwkeurigheid in de orde van een decimeter over vlak terrein en een horizontale nauwkeurigheid in de orde van enkele meters. Het terrein dat door een enkel GLAS lasersignaal wordt belicht en daardoor ingemeten, heeft een diameter van ongeveer 70 m, veel

kleiner dan de voetafdrukken van radar altimeters. ICESat kon alleen direct onder zijn eigen baan meten, maar leverde wel elke 170 m een nieuwe meting af. Door zijn kleine voetafdruk zijn de ICESat/GLAS metingen in principe beter geschikt voor het in kaart brengen van veranderingen in waterstanden en diktes van gletsjers op het Tibetaanse Plateau dan andere remote sensing technieken.

De veranderingen in de waterstanden van meren en diktes van gletsjers kunnen direct worden omgezet in watervolumes, die weer kunnen worden gebruikt als invoer voor waterbalans modellen. Zulke modellen dragen bij aan het begrip van veranderingen in de waterhuishouding van het Tibetaanse Plateau. Daarnaast levert directe analyse van de veranderingen ook veel nieuwe informatie op. Dit geeft het potentiële nut aan van het onderzoek beschreven in dit proefschrift. Het onderzoek bestaat uit drie delen: i) het monitoren van waterstanden in meren, ii) het monitoren van veranderingen in de dikte van gletsjers, en, iii) het bepalen van verbanden tussen meren en gletsjers.

Het monitoren van waterstanden in meren: de ICESat GLA14 landhoogtes in combinatie met het MODIS land-water sjabloon worden gebruikt om waterstanden van Tibetaanse meren te verkrijgen. Om GLA14 metingen van het wateroppervlak te krijgen, is gekeken welke GLA14 metingen binnen de omtrek van een meer vallen. Hiervoor is het MODIS land-water sjabloon gebruikt. Vervolgens worden foute metingen verwijderd met behulp van het RANSAC algoritme. Zulke fouten metingen worden onder meer veroorzaakt door bewolking. Uit de correcte metingen wordt een gemiddelde waterstand bepaald, die gekoppeld wordt aan de tijd dat ICESat het meer passeerde. Bij voldoende passages kan bovendien een trend worden geschat door de verschillende waterstanden die voor een enkel meer verkregen ziijn. In totaal konden op deze manier trends voor 154 verschillende meren worden verkregen, verspreid over het Tibetaans Plateau. De meeste meren die gemiddeld zakken bevinden zich in het zuiden van Tibet en langs de Himalaya, terwijl de meren in het midden van Tibet juist gemiddeld stijgen tussen 2003 en 2009.

De waterstanden die aan de hand van de GLA14 metingen bepaald werden, konden gegroepeerd worden in drie verschillende seizoenen, die corresponderen met de jaargetijden waarin ICESat actief was: het late droge seizoen, het natte seizoen, en het begin van het droge seizoen. Trends per seizoen werden geschat en deze werden vergeleken met trends verkregen uit alle waterstanden tesaman. De resultaten geven aan dat seizoensinvloeden sterker zijn in het zuidoosten van Tibet en dat deze invloed afneemt richting noordwesten. Deze resultaten komen overeen met trends in neerslag, temperatuur en vochtigheid zoals door anderen zijn gedocumenteerd in recent onderzoek over klimaatverandering in Tibet.

Het monitoren van veranderingen in de dikte van gletsjers: de ICESat GLA14 hoogtemetingen zijn gebruikt in combinatie met het SRTM hoogtemodel en het GLIMS gletsjer sjabloon om veranderingen in diktes van gletsjers te schatten. Daartoe is steeds het verschil bepaald tussen de GLA14 hoogte en de SRTM hoogte op dezelfde locatie. Hoogtemetingen van verschillende gletsjers werden daarbij gegroepeerd als de gletsjers bij elkaar in de buurt lagen en bovendien op een soortgelijke manier waren georiënteerd. Deze procedure resulteerde in een beperkt aantal gletsjer zones. Uit alle correct geachte verschillen tussen GLA14 en SRTM werd vervolgens voor elke gletsjerzone een trend geschat die aangeeft hoeveel ijs er gemiddeld per jaar verloren ging of bijkwam tussen 2003 en 2009. Op deze manier werden trends voor de verandering in de dikte van gletsjers verkregen voor 90 verschillende gletsjer zones. De resultaten laten zien dat in de meeste zones de gletsjer flink dunner worden, met uitzondering van de op het noorden georiënteerde gletsjers in de westelijke Kunlun. Bovendien blijkt dat veranderingen sterk afhankelijk zijn van de relatieve positie van een gletsjerzone in een gebergte.

Het bepalen van verbanden tussen meren en gletsjers: geometrische verbanden tussen gletsjers en meren op het Tibetaanse Plateau werden bepaald aan de hand van een netwerkanalyse van het volledige Tibetaanse riviernetwerk. Als invoer voor deze analyse is het zogenaamde HydroSHEDS riviernetwerk product gebruikt, dat op zijn beurt weer is afgeleid van het SRTM hoogtemodel. Wel waren correcties noodzakelijk op verschillende locaties. De resultaten geven aan dat 25,3% van de gletsjers hun smeltwater direct afvoeren naar 244 meren. Bovendien kon de verhouding tussen de totale oppervlakte van alle gletsjers die afwateren in een meer en de oppervlakte van het toevoersgebied van dat meer worden bepaald als proxy voor de afhankelijkheid van een meer van gletsjerwater. De resultaten laten duidelijk zien welke meren meer of minder afhankelijk zijn van gletsjerwater en welke meren daarom naar verwachting sterker zullen worden beïnvloed door het krimpen van de gletsjers op de Tibetaanse hoogvlakte.

Door de beperkingen in de meetcapaciteit van ICESat, heeft ICESat slechts een beperkt aantal gletsjers en meren op het Tibetaanse Plateau kunnen waarnemen. Op grond van alle beschikbare metingen zijn trends bepaald in de verandering in waterstanden van veel meren en diktes van 90 gletsjer zones. Daarnaast is de geometrische afhankelijkheid van gletsjerwater bepaald voor alle Tibetaanse meren. Een spatiële analyse van deze verschillende veranderingen in water volume in vergletsjerde gebieden kan worden uitgevoerd om een mogelijke correlatie te bepalen. De resultaten van zo'n analyse zouden een eerste volgende

stap kunnen zijn om verdere verbanden in de waterhuishouding van het Tibetaanse Plateau te kunnen onthullen.

Tóm tắt

Giám sát những biến đổi mực nước hồ và độ dày băng trên Cao nguyên Tây Tạng với thiết bị đo cao bằng laser từ vệ tinh ICESat

Cao nguyên Tây Tạng là một cao nguyên cao và rộng lớn ở Trung tâm châu Á. Nó chiếm diện tích ~2.5 triệu km^2 và có cao độ trung bình trên 4,500 m. Cao nguyên Tây Tạng không những là cao nguyên cao nhất và rộng nhất trên thế giới, mà còn chứa một lượng lớn băng. Ngoài ra, có hàng ngàn hồ trên khu vực này. Hầu hết những hồ này cung cấp nước ngọt cho người dân, thú nuôi và nông nghiệp trong khi đó một số là hồ nước mặn. Cao nguyên Tây Tạng cũng là nguồn của những con sông lớn của châu Á như Brahmaputra, Ganges, Indus, Mekong, Salween, Yellow River, và Yangtze. Nước băng tan cung cấp một lượng lớn cho các con sông trong suốt đợt gió mùa vào mùa hè và là nguồn nước thiết yếu trong mùa khô. Điều này có nghĩa là Cao nguyên Tây Tạng giữ những nguồn nước quan trọng cung cấp cho khu vực Đông Nam Á, khu vực có mật độ dân số cao nhất thế giới. Tuy nhiên, những nghiên cứu gần đây báo cáo rằng diện tích băng đã mất dần một cách rõ rệt trong vài thập kỷ qua. Điều này được cho là ảnh hưởng đến trữ lượng nước của khu vực này. Do vậy, việc hiểu biết những quy trình thủy văn và định lượng trữ lượng nước của Cao nguyên Tây Tạng là cần thiết.

Nhìn chung, trữ lượng nước của Cao nguyên Tây Tạng được xác định bởi lượng mưa, dòng chảy bề mặt, sự bốc hơi nước và sự thẩm thấu. Do địa hình cao, rộng lớn và khí hậu phức tạp, chỉ có một lượng giới hạn các trạm khí tượng thủy văn ở khu vực này. Thế nên, rất khó khăn để định lượng trữ lượng nước này. Tuy nhiên, trữ lượng tĩnh của một lưu vực hồ hoặc sông, được xem như một mô hình cân bằng nước đơn giản, là một thành phần của tổng trữ lượng nước của Cao nguyên Tây Tạng. Những biến đổi trữ lượng nước của những nguồn nước mặt có thể được đánh giá bằng cách phân tích những biến đổi mực nước của chúng. Hơn nữa, một trong những yếu tố ảnh hưởng trực tiếp đến mực nước hồ và sông trên Cao nguyên Tây Tạng là nước băng tan. Do đó, việc giám sát những biến đổi độ dày băng và mực nước đóng góp rất hữu ích để hiểu những quy trình thủy văn và cân bằng nước của Cao nguyên Tây Tạng.

Tháng 1 năm 2003, vệ tinh ICESat được phóng để đo cân bằng khối của các tảng băng, độ cao của mây và aerosol, cũng như cấu trúc thực vật và địa hình mặt đất. Dữ liệu độ cao bề mặt đất từ thiết bị đo cao bằng laser GLAS trên vệ tinh ICESat có độ chính xác theo phương đứng ~10 cm trên địa hình phẳng và độ chính xác theo phương ngang ~5 m. Footprint thể hiện cho diện tích tương tác trên bề mặt địa hình của một xung Gauss được phát đi để thực hiện trị đo. Footprint từ phép đo cao bằng xung laser được phát từ GLAS trên vệ tinh ICESat có đường kính

~70 m, nhỏ hơn nhiều so với các footprints từ phép đo cao bằng xung radar trên các vệ tinh khác như Topex/Poseidon, Jason-1&2, hoặc ENVISat. Ngoài ra, ICESat chỉ thu được các trị đo dọc theo tuyến với khoảng cách dọc tuyến giữa hai footprints liên tiếp là 170 m. Với đặc tính footprint nhỏ, thiết bị đo cao bằng laser ICESat/GLAS có nhiều ưu điểm trong việc giám sát những biến đổi mực nước và độ dày băng trên Cao nguyên Tây Tạng hơn những kỹ thuật viễn thám khác.

Những biến đổi mực nước và độ dày băng có thể được chuyển đổi thành các thể tích nước mà có thể được sử dụng như thông số đầu vào của các mô hình cân bằng nước. Những điều này góp phần nâng cao sự hiểu biết về những biến đổi trữ lượng nước của Cao nguyên Tây Tạng. Đó là lí do việc giám sát những biến đổi mực nước và độ dày băng trên Cao nguyên Tây Tạng với thiết bị đo cao bằng laser trên vệ tinh ICESat là cần thiết. Nghiên cứu này bao gồm ba phần chính: i) giám sát biến đổi mực nước hồ, ii) giám sát biến đổi độ dày băng, và iii) đánh giá những mối quan hệ giữa những biến đổi mực nước và độ dày băng.

Giám sát biến đổi mực nước: dữ liệu cao độ bề mặt đất ICESat GLA14 kết hợp với mặt nạ nước mặt MODIS được sử dụng để lấy những biến động mực nước của các hồ trên Cao nguyên Tây Tạng. Về cơ bản, dữ liệu độ cao GLA14 thể hiện cao độ bề mặt nước được chọn bằng cách sử dụng đường bao của hồ, trích lọc từ mặt nạ nước mặt MODIS. Với mỗi hồ được ICESat lấy mẫu, những dị thường trong tập cao độ bề mặt do mây, sự bảo hòa của tín hiệu phản hồi, hoặc các đặc tính bề mặt tương tác được loại bỏ bằng cách áp dụng giải thuật RANSAC. Sau đó, những cao độ trung bình tương ứng với những thời điểm ICESat thu thập dữ liệu được xác định. Chúng thể hiện cho những mực nước trung bình trong suốt giai đoạn giám sát. Theo đó, xu hướng mực nước hồ theo thời gian được ước tính bằng mô hình hồi quy tuyến tính. Những kết quả chỉ ra rằng giám sát được biến đổi mực nước của 154 hồ trải khắp Cao nguyên Tây Tạng giai đoạn năm 2003 và 2009. Hơn nữa, hầu hết các hồ có xu hướng giảm mực nước nghiêm trọng ở phía nam của Cao nguyên Tây Tạng và dọc theo dải núi Himalaya, ngược lại hầu hết các hồ có xu hướng tăng mực nước ở bên trong Cao nguyên.

Ngoài ra, dữ liệu cao độ GLA14 được nhóm thành ba tập dữ liệu theo mùa dựa trên lịch trình thu thập dữ liệu của ICESat: cuối mùa khô, mùa ẩm ướt, và đầu mùa khô. Những xu hướng biến đổi mực nước hồ hàng năm được ước lượng theo cùng một mùa và giữa các mùa trong năm. Những kết quả chỉ ra rằng những ảnh hưởng của mùa đối với mực nước hồ ở phía nam của Cao nguyên Tây Tạng rõ ràng hơn ở phía tây bắc. Ảnh hưởng của mùa đối với mực nước giảm dần đều từ phía đông nam đến phía tây bắc của Cao nguyên Tây Tạng. Những kết quả này phù hợp với những xu hướng biến đổi lượng mưa, nhiệt độ và độ ẩm được trình bày trong có nghiên cứu gần đây về biến đổi khí hậu trên Cao nguyên Tây Tạng.

Giám sát biến đổi độ dày băng: dữ liệu độ cao bề mặt đất ICESat GLA14 kết hợp với mô hình độ cao số SRTM và mặt nạ băng GLIMS được sử dụng để thu được những biến đổi độ dày băng. Ở đây, hướng tiếp cận cho việc ước lượng độ dày băng là ước lượng sự khác biệt giữa cao độ bề mặt đất GLA14 và mô hình độ cao số SRTM tham chiếu. Bằng cách xem xét những khu vực ICESat lấy mẫu những khối băng, những khối băng được ICESat lấy mẫu nằm kề nhau và có cùng hướng được nhóm lại thành những khu vực băng được lấy mẫu. Theo đó, những cao độ GLA14 trên những khu vực băng này được chọn. Với mỗi khu vực băng được giám sát, những trị đo GLAS không chắc chắn được loại dựa trên những đặc tính được áp dụng cho hồ, tuy nhiên ngoài ra, độ dốc và độ gập ghềnh bề mặt địa hình cũng được xem xét. Theo đó, trị đo trung bình của sự khác biệt cao độ giữa những cao độ GLA14 được chấp nhận và mô hình độ cao số SRTM được xác định, tương ứng với mỗi thời điểm thu thập dữ liệu của ICESat. Dựa trên những trị đo trung bình của sự khác biệt cao độ này, xu hướng băng mỏng đi hay dày lên theo thời gian được ước tính bằng mô hình hồi quy tuyến tính. Kết quả là ước tính được những xu hướng biến đổi độ dày của 90 khu vực băng trên Cao nguyên Tây Tạng từ năm 2003 đến 2009. Hầu hết những khu vực băng được giám sát trên Cao nguyên Tây Tạng đang trải qua việc mỏng dần nghiêm trọng, ngoại trừ những khối băng ở những ngọn núi phía tây Kunlun. Những biến đổi độ dày băng diễn ra phụ thuộc rất nhiều vào vị trí tương đối ở một dải núi. Ngoài ra, hầu hết những khối băng hướng về phía bắc có xu hướng tăng độ dày, mặc dù một số có xu hướng giảm nhưng trong những trường hợp đó thì tốc độ mỏng dần thấp hơn so với tốc độ mỏng dần của khu vực băng tương ứng hướng về phía nam.

Đánh giá những mối quan hệ giữa biến đổi mực nước và biến đổi độ dày băng: những liên kết hình học giữa những khối băng và hồ trên Cao nguyên Tây Tạng được xác định bằng cách áp dụng phân tích mạng dòng chảy bề mặt trong những lưu vực đối với mỗi khối băng và mỗi hồ. Mạng dòng chảy bề mặt được trích lọc từ sản phẩm dữ liệu thủy văn HydroSHEDS được tạo ra từ mô hình độ cao số SRTM, tuy nhiên cần hiệu chỉnh ở vài khu vực. Những kết quả chỉ ra rằng 25.3% của tổng diện tích bề mặt băng giải phóng nước băng tan chảy trực tiếp đến 244 hồ. Hơn nữa, tỉ số giữa tổng diện tích bề mặt băng có nước băng tan chảy xuống một hồ và diện tích lưu vực của hồ đó được giới thiệu như một biến tham khảo cho sự phụ thuộc của một hồ vào dòng chảy nước băng tan. Những kết quả liệt kê rõ ràng những hồ nào phụ thuộc nhiều hơn hoặc ít hơn vào dòng chảy nước băng tan và như vậy xác định được những hồ nào được mong đợi bị ảnh hưởng nhiều bởi sự co lại của các khối băng trên Cao nguyên Tây Tạng.

Do đặc điểm quỹ đạo vệ tinh, các khối băng và hồ được ICESat lấy mẫu nằm rải rác trên khắp Cao nguyên Tây Tạng. Những tốc độ biến đổi mực nước và độ dày băng giai đoạn năm 2003 và 2009 được ước tính dựa trên dữ liệu đo cao bằng laser từ vệ tinh ICESat. Ngoài ra, mức độ phụ thuộc của những hồ trên Cao

nguyên Tây Tạng vào dòng chảy nước băng tan cũng được xác định. Phân tích kiểu mẫu không gian những biến đổi thể tích nước của những khối băng và hồ có thể được thực hiện để xác định mức độ tương quan giữa chúng. Những kết quả của phân tích như thế sẽ là bước bổ sung đầu tiên để hiểu những quy trình thủy văn trên Cao nguyên Tây Tạng.

Chapter 1

INTRODUCTION

This chapter presents scientific reasons and methods for monitoring changes in glacial thickness and lake level on the Tibetan Plateau. First we introduce the Tibetan Plateau and the importance of studying the water balance of this region. The Tibetan Plateau has the largest glacier-covered area outside the Poles, containing ~37,000 glaciers that together occupy an area of ~56,560 km^2. There are thousands of lakes on this region, ~900 lakes of which have an area of over 1 km^2. It is also known as The Water Tower of Asia as it is the origin of major rivers that flow to Bangladesh, Burma, Cambodia, China, India, Nepal, Pakistan, Thailand and Vietnam. Thus the water of the Tibetan Plateau is an important fresh water source for more than one billion people living in the basins of these rivers. In general, glacial melt water from mountains feeds lakes and rivers on the Tibetan Plateau. Moreover, changes in water storage of open water bodies can be assessed by analyzing changes in their water levels. Therefore, estimating the water storage change of the Tibetan Plateau requires estimating changes in glacial thickness and lake level. As an alternative to other remote sensing techniques, satellite laser altimetry is a potential solution to assess hydrologic processes in this region. This technique is implemented in the ICESat satellite mission, and advantages and challenges of using its data products for monitoring changes in glacial thickness and lake level on the Tibetan Plateau are described. Accordingly a research question is proposed and divided into sub-questions. A short introduction will be given to the methodology applied to answer the research question. Finally the thesis structure is outlined.

1.1. The water balance of the Tibetan Plateau

The Tibetan Plateau, also known as the Qinghai-Tibetan Plateau, is a vast, elevated plateau in Central Asia covering most of the Tibet Autonomous Region and Qinghai Province in China and Ladakh in India, as illustrated in Figure 1.1. It occupies an area of ~2.5 million km^2 (73^{0}30'E – 104^{0}30'E and 26^{0}30'N – 39^{0}30'N), and has an average elevation of over 4,500 m. The Tibetan Plateau is surrounded by large mountain ranges, the Himalaya in the South, the Karakorum in the Southwest, the Kunlun in the Northwest and the Qilian Mountains in the Northeast. It is not only the highest and largest plateau of the world, but also contains a large amount of glaciers. Therefore, it keeps the water resources under control for Southeast Asia, the most densely populated region on Earth.

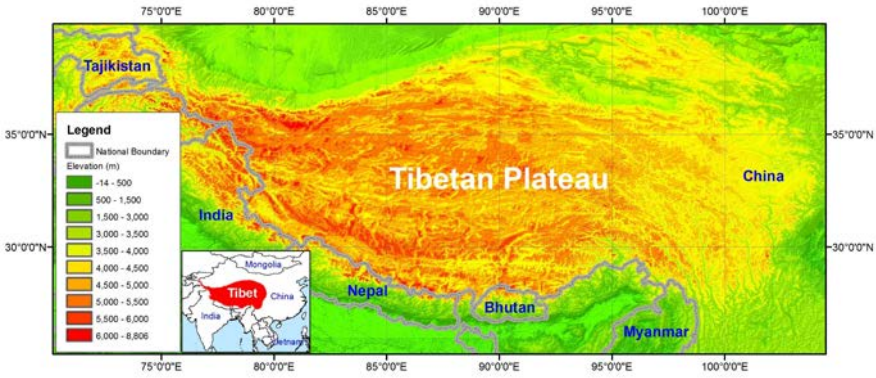

Figure 1.1: The Tibetan Plateau (Tibet). This map was designed based on the SRTM 90 m DEM.

The Tibetan Plateau knows two different seasons: the dry season, in winter, and the wet or rainy season, in summer. Winters from November to March are cold with an average temperature of below 0 ^{0}C. Summers from May to September have warm days with strong sunshine and daily mean temperature from 10 to 20 ^{0}C. The climate in the West and the North of the Tibetan Plateau is warmer and drier than in the South and East (Tao et al., 2004). Precipitation on the Tibetan Plateau is dominated by annual monsoons such as the Indian summer monsoon on the plateau's Southern and Southeastern flanks, the Asian summer monsoon to the East, and the winter monsoon, also called the westerflies, along the plateau's

Southwestern and Northwestern flanks (Zhisheng et al, 2001; Yao et al., 2012). This makes it likely that different patterns of glacial changes and water level changes occur at different parts of the Tibetan Plateau.

Figure 1.2: The Kyetrak Glacier, located on the northern slope of Cho Oyu in the Tibetan Plateau, as photographed in 1921 by Major E.O. Wheeler and in 2009 by David Breashears (Source: Yale, 2014).

The Tibetan Plateau has the largest glacier-covered area outside the Poles. It contains ~37,000 glaciers, occupying an area of ~56,560 km^2 (Li, 2003). There are thousands of lakes in this region. About 900 lakes have an area of over 1 km^2, occupying a total area of ~38,800 km^2 (Carroll et al., 2009). Most of them supply fresh water for people, livestock and agriculture while some are salt water lakes. The Tibetan Plateau is also the origin of Asia's big rivers such as Brahmaputra, Ganges, Indus, Mekong, Salween, Yellow River, and Yangtze. Glacial melt water supplies large inflow for the rivers during the summer monsoon and is a primary water source in the dry season (Xu et al., 2007). More than 1.4 billion people depend for their living and food security on the water resources from the Tibetan Plateau (Immerzeel et al., 2010). Recent research reported that the glaciers have been retreating significantly in the last decades. One example is shown in Figure

1.2, which shows two photographs of the North Side of the Cho Oyu Mountain on the border between Nepal and Tibet. The glacier that is prominently visible in the 1921 photo appears to have almost completely disappeared in 2009 and has been partly replaced by a lake. Therefore, understanding hydrologic processes and quantifying the water storage of the Tibetan Plateau is essential.

In general, hydrologic processes in the Tibetan Plateau conform to the water cycle, as described in Figure 1.3. Accordingly, the water storage of the Tibetan Plateau is determined by precipitation, surface runoff, evaporation and infiltration. Due to the vastness, high relief and the complicated climate, only a limited number of hydrometeorologic gauge measurements are available in this region. Thus it is difficult to quantify this water storage. However, the net annual water storage of a lake or river basin, considered as a simple water balance model, is one component of the total water storage of the Tibetan Plateau. Changes in water storage of open water bodies can be assessed by analyzing changes in their water levels. Moreover, one of the variables directly affecting water levels of lakes and rivers on the Tibetan Plateau is glacial melt water. Therefore, monitoring changes in glaciers and water levels is a potential useful contribution to the understanding of the hydrologic processes and the water balance of the Tibetan Plateau.

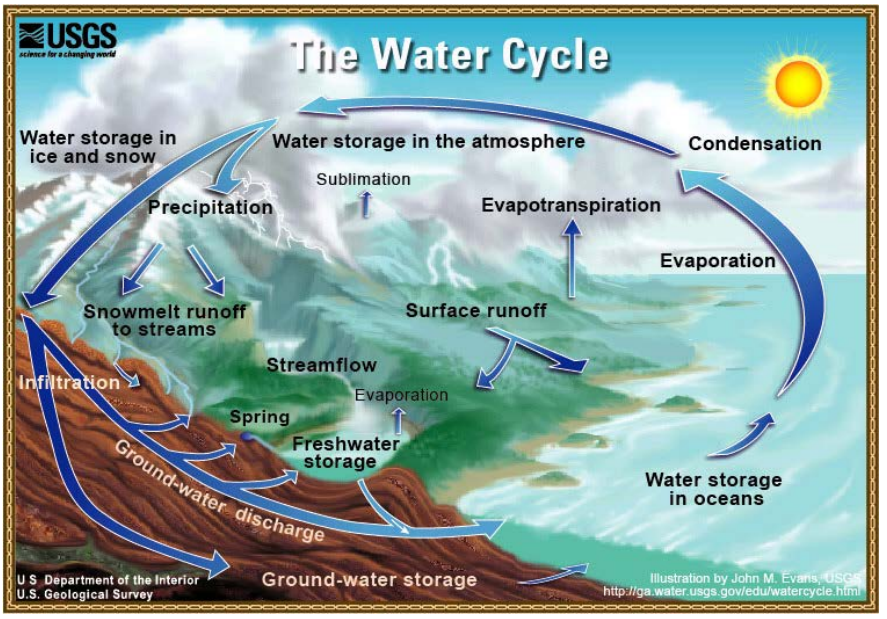

Figure 1.3: The water cycle. (Source: USGS, 2014)

The Tibetan Plateau has steep and rough relief, and often harsh climatic conditions. It is therefore difficult to reach mountain glaciers, lakes and upstream rivers. Thus using remote sensing techniques is a potential solution to assess hydrologic processes at the regional scale. Many different techniques are available with different sensor characteristics and different spatial and temporal resolution, including spectral imagery, photogrammetry, synthetic aperture radar (SAR) interferometry, radar altimetry, and laser altimetry.

Firstly imagery by e.g. Landsat and MODIS has the big advantage of covering the full Tibetan Plateau. It is possible to extract glacier and lake outlines from this imagery and to generate glacier and land-water masks. Multi-temporal imagery enables to detect area changes in glacier and water surface. For example, recent research reported glacial shrinkage in individual sub-regions on the Tibetan Plateau and surroundings using Landsat images at the Himalayas (Ye et al., 2009; Yao et al., 2012; Tian et al., 2014), the Tien Shan Mountains (Sorg et al., 2012), the Qilian Mountains (Wang et al., 2011), the Nyaiqentanglha Range (Bolch et al., 2010), and the inner plateau (Zhang et al., 2008; Wei et al., 2014). On the other hand, a 250 m MODIS land-water mask was produced combining MODIS images and SRTM DEM data (Carroll et al., 2009). Moreover, satellite images provide information on floodings occurring in river basins (Long et al., 2013; Bhatt et al., 2013). However, it is difficult to convert obvious changes in glacier and water body extent into water volumes that can be used as input for water balance models, as this requires in addition the availability of high quality digital terrain models.

Secondly a comparison between two digital elevation models at different times can reveal volume changes in glaciers and water bodies. For example, Gardelle et al. (2012) compared two digital elevation models from 1999 and 2008 and revealed that ice thinning and ablation is occurring at high rates in the central Karakoram and the Himalaya mountain ranges. Photogrammetry provides a good coverage for the whole Tibetan Plateau, as e.g. the global ASTER GDEM digital elevation model demonstrates. Photogrammetry requires however matches at pixels in overlapping image parts. These matches are difficult to obtain at areas with homogenous texture, such as glaciers and lakes. Therefore, it is very challenging to obtain photogrammetric digital elevation models of a quality that is sufficient to extract changes in lake level or glacial thickness.

Thirdly SAR interferometry has been applied to determine glacial velocities. Quincey et al. (2009) quantified the extent of stagnation in 20 glaciers across the Mt. Everest region and subsequently examined the relationship between local catchment topography and ice dynamics. However, it is not obvious how to relate such results to glacial thickness changes. Moreover, digital elevation model data

based on SAR interferometry, e.g. SRTM 90 m DEM, has in general insufficient accuracy to assess changes in glaciers and water bodies, reported with its vertical error of ~16 m on steep and rough areas (Zandbergen, 2008).

Fourthly satellite radar altimetry data has effectively been used for estimating annual water level changes since the seventies. For example, a limited number of large lakes on the Tibetan Plateau, like Namtso, Seilin, and Qinghai, have been observed using a composition of TOPEX/Poseidon, Jason 1 and 2, ENVISAT and GFO data (Crétaux et al., 2011). However, the relatively large footprints [(1)] of several kilometers of satellite radar altimeters are not appropriate for monitoring vertical changes in mountain glaciers and smaller and medium sized lakes in the steep and rough terrain that characterizes the Tibetan Plateau.

The alternative that will be used in this research is satellite laser altimetry. So far, one satellite laser altimetry mission was operational at our planet, the ICESat mission carrying the GLAS instrument.

1.2. ICESat laser altimetry

The Geoscience Laser Altimetry System (GLAS) instrument on board of ICESat was operational between 2003 and 2009. Its primary purpose was the detection of ice sheets elevation changes. Other objectives consist of measurements of sea ice, ocean, and land surface elevations and surface roughness, tree height estimation, and cloud studies. Figure 1.4a shows ICESat on its orbit while Figure 1.4b shows ICESat collecting measurements of the Earth's surface and atmosphere. During its lifetime, the GLAS instrument did not collect elevations continuously, but only in 18 one-month campaigns. The ICESat/GLAS instrument only obtained measurements along track with an along track distance between consecutive footprints of 170 m. The ICESat laser measurements have a vertical accuracy of ~10 cm over flat terrain and a horizontal accuracy of ~5 m (Schutz, 2002; Schutz et al., 2005; Duong et al., 2008). In fact, the tracks from the ICESat/GLAS campaigns only sparsely sampled the Tibetan Plateau, as illustrated in Figure 1.5. However a large number of glacial areas and lakes were still observed. In addition, the ICESat 1064 nm wavelength for assessing land surface elevations is strongly affected by clouds and terrain characteristics, like slope and roughness. Nevertheless with its small laser footprints, ICESat/GLAS data are advantageous in monitoring changes in glacial thickness and water level on the Tibetan Plateau.

[(1)] The footprint of a laser or radar altimeter is the spot on the terrain surface, illuminated by a single laser or radar pulse.

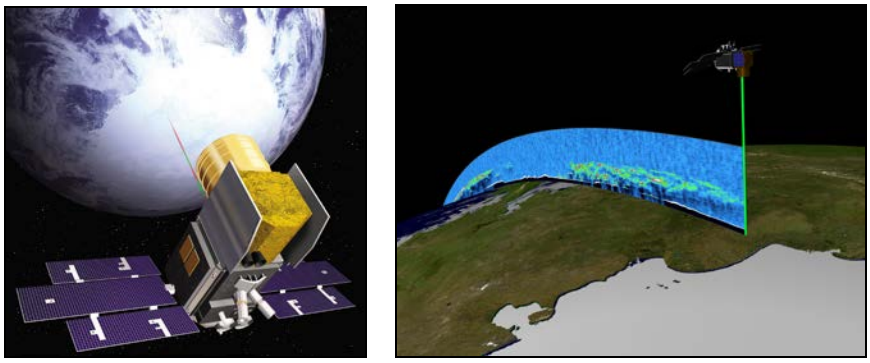

a) b)

Figure 1.4: a) ICESat on orbit, and b) Illustration of the GLAS instrument on board of ICESat, emitting pulses of green and infrared light straight down toward the Earth to collect three-dimensional measurements of the Earth's surface and atmosphere (NASA, 2014).

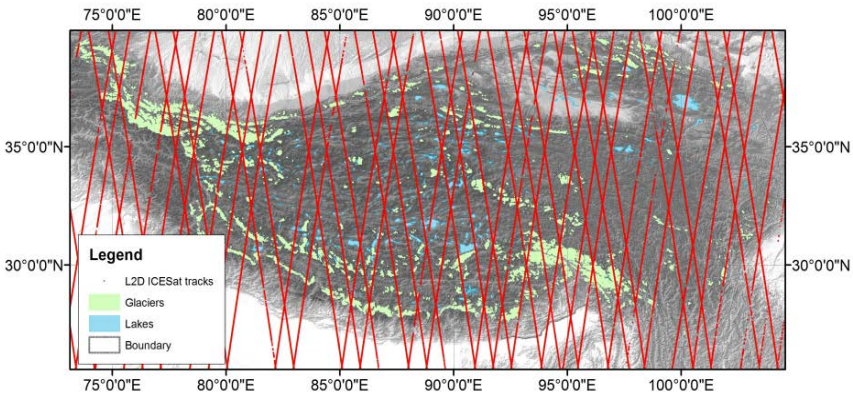

Figure 1.5: Distribution of glaciers and lakes with an area of over 1 km^2, and tracks of the ICESat L2D campaign passing over the Tibetan Plateau.

After the success of the ICESat mission, ICESat-2 is scheduled for launch in 2017 (NASA, 2014). The primary purpose of the ICESat-2 mission is again to measure ice sheet elevation change and sea ice thickness, while its data will also be used to estimate global vegetation biomass. The Advanced Topographic Laser Altimeter System (ATLAS) is the only instrument on board of ICESat-2. ATLAS

will emit green laser pulses at 532 nm wavelength. The ICESat-2/ATLAS mission designed using micro-pulses and multi-beams will improve both the cross-track and along-track sampling and the estimation of elevations in sloped and rough surface areas.

1.3. Research question

The main research question reads:

How to monitor changes in glacier thickness and lake levels on the Tibetan Plateau exploiting ICESat laser altimetry?

This research question is divided into the following sub-objectives:

i) How to exploit ICESat laser altimetry and additional data to retrieve lake levels in the Tibetan Plateau?

ii) How to exploit ICESat laser altimetry and additional data for estimating changes in glacial thickness on the Tibetan Plateau?

iii) How to validate changes in glacial thickness and lake levels derived from ICESat laser altimetry?

iv) How to link changes in glaciers and lakes on the Tibetan Plateau?

v) Is any relationship observable between changes in glacier thickness and lake levels at the Tibetan Plateau?

1.4. Methodology

In general the monitoring of changes in glacial thickness and lake level on the Tibetan Plateau is based on exploiting ICESat/GLAS data in combination with other available remote sensing data products including a glacier mask, a land-water mask, a digital elevation model (DEM), and hydrographic data. The glacier mask represents glacial outlines in mountains while the land-water mask locates lakes on the Tibetan Plateau. The DEM data is used as reference surface to estimate changes using ICESat elevations over glaciers, to estimate terrain slope and roughness, and to derive hydrographic data such as surface flow and watersheds.

The main tasks are as follows:

- Convert all input remote sensing data to the WGS84 Geographic Coordinate System in horizontal and the EGM2008 datum in vertical.
- Extract candidate ICESat elevations based on the glacier mask and the land-water mask.
- Explore the ICESat candidate elevations on lakes and glaciers using criteria such as cloud cover, saturation, slope, and roughness.
- Remove ICESat candidate elevations that are identified as anomalies.
- Estimate annual change trends in glacier thickness and lake level using adjustment theory.
- Determine geometric links between glaciers and lakes using a surface flow network analysis.

1.5. Organization of this thesis

This thesis exploits ICESat laser altimetry to monitor changes in lake levels and glacier thickness at the Tibetan Plateau between 2003 and 2009. The ICESat GLA14 land surface elevation data, used as a main data source, is described in Chapter 2. Additionally other products derived from remote sensing data including notably glacier and lake masks are also described in Chapter 2. In Chapter 3, glacial thinning or thickening trends in the glacial areas sampled by ICESat campaigns are estimated. In Chapter 4, annual water level trends of Tibetan lakes using ICESat laser altimetry in combination with a land-water mask are described. Accordingly seasonal and inter-seasonal lake level variations are analyzed and represented in Chapter 5. The results on seasonal trends seem to confirm different spatial patterns of temperature, precipitation, and humidity on the Tibetan Plateau. Chapter 6 presents how to determine geometric links between glaciers and lakes on the Tibetan Plateau. An indicator for dependency of a Tibetan lake on glacial runoff is defined and discussed as well. Chapter 7 gives the thesis conclusions, listing both achievements and recommending future work related to hydrological mass balance estimation at the Tibetan Plateau.

Chapter 2

EXPLOITED REMOTE SENSING DATA

This chapter describes input data sources used for studying changes in glacier thickness and lake levels on the Tibetan Plateau. The main data source exploited in this study is the ICESat laser altimetry data in which the GLA14 product provides global land surface elevations between 2003 and 2009. In addition to the GLA14 data, other data products derived from remotely sensed data are used such as the SRTM DEM, the GLIMS glacier mask, the 250 m MODIS land-water mask, and the HydroSHEDS hydrographic data. The HydroSHEDS river network and drainage basins are used to determine geometric links between glaciers and lakes at the Tibetan Plateau. Moreover a suitable set of Landsat TM images is used to validate the MODIS lakes and to visualize the GLIMS glaciers in the case study areas. These data products all are freely distributed on the internet and are useful for research on climatic change and water mass balances at regional and global scales.

2.1. Introduction

Currently a lot of remote sensing data that is potentially useful for estimating water mass balance and monitoring climatic changes is available on public websites. In this research on changes in glacier thickness and lake levels on the Tibetan Plateau, we exploit elevation data derived from ICESat laser altimetry. This product provides global multi-year elevations using relatively small laser footprints or laser spots. In addition, other remote sensing products are used such as the SRTM DEM, the GLIMS glacier mask, the MODIS land-water mask, and the HydroSHEDS river network and basin product. Compositions from these products are applied for research objectives such as estimating glacier thickness and lake level changes, and deriving geometric links between glaciers and lakes.

2.2. ICESat/GLAS data

In this section, first we introduce the ICESat mission. Then relevant data products from ICESat/GLAS data are described. Finally, we present the processing of ICESat GLA14 elevation data, used as a main input source for monitoring changes in glacial thickness and lake levels on the Tibetan Plateau.

2.2.1. ICESat mission

ICESat (Ice, Cloud, and Land Elevation Satellite) was NASA's benchmark Earth Observing System mission for measuring ice sheet mass balance, cloud and aerosol heights, as well as land topography and vegetation characteristics (NASA, 2014). ICESat was launched on 12-Jan-2003 and retired in February 2010 due to a technical malfunction. Between 2003 and 2009, the ICESat mission provided multi-year elevation data needed to determine ice sheet elevation changes as well as cloud property information over polar areas. In addition, it also provided topography and vegetation data around the globe.

The Geoscience Laser Altimeter System (GLAS) instrument on board of ICESat measured the distance from the satellite to the Earth surface and to intervening clouds and aerosols (GLAS, 2014). This distance was precisely determined based on the flight of duration of a laser pulse to the reflecting surface and back to the platform. The GLAS instrument performed the measurements 40 times a second when it was moving on orbit at a rate of 26,000 km/h. Figure 2.1 illustrates the GLAS instrument making measurements while orbiting the Earth. Attributes of the ICESat/GLAS operation are described in Table 2.1. Subsequently, altitude and geodetic location of each laser measurement were

calculated based on the distance from ICESat to the surface in combination of the position of ICESat in space and the pointing direction of the laser beam towards the surface. Up to now the GLAS instrument on ICESat is the only satellite laser altimetry instrument that provided elevation data all over the world.

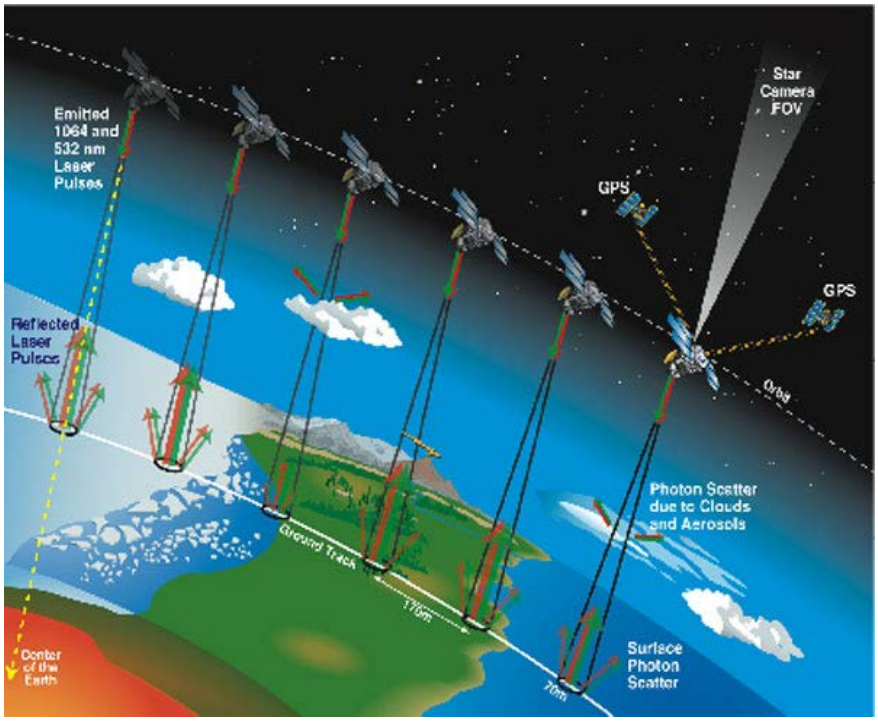

Figure 2.1: Schematic illustration of the GLAS instrument making measurements from ICESat while orbiting the Earth (GLAS, 2014).

Table 2.1: Attributes of the ICESat/GLAS operation.

Attribute	Value
Instrument	Geoscience Laser Altimeter System
Orbit Height	600 km
Inclination	94°
Laser Wavelength	1064 nm and 532 nm

Orbit Repeat	8 days and 91 days
Pulse length, given as Full Width at Half Maximum	5 ns
Laser Footprint Diameter on the ground	70 m
Sample interval on the ground	170 m
Sample Rate	40 laser shots per second

The ICESat/GLAS instrument was equipped with three lasers, each of which had 1064 nm and 532 nm channels. The infrared laser channel was used for measuring surface altimetry and dense cloud heights while the green lidar channel was used for determining the vertical distribution of clouds and aerosols. These three lasers were only operated one at a time, sequentially throughout the mission. During its lifetime from 2003 to 2009, the ICESat/GLAS instrument captured elevations in 18 designated campaigns, as summarized in Table 2.2.

Table 2.2: ICESat laser altimetry campaigns between 2003 and 2009.

Start date	End date	Days	Laser	Orbit repeat (days)
2003-02-20	2003-03-29	38	1AB	8
2003-09-25	2003-11-19	55	2A	8 and 91
2004-02-17	2004-03-21	34	2B	91
2004-05-18	2004-06-21	35	2C	91
2004-10-03	2004-11-08	37	3A	91
2005-02-17	2005-03-24	36	3B	91
2005-05-20	2005-06-23	35	3C	91
2005-10-21	2005-11-24	35	3D	91
2006-02-22	2006-03-28	34	3E	91
2006-05-24	2006-06-26	33	3F	91
2006-10-25	2006-11-27	34	3G	91
2007-03-12	2007-04-14	34	3H	91
2007-10-02	2007-11-05	37	3I	91
2008-02-17	2008-03-21	34	3J	91
2008-10-04	2008-10-19	16	3K	91

2008-11-25	2008-12-17	23	2D	91
2009-03-09	2009-04-11	34	2E	91
2009-09-30	2009-10-11	12	2F	91

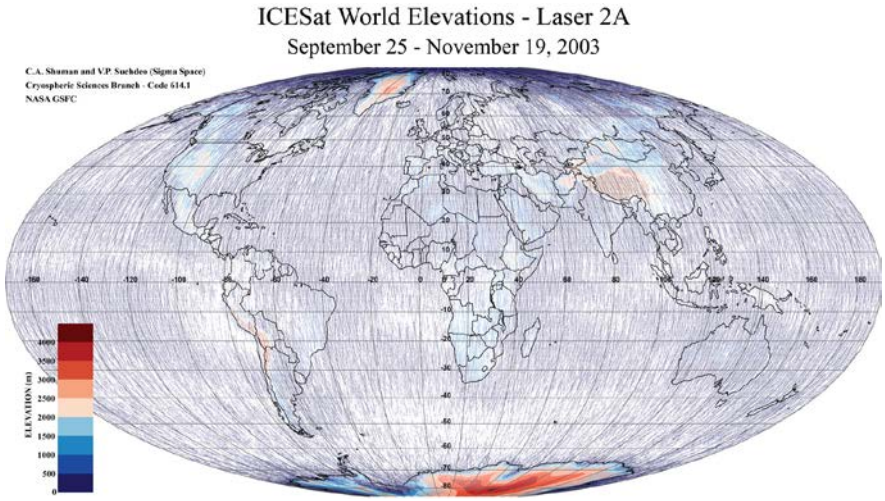

a)

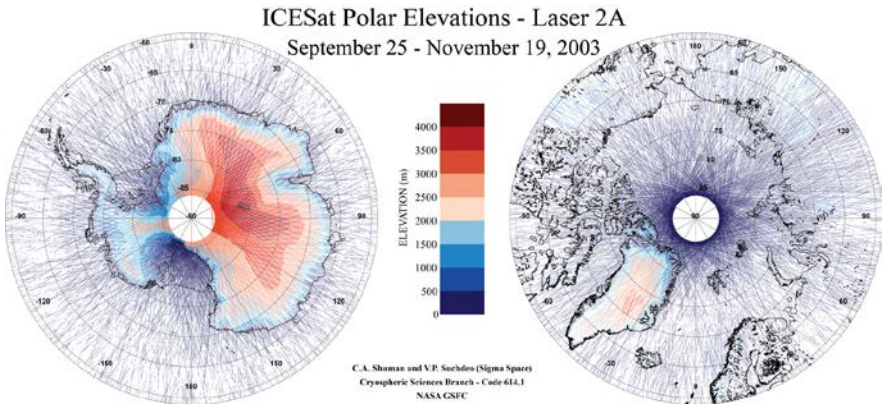

b)

Figure 2.2: a) World elevations and b) Polar elevations from the ICESat L2A campaign (NSIDC, 2014).

The temporal and spatial coverage is visualized by elevations obtained from the ICESat L2A campaign, as illustrated in Figure 2.2. Here the lowest elevations, sea level to 500 m, are shown in dark blue, and the other colors define higher elevations at 500 m increments. All elevations above 4,000 m are represented by a dark red color. White spaces are areas where no elevation data were obtained. This includes gaps along any individual track, generally due to atmospheric losses and between adjacent tracks because of the 8 day and partial 91 day orbit repeat cycles.

2.2.2. GLAS data products

GLAS data consists of 15 products at different data processing levels (Level-1A, Level-1B, and Level-2) (NSIDC, 2014). Here Level-0 represents raw data, while Level-4 data have had the greatest amount of processing applied (Parkinson et al., 2006). These products are shortly named as GLA01 - GLA15 in which the Level-2 data products from GLA08 to GLA15 provide global elevation measurements to different reflecting surfaces such as aerosols, clouds, ice sheets, sea ice, land surface, and ocean. For example, GLA14 provides global land surface elevations. All products are distributed by the National Snow and Ice Data Centre (NSIDC). They are in a flat binary format. However, the final Release 33 data products exist in two formats: the original binary format and HDF5 (Hierarchical Data Format).

2.2.3. ICESat GLA14 land surface elevation data

In this study, we exploit the ICESat GLA14 land surface elevation data in version 31, released in 2010 (Zwally et al., 2011). The GLA14 data for all 18 campaigns are available from the NSIDC website. The GLA14 data of each campaign is stored as a separate binary file. In addition to providing all ICESat/GLAS data products, NSIDC also provide tools for reading and viewing these data. The processing of the GLA14 data consists of 4 steps, as follows:

- Download ICESat GLA14 land surface elevation data: define the study area and the observed period. For example, the study area is the whole Tibetan Plateau, $73^0$30'E – $104^0$30'E and $26^0$30'N – $39^0$30'N, and the observed period is from 2003 to 2009, including all 18 ICESat campaigns. The Release 31 GLA14 data is in binary format.

- Convert the GLA14 binary data into ASCII text format: use the IDL Readers tool. This tool reads data from an ICESat/GLAS file and saves all the variables in ASCII format.

- Extract some variables from the GLAS altimetry data and output them in ASCII columns: use the NSIDC GLAS Altimetry elevation extractor Tool (NGAT). For example, for each laser measurement on a reflecting surface, the variables necessary to further analysis in this study consist of arrival time of the laser pulse, latitude, longitude, elevation, geoid height, saturation flag, and number of peaks found in the return echo.

- Convert between GLAS and WGS84 ellipsoids: use the IDL Ellipsoid Conversion tool. This tool converts latitudes and elevations between the WGS84 and the TOPEX/Poseidon ellipsoids. The latter ellipsoid is the ellipsoid used for all ICESat/GLAS elevations.

ICESat/GLAS geo-located products are given in terms of geodetic latitude, longitude, and elevation above a reference ellipsoid. ICESat/GLAS uses the same ellipsoid as TOPEX/Poseidon and Jason-1 where the equatorial radius is 6,378,136.30 m and reciprocal flattening (1/f) is 298.257. Differences between the ellipsoid used by ICESat/GLAS and the WGS84 ellipsoid are summarized in Table 2.3.

Table 2.3: Comparison between the ICESat/GLAS ellipsoid and WGS84 ellipsoid parameters.

	ICESat/GLAS	**WGS84**
Equatorial radius (a)	6,378,136.300000 m	6,378,137.000000 m
Polar radius (b)	6,356,751.600563 m	6,356,752.314245 m
Reciprocal flattening (1/f)	298.25700000	298.25722356
Eccentricity (e)	0.081819221456	0.081819190843

According to Table 2.3, the ICESat/GLAS ellipsoid is about 70 cm smaller than the WGS84 ellipsoid. As a consequence, comparison of GLAS elevations to those obtained from other sources must take into account the potential effect of ellipsoidal differences. The dominant difference is in geodetic elevation, with GLAS elevations higher than those obtained using the WGS84 ellipsoid. However, the differences in geodetic latitude and longitude will produce a horizontal displacement of only a few centimeters. The horizontal displacement caused by different ellipsoids is well below the GLAS accuracy in horizontal geo-location, so it can be ignored. The adjustment of elevation to account for

different ellipsoids with adequate accuracy is a straightforward function of latitude. Therefore the IDL Ellipsoid conversion tool helps to convert geodetic locations of ICESat footprints referencing to the ICESat/GLAS ellipsoid into the WGS84 ellipsoid.

In addition to geodetic latitude, longitude and elevation above the ICESat/GLAS ellipsoid, the GLA14 data provides geoid heights in the Earth Gravitational Model 2008 (EGM2008). These geoid height values present elevation differences between the EGM2008 geoid surface and the WGS84 ellipsoidal surface. Thus NSIDC also supports a function used to correct geoid height values from a particular data release so that the resulting values are relative to the ICESat/GLAS ellipsoid, and are in a mean-tide system. This function is included in the IDL Ellipsoid Conversion tool.

As a result, ICESat GLA14 binary data of all 18 campaigns were converted into the text-column format, with one file for each campaign. Using geodetic latitude and longitude, each file in text-column format was converted into a GIS shapefile in point vector format. Thus there are 18 GIS shapefiles, corresponding to 18 ICESat campaigns, in which each point represents an ICESat laser footprint with attributes including arrival time of the laser pulse, latitude, longitude, elevation, geoid height, saturation flag, and the number of peaks found in the return echo. Here the geo-location of each ICESat footprint is referenced to WGS84 in horizontal and to EMG2008 in vertical. Figure 2.3 illustrates elevations derived from ICESat L2D campaign data from 25-Nov-2008 to 17-Dec-2008 at the Tibetan Plateau.

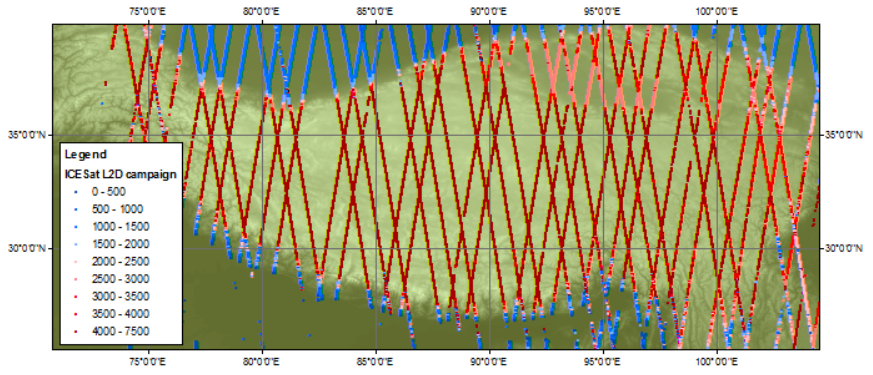

Figure 2.3: Tracks of the ICESat L2D campaign from 25-Nov-2008 to 17-Dec-2008 over the Tibetan Plateau.

The geospatial accuracy of each footprint is reported as ~5 m in the horizontal datum and ~10 cm in the vertical datum for slopes below 1 degree (Schutz, 2002; Schutz et al., 2005; Duong et al., 2008). Schutz (2002) also indicated that the vertical accuracy of each footprint strongly depends on the reflecting surface roughness and slope. However, the quality of the elevations can be assessed by GLA14 attributes describing possible effect of saturation and the number of peaks in the decomposition the full waveform return signal. The saturation correction flag identifies possible saturation issues while the number of peaks relates to land surface geometry (Duong, 2010). In addition, in 2011 the ICESat Science Team detected inter-campaign elevation biases for different areas and various surface types (NSIDC, 2014). These biases were below 15 cm and were included in the Release 33 products. However, it is noted that they should not be used.

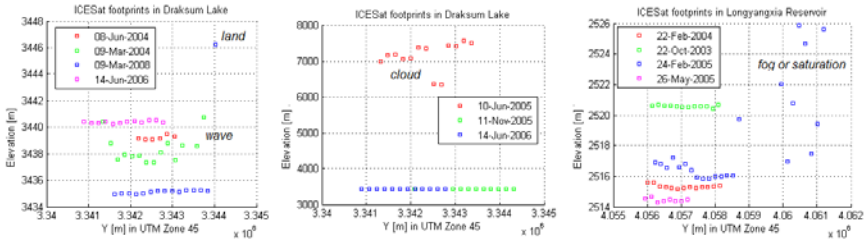

a) b) c)

Figure 2.4: The distribution of the ICESat GLA14 elevations affected by different surface characteristics: a) Waves: elevation variations of a few meters within consecutive shots, b) Clouds: elevation variations within one track are very big, e.g. ~1,000 m, while the altitude difference with other campaigns is high, e.g. more than 3,500 m, and c) Fog or saturation: elevation variations in the order of 10 m.

For considering the quality of the laser measurements on land surface, we explored the ICESat GLA14 land surface elevation data at flat surfaces, lakes. The result of these explorations indicated that the GLA14 elevations were significantly affected by different surface characteristics. Figure 2.4 shows the distribution of GLA14 elevations whose footprints were located within Draksum Lake and Longyangxia Reservoir on the Tibetan Plateau. Here the lake outlines were obtained from the 250 m MODIS land-water mask. Waves at a lake-surface or snow on top of lake ice may be an explanation for a slightly larger variation in

lake elevations between points from one track, as shown in Figure 2.4a. If elevations over a lake are affected by clouds, the elevation variation within one track may be very big, for example about 1,000 m, while the altitude difference with other campaigns is high, for example more than 3,500 m at Draksum Lake as illustrated in Figure 2.4b. If GLA14 elevations are affected by fog or if the reflected elevation signals are saturated, the elevation variation may further increase. Here saturation refers to the effect that the GLAS waveform signal is clipped by the receiver because the receiver obtains more signal than it can handle (Duong, 2006). In Figure 2.4c, such variations in an order of 10 m are shown.

2.3. Other remote sensing products

In this section, we introduce other remote sensing products used in this study. Firstly, the GLIMS glacier mask, representing glacier outlines on the Tibetan Plateau, is used in Chapters 3 and 6. Secondly, the MODIS land-water mask is used to obtain Tibetan lake outlines in Chapters 4, 5 and 6. Thirdly, the SRTM DEM data is referenced to ICESat/GLAS elevations as a base map in Chapter 3 and to create several individual drainage catchments in Chapter 6. Finally, the HydroSHEDS river network and drainage basin data are used to analysis links between glaciers and lakes on the Tibetan Plateau in Chapter 6. The river network provides information on the direction of surface runoff, while the drainage basin data describes the catchment areas. Moreover, Landsat images are used on several occasions for checking the existence of lakes and glaciers as well.

2.3.1. GLIMS / CAREERI glacier mask

Global Land Ice Measurements from Space is a project to monitor the world's glaciers, primarily using data from optical satellite instruments (GLIMS, 2014). Now over 60 institutions world-wide are involved in GLIMS for inventorying the majority of the world's estimated 160,000 glaciers. The resulting glacial outlines are distributed in the GIS shapefile format and are referenced to the WGS84 datum. Each glacier is represented by a polygonal vector with attributes such as identification code, area, width, length, min elevation, max elevation, and name.

In Chapter 3, the GLIMS glacier mask presenting glacial outlines on the whole Tibetan Plateau is used for the research on glacier thickness changes, as shown in Figure 2.5. For this study area, the glacier mask consists of ~37,000 glaciers, occupying an area of ~56,560 km^2. This product was submitted by Li (2003),

Chinese Academy of Sciences. The GLIMS glacier mask is a copy of original data collected and digitized by the Cold and Arid Regions Environmental and Engineering Research Institute, Chinese Academy of Science (CAREERI).

In Chapter 6, we use the CAREERI glacier mask to determine dependency of Tibetan lakes on glacial runoff. The CAREERI glacier mask is developed and distributed by the World Data Center for Glaciology and Geocryology, Lanzhou, China. The glacier inventory was based on topographic maps, aerial photography, optical remote sensing images and in situ measurements from 1978 to 2002 (Shi et al., 2009) during several individual periods. This product is distributed as ArcInfo coverage data, a GIS file format. It uses the Projected Coordinate System, named as the Beijing Coordinate Projection, based on the Krasovsky spheroid and the Albers map projection. Its attributes consist of the area of each glacier, perimeter, and glacier identification codes.

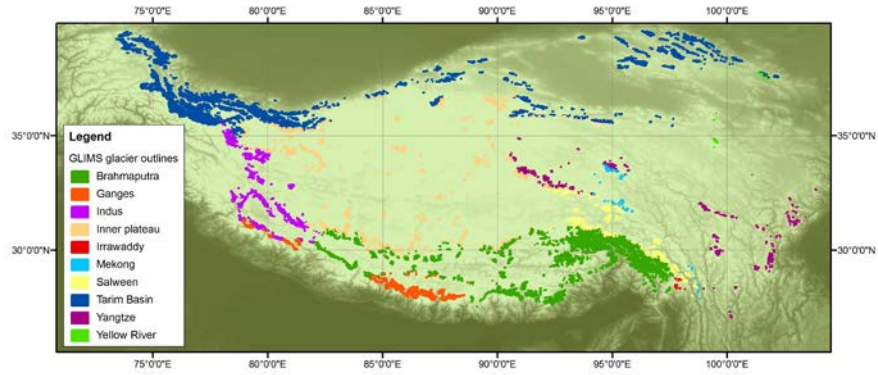

Figure 2.5: GLIMS glacier outlines colored per basin on the Tibetan Plateau.

In this study, initially we used the CAREERI glacier mask to determine geometric dependency of Tibetan lakes on glacial runoff. This glacier mask is referenced to the Beijing Coordinate System, but missing the datum parameters. Therefore it is difficult to integrate it with other data, e.g. reference it to the WGS84 Geographic Coordinate System. Therefore when the GLIMS glacier inventory was updated in 2013, we switched to the GLIMS glacier mask to monitor changes in glacier thickness at the Tibetan Plateau. The GLIMS glacier mask is a copy of the CAREERI glacier mask but it is referenced to the WGS84 Geographic Coordinate System.

2.3.2. MODIS land-water mask

The 250 m MODIS land-water mask, called MOD44W, was produced using over 8 years of Terra MODIS spectral data, over 6 years of Aqua MODIS spectral data and Shuttle Radar Topography Mission (SRTM) elevation data (Carroll et al., 2009). This product is distributed in raster format and referenced to the WGS84 coordinate system. For each pixel of 250 m, the MODIS land-water mask indicates in different ways whether one of the contributing algorithms decided that the pixel represents water. In addition to lakes, the land-water mask also shows some parts of rivers and seasonally empty depressions.

In this study, we selected lakes with an area of over 1 km^2 on the whole Tibetan Plateau. This limit is a trade-off: selecting only larger lakes would decrease the number of lakes in the analysis, while applying a lower threshold would stretch the possibilities of the 250 m MODIS land-water mask too much. The lakes in the land-water mask are compared to Google Earth and appropriate Landsat TM images to remove parts of rivers and empty depressions. This selection returns 891 lakes with an area of over 1 km^2 on the Tibetan Plateau. They occupy a total area of ~38,800 km^2, as shown in Figure 2.6. These Tibetan lakes were stored into a GIS shapefile in polygon vector format and referenced to the WGS84 Geographic Coordinate System.

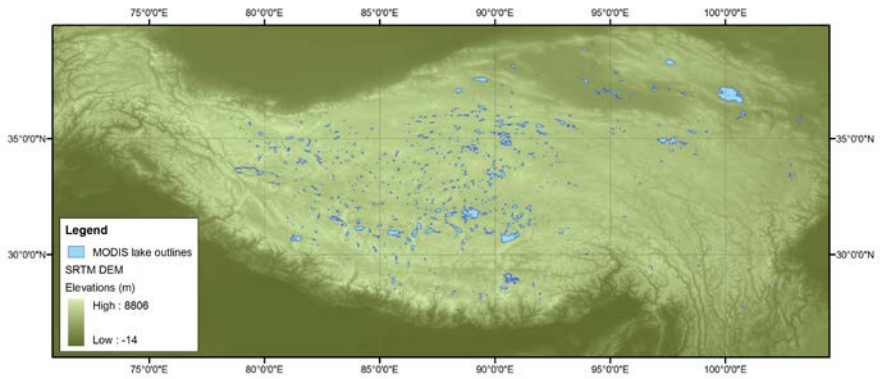

Figure 2.6: Tibetan lakes with an area over 1 km^2, derived from the 250 m MODIS land-water mask, superimposed on the elevation layer merged by 21 SRTM DEM 5^0x5^0 tiles.

2.3.3. SRTM DEM

The Shuttle Radar Topography Mission (SRTM) was flown in February 2000 and collected the first ever high resolution near-global digital elevation data. In this study, we use the SRTM 90 m DEM, produced by NASA (Jarvis et al., 2008). This DEM has a resolution of 90 m at the equator corresponding to 3-arc seconds and is distributed in 5^0 x 5^0 tiles. To cover the full Tibetan Plateau as shown in Figure 2.6, 21 SRTM DEM tiles are concatenated. The tiles are available in both ArcInfo ASCII and GeoTiff format. The digital elevation data were stored in a grid as m x n matrix. The data is projected in a Geographic (latitude / longitude) projection, with the WGS84 horizontal datum and the EGM96 vertical datum. The vertical error of the DEM's is reported to be less than 5 m on relative flat areas and 16 m on steep and rough areas (Zandbergen, 2008).

2.3.4. HydroSHEDS hydrographic data

HydroSHEDS stands for Hydrological data and maps based on SHuttle Elevation Derivatives at multiple Scales (HydroSHEDS, 2014). HydroSHEDS provides hydrographic information in a consistent and comprehensive format for regional and global-scale applications. HydroSHEDS offers a suite of geo-referenced data sets (vector and raster), including stream networks, watershed boundaries, drainage directions and ancillary data layers such as flow accumulations, distances and river topology information. It is derived from elevation data of the STRM DEM at 3 arc-second resolution (a grid cell size of ~87 m on the Tibetan Plateau). The processing methods include void filling, filtering, stream burning, and up-scaling techniques. Manual corrections were made where necessary (Lehner et al, 2008).

The HydroSHEDS river data are directly derived from drainage directions and flow accumulation layers. The river data are built at 15 arc-second resolution (~410 m on the Tibetan Plateau). Grid cells with an upstream drainage area exceeding a threshold of 100 upstream cells were considered as belonging to a stream or a river segment. The river data are formatted in polyline vectors where each line is formed by a from-node (starting point), a list of vertices and a to-node (end point). The river network is referenced to WGS84. Each river segment has a pointer to its corresponding flow accumulation given as a number of grid cells. For example, the inset in Figure 2.7 shows the river network in the Kekexili Lake catchment, and the flow route from Yinma Lake to Kekexili Lake is indicated.

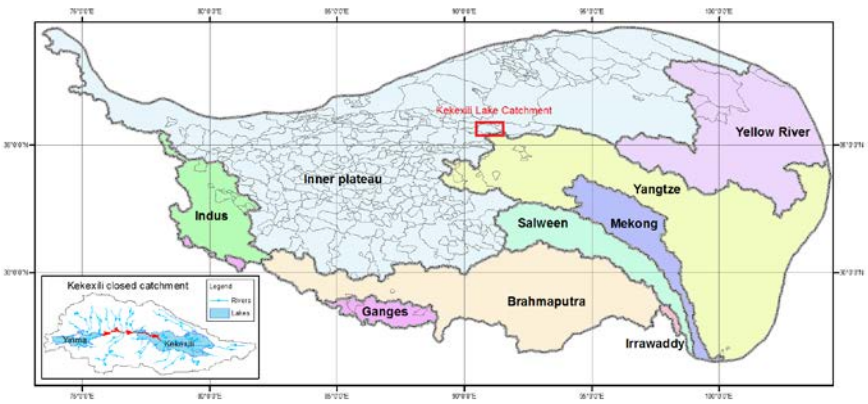

Figure 2.7: Tibetan catchments derived from the HydroSHEDS hydrographic data. Inset: the river network at the Kekexili catchment.

The HydroSHEDS drainage basin data, describing the catchment areas or the watershed boundaries, are also built at 15 arc-second resolution. This product is formatted as polygons, as shown in Figure 2.7. It is also referenced to WGS84. Catchments are attributed with an area in square kilometer, e.g. the Kekexili Lake catchment occupies an area of 2,636.5 km^2.

2.3.5. Landsat TM images

The Landsat program provided satellite images of the Earth to monitor natural resources of the globe from 1972 to present. Their temporal resolution is 16 days while their spatial resolution is 15 m for panchromatic, 30 m for multi-spectral and 60 m for thermal bands. In this study, however, we exploited this data source to validate the glacier outlines obtained from the GLIMS glacier mask and to check the existence of the lake outlines obtained from the MODIS land-water mask.

a) Representing the GLIMS glacier outlines: some Landsat 8 images in 2013 were collected at glacial mountain regions. These true color composite images were used as base maps for superimposing the GLIMS glacier layer at Hengduan Mountain and Western Kunlun Mountain, see Section 3.3.

b) Checking the existence of the MODIS lakes: an appropriate set of Landsat 7 ETM images around 2001 and 2002 was collected. These images were below 10% cloud coverage. False color images were composited from

Landsat ETM bands to emphasize water bodies. Then, the MODIS lake layer was overlaid on the false color composite images. To check if a lake is seasonal, e.g. empty depressions or holes in summer, the Landsat images containing the lakes were collected at least twice per year, corresponding to summer and winter at the Tibetan Plateau. In addition, the MODIS lake layer was explored in Google Earth as well.

2.4. Conclusions

All data products described in this chapter are distributed at public professional websites. Initially they were built for different research objectives such as the ICESat/GLAS data to detect ice sheets elevation changes, the 250 m MODIS land-water mask to manage natural resources, the HydroSHEDS data to provide hydrographic information at regional and global scale, etc. However combining these data products has strong potential for monitoring the impact of climate change and estimating mass balances at sensitive areas. Note that a reference coordinate system is important in the integration of remote sensing data, e.g. the WGS84 Geographic Coordinate System is suitable for regional and global scale studies. These applications exploiting fused data products are useful to understand hydrological systems all over the world. For example, this research on changes in glacier thickness and lake levels is expected to contribute to the understanding of hydrologic mass balance of the Tibetan Plateau.

Chapter 3

ASSESSING GLACIAL THICKNESS CHANGES AT THE TIBETAN PLATEAU USING ICESAT LASER ALTIMETRY [(2)]

Monitoring glacier changes is essential for estimating the water mass balance of the Tibetan Plateau. Recent research indicates that glaciers at individual regions on the Tibetan Plateau and surroundings are shrinking and thinning during the last decades. Studies considering large regions often ignored however the impact of locally varying weather conditions and terrain characteristics on glacial evolution, i.e. the impact of orographic precipitation and variation in solar radiation. Our hypothesis is therefore that adjacent glaciers of opposite orientation change in a different way. In this chapter, we exploit ICESat laser altimetry data in combination with the SRTM DEM and the GLIMS glacier mask to estimate glacial thickness change trends between 2003 and 2009 on the whole Tibetan Plateau. Considering acquisition conditions of ICESat measurements and terrain surface characteristics, annual glacial elevation trends were estimated for 15 different settings with respect to terrain slope and roughness. In the end, we only included ICESat elevations acquired over terrain with a slope below 20 deg and a roughness at the footprint scale below 15 m. With this setting, 90 glacial areas could be distinguished. The results show that most of observed glacial areas on the Tibetan Plateau are thinning, except for some glaciers in the Northwest. In general, glacial elevations on the whole Tibetan Plateau decreased at an average rate of -0.17 ± 0.47 meters per year (m a^{-1}) between 2003 and 2009, taking together glaciers of any size, distribution, and location of the observed glacial area. Moreover, the results show that glacial elevation changes indeed strongly depend on the relative position in a mountain range.

[(2)] Published as: Phan, V.H., Lindenbergh, R.C., Menenti, M.: Orientation dependent glacial changes at the Tibetan Plateau derived from 2003 – 2009 ICESat laser altimetry. *The Cryosphere Discussion*, 8, 2425-2463, 2014.

3.1. Introduction

The Tibetan Plateau has steep and rough terrain and contains ~37,000 glaciers, occupying an area of ~56,560 km^2 (Li, 2003). Recent studies report that the glaciers have been retreating significantly in the last decades. According to Yao et al. (2012), the magnitude of glacial change in the last 30 years is location dependent, with the largest reduction in glacial length and area occurring in the Himalayas (excluding the Karakoram). Sorg et al. (2012) showed that glacier shrinkage has also occurred in the Tien Shan Mountains in the Northwest of the Tibetan Plateau during the period between 1950 and 2000. As reported in Wang et al. (2011), 910 glaciers in the Middle Qilian Mountain Region have rapidly reduced in area between 1956 and 2003, with a mean reduction of 0.10 km^2 per individual glacier, corresponding to a mean rate of 2,127 $m^2 a^{-1}$. In addition to generating a glacier inventory for the western Nyaiqentanglha Range for the year ~2001, based on Landsat ETM+ and SRTM3 DEM data, Bolch et al. (2010) reported that the glacier area in that region decreased by -6.1 ± 3 % between 1976 and 2001 and glaciers continued to shrink during the period 2001 – 2009. Recently, Tian et al. (2014) semi-automatically delineated the glacier outlines of ~1990, ~2000 and ~2010 in the Qilian Mountains using Landsat imagery with the help of ASTER GDEM and SRTM DEM elevations, and after combining their results with previous studies found that the total glacier area shrank by 30 ± 8 % between 1956 and 2010. Similarly using Landsat images between 2004 and 2011 and topographic maps in 1970s, Wei et al. (2014) reported that the total glacier area in the inner Tibetan Plateau decreased at a rate of 0.27 % a^{-1}. In addition, glaciers in the Tuotuo River basin, the source of the Yangtze River in the inner plateau, have also retreated between 1968 and 2002 (Zhang et al., 2008) as have glaciers in the Mt. Qomolangma (Mt. Everest) region in the Himalayas in the last 35 years (Ye et al., 2009). Most of the above results were analyzed from topographic maps, in situ measurements, and optical remotely sensed images during the observed periods. Recently, however, new remote sensing techniques such as interferometry and radar / laser satellite altimetry have been used for research on glacier and ice-sheet changes.

The ICESat mission provided global elevation data between 2003 and 2009 that were mostly used to study ice sheet mass balance over polar areas. However, recently the ICESat laser altimetry data have also been exploited to monitor glaciers in mountain regions such as Himalayas, Alps and the Tibetan Plateau. Kaab et al. (2012) quantified the glacial thinning in the Hindu Kush-Karakoram-Himalaya region from 2003 to 2008, based on the ICESat/GLAS data and the SRTM DEM. Similarly using ICESat/GLAS data and digital elevation models including SRTM DEM, Advances Spaceborne Thermal Emission and Reflection Radiometer Global Digital Elevation Model (ASTER GDEM) and airphoto

DEMs, Kropacek et al. (2013) estimated volume changes of the Aletsch Glacier in the Swiss Alps by two approaches based on elevation differences with respect to a reference DEM and elevation differences between close by tracks. Estimating thickness change rates for high-mountain Asian glaciers based on ICESat/GLAS data is part of regional glacier mass budget studies all over the world (Gardner et al., 2013).

In addition, Neckel et al. (2014) applied a method similar to Kaab et al. (2012) for estimating glacier mass changes at eight glacial sub-regions on the Tibetan Plateau between 2003 and 2009. The results indicated that most of the glacial sub-regions had a negative trend in glacial thickness change, excluding one sub-region in the western Mt. Kunlun in the Northwest of the Tibetan Plateau. The glacial thickness changes on the Tibetan Plateau and surroundings obtained from the ICESat/GLAS data provided useful information about the status of glacial sub-regions between 2003 and 2009. However, sampled glacial sub-regions were relative large. As a consequence, the glacial conditions were not homogeneous, due to e.g. orographic precipitation and variation in solar radiation. The significant influence of climatic parameters (Bolch et al., 2010) and spatial variability (Quincey et al., 2009) on glacial change rates has already been demonstrated for several individual glaciers on the Tibetan Plateau. In addition, the quality of ICESat elevations is known to be strongly dependent on terrain characteristics.

Therefore, in this study we exploit ICESat/GLAS data for monitoring glacial thickness changes on the whole Tibetan Plateau, identifying sampled glacial areas based on ICESat footprints and glacier orientation. In addition, we explore the ICESat/GLAS data by applying criteria impacting the quality of footprints including acquisition condition and terrain surface characteristics. The results are expected to complement to previously estimated water level changes of the Tibetan lakes, see Chapter 4 and (Zhang et al., 2011). Using additional explicit runoff relations between glaciers and lakes shown in Chapter 6, correlations between glacial and lake level changes can be determined to improve understanding of water balance on the Tibetan Plateau.

3.2. Methodology

To estimate a glacial thickness change trend, we consider differences between glacial surface elevations derived from 2003 – 2009 ICESat laser altimetry and a digital elevation model. Here the digital elevation model is used as a reference surface. In addition, a glacier mask is used to identify ICESat elevations that are likely to sample glaciers. Each difference is time-stamped by the ICESat

acquisition time. Valid differences obtained during the same ICESat campaign track over a certain homogeneous glacial area, also called a sampled glacial area, are used to estimate a mean difference. Mean differences for each sampled glacial area are grouped to form a time series. Consecutively, a temporal trend is estimated through the mean differences per area, resulting in a temporal trend of glacial thickening or thinning.

The input data sources consist of the ICESat GLA14 land surface elevation data, the SRTM DEM, and the GLIMS glacier mask, see sections 2.2.3, 2.3.3, and 2.3.1 respectively in Chapter 2. Figure 3.1 illustrates the SRTM elevations, GLIMS glacier outlines and ICESat L2D campaign tracks on the Tibetan Plateau. Differences between the ICESat GLA14 elevations and the reference SRTM DEM may correspond to glacial thickness change between 2003 and 2009. However, the vertical accuracy of each ICESat footprint strongly depends on terrain surface characteristics, so we have to remove uncertain footprints before the estimation. Firstly, therefore, we estimate surface slope and roughness from the SRTM DEM. Then we determine those glacial areas that are sufficiently sampled. Next we identify valid thickness changes for each sampled glacial area. Finally we estimate glacial thickness change trends per area.

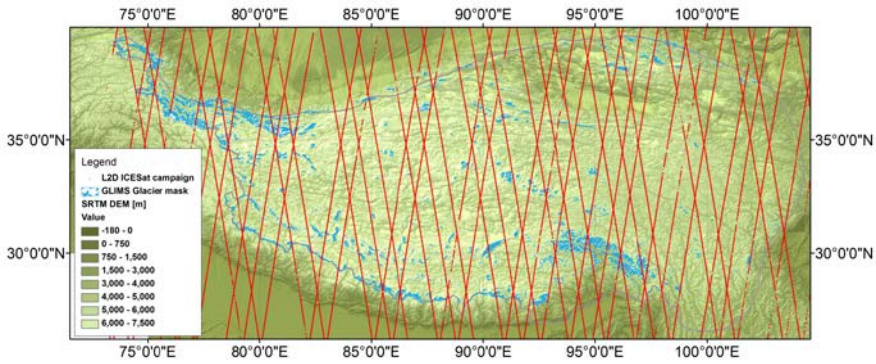

Figure 3.1: GLIMS glacier outlines and ICESat L2D-campaign tracks superimposed on the SRTM DEM over the Tibetan Plateau.

3.2.1. Estimating surface slope and roughness from SRTM DEM

Based on the SRTM DEM, the terrain surface parameters slope S and roughness R are estimated, using a 3x3 kernel scanning over all pixels of the grid, as

illustrated in Figure 3.2. For each pixel, the slope S in decimal degrees is locally estimated by formula (3.1) (Verdin et al., 2007, Shi et al., 2013).

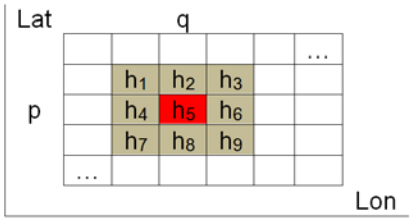

Figure 3.2: Illustration of the 3 by 3 kernel at pixel (p, q) where the h_i values (i = 1÷9) are corresponding to the DEM elevations.

$$S = \frac{180}{\pi} * \arctan\sqrt{\left(\frac{dz}{dx}\right)^2 + \left(\frac{dz}{dy}\right)^2} \tag{3.1}$$

$$\frac{dz}{dx} = \frac{(h_3 + 2*h_6 + h_9) - (h_1 + 2*h_4 + h_7)}{8*\Delta lon} \tag{3.2}$$

$$\frac{dz}{dy} = \frac{(h_7 + 2*h_8 + h_9) - (h_1 + 2*h_2 + h_3)}{8*\Delta lat} \tag{3.3}$$

Here, Δlat and Δlon are the width and the height of a grid cell in meters, estimated by distance formula (3.4) (Sinnott, 1984).

$$\begin{aligned} d &= r * 2 * a \tan 2(\sqrt{a}, \sqrt{1-a}) \\ a &= \sin^2\left(\frac{\varphi_2 - \varphi_1}{2}\right) + \cos(\varphi_1) * \cos(\varphi_2) * \sin^2\left(\frac{\lambda_2 - \lambda_1}{2}\right) \end{aligned} \tag{3.4}$$

Here, d is the shortest distance over the earth's surface – the 'as-the-crow-flies' distance between the two points (λ_1, φ_1) and (λ_2, φ_2) in radians in a geographic coordinate system and r is the earth's radius (mean radius = 6,371 km).

The roughness R in meters is defined as the root mean square of the differences $\hat{e}_i$ between the grid heights and the local 3x3 plane, best fitting in the least squares sense, Lay (2003) and Shi et al. (2013).

$$R = \sqrt{\frac{\sum_{i=1}^{i=9} \hat{e}_i^2}{9}} \qquad (3.5)$$

3.2.2. Determining a sampled glacial area

Because of the orbital configuration of ICESat and its along track only sampling, Tibetan glacial areas are only sampled sparsely by ICESat. In addition, surface elevation changes on these mountain glaciers are expected to be affected significantly by the orientation and face of the corresponding mountain range. For example, the South face of the Himalayas is experiencing more precipitation than the North face, while on the other hand North faces experience less incoming sunlight. Therefore we decided to group nearby glaciers having similar orientation into one sampled glacial area while, on the other hand, glaciers on different sides of a mountain range ridge were grouped into different areas. First we extracted footprints of all ICESat campaigns within the GLIMS glacier outlines, as illustrated in Figure 3.3. Then each glacial area outline was manually determined, by considering the locations of the glaciers and the ICESat footprints. For example, in Figure 3.3 the ICESat-sampled glaciers having a northern orientation were grouped into one glacial area, A, while those on the other side of the mountain ridge were grouped into another glacial area, B. Finally each glacial area was coded by an identification number.

3.2.3. Identifying a glacial elevation difference

A glacial elevation difference Δh is identified as the difference between an elevation of an ICESat footprint within a sampled glacial area and the reference SRTM DEM, compare formula (3.6), where Δh is in meters above EGM2008.

$$\Delta h = h_{ICESat} - h_{SRTM} = (Elev - GdHt) - (SRTM\_elev + 96\_08\_Ht) \qquad (3.6)$$

Each glacial elevation difference Δh depends on the characteristics of the terrain illuminated by the ICESat pulse and the characteristics of the ICESat measurement itself. It is in principle also affected by the local quality of the SRTM reference elevation, but in this study it is assumed that the quality of the STRM DEM is not location dependent. What is assessed in this study is the quality of the elevation difference with respect to the attributes described in Table 3.1. For this purpose, we extract ICESat footprints within the sampled glacial areas and obtain their full attributes.

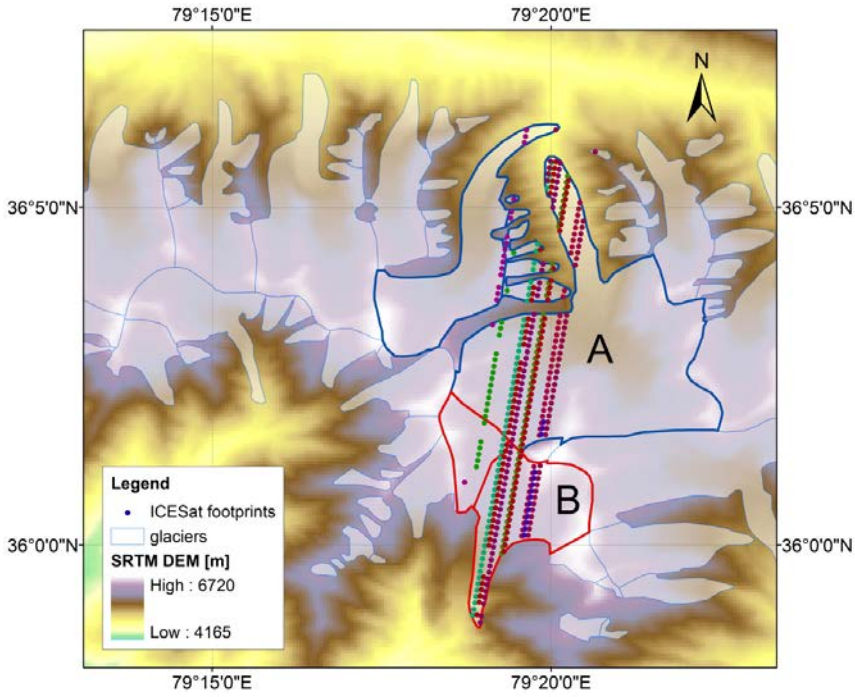

Figure 3.3: ICESat footprints superimposed over the GLIMS glacier mask. The ICESat-sampled glaciers having similar orientation were grouped into glacial areas A and B.

Table 3.1: The attributes related to each ICESat measurement.

Name	Attribute description
Time	ICESat acquisition time or arrival time of the laser pulse on the reflecting surface in UTC 'dd-MM-yyyy' format, derived from the GLA14 data
Lat	Geodetic latitude in degrees, derived from the GLA14 data
Lon	Geodetic longitude in degrees, derived from the GLA14 data
Elev	Elevation in meters above WGS84, derived from the GLA14 data
GdHt	Geoid height in meters in the EGM2008 datum, derived from the GLA14 data
SatFlg	Saturation correction flag, identifying possible saturation

	issues, derived from the GLA14 data
NumPk	Number of peaks in the Gauss waveform decomposition from the return echo, derived from the GLA14 data
SRTM_elev	Elevation in meters above EGM1996, derived from the SRTM DEM
S	Surface slope in degrees, derived from the SRTM DEM
R	Surface roughness in meters, derived from the SRTM DEM
96_08_Ht	Geoid height difference between EGM1996 and EGM2008 in meters (Pavlis et al., 2008)
GID	Identification code of the observed glacial area

A glacial elevation difference Δh is maintained for further analysis if the corresponding ICESat measurement is considered good according to the following criteria. First we select those footprints whose return echo is not or only lightly saturated and moreover have only one peak in its Gauss decomposition. That is the value of *SatFlg* should equal 0 or 1, and the value of *NumPk* should equal 1. A footprint with one mode is expected to correspond to homogeneous land surface. Then we remove footprints affected by clouds. If ICESat footprints are affected by clouds, the elevation variation within one track can be very large, while the altitude difference with other tracks is high, shown at Section 2.2.3 in Chapter 2. In this study, if the ICESat elevation difference to the SRTM DEM Δh is larger than 100 m, the footprint is assumed to be affected by clouds and removed from further analysis.

3.2.4. Different settings with respect to slope and roughness

Here we analyze different settings incorporating the terrain surface characteristics slope and roughness. We remove footprints with a slope S bigger than a threshold S_0 and roughness R bigger than a threshold R_0. Applying strict thresholds will result in a relative small number of remaining glacial elevation differences albeit of relatively high quality. A slope S below 10 deg is always considered good while a slope of over 30 deg results in an inacceptable bias. The roughness R is estimated directly from the SRTM data, its lower limit of 5 m corresponds to relative flat areas while its upper limit of 15 m corresponds to high relief and rough areas. In the following we consider 15 different settings with slope and roughness values within these outer limits, as described in Table 3.2. Each record in Table 3.2, corresponding to one such setting, also

summarizes the corresponding resulting trend in glacial thinning/thickening for the whole Tibetan Plateau between 2003 and 2009, as determined by the following steps.

3.2.5. Obtaining mean glacial elevation differences

For each sampled glacial area, glacial elevation differences all are time-stamped by ICESat acquisition time. The ICESat acquisition time t_i is defined per ICESat track segment, where one track is sampling a glacial area with consecutive individual footprints. A mean glacial elevation difference $\overline{\Delta h_i}$ is considered representative for the height of the glacial area above the SRTM base map at ICESat acquisition time t_i. The mean difference $\overline{\Delta h_i}$ and its standard deviation s_i is computed using formulas (3.7) and (3.8), where k is the number of ICESat footprints in the track segment that are sampling a glacial area at ICESat acquisition time t_i and Δh_{ij} is the jth elevation difference, j = 1÷k.

$$\overline{\Delta h_i} = \frac{1}{k}\sum_{j=1}^{j=k}\Delta h_{ij} \tag{3.7}$$

$$s_i = \sqrt{\frac{1}{k}\sum_{j=1}^{j=k}\left(\Delta h_{ij} - \overline{\Delta h_i}\right)^2} \tag{3.8}$$

Each ICESat acquisition time t_i is considered as an epoch in the time series used to estimate a temporal trend using linear regression. Here we only use the mean glacial elevation difference $\overline{\Delta h_i}$ in a time series if its standard deviation s_i is less than a threshold Std_0 and the number of ICESat footprints k is at least six footprints. The threshold Std_0 is defined to be equal to the roughness threshold R_0 for each setting with respect to terrain slope and roughness. To remove unreliable elevation differences, we build an iterative algorithm. That is, if s_i is bigger than Std_0 and $\left|\Delta h_{ij} - \overline{\Delta h_i}\right|$ is maximal for j in 1÷k, the jth elevation difference Δh_{ij} is removed. Then $\overline{\Delta h_i}$ and s_i are re-computed. This process is repeated until s_i drops below Std_0 or k is less than six. In Figure 3.4, the values $\overline{\Delta h_i}$ and s_i representing mean glacial elevation differences and their standard deviations are shown between 2003 and 2009 for two glacial areas A and B in case that S_0, R_0, and Std_0 are 15 deg, 10 m, and 10 m, respectively.

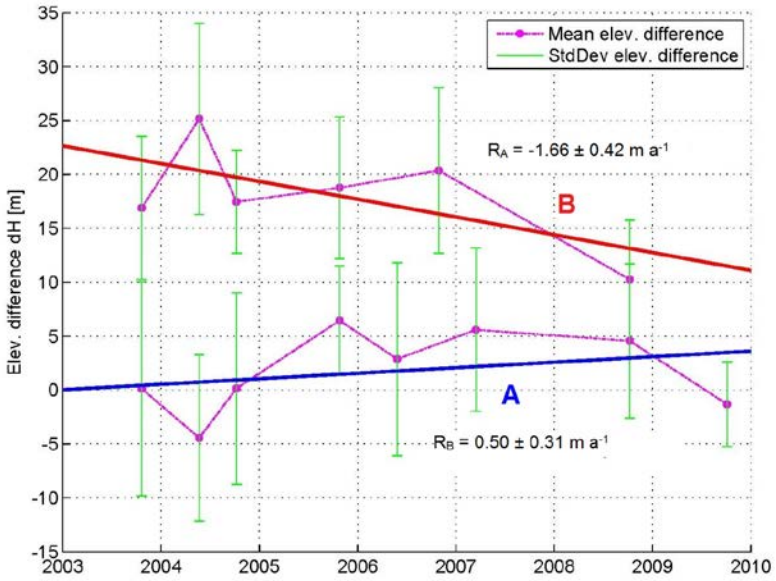

Figure 3.4: Distributions of the mean elevation differences and temporal glacial thickness change trends between 2003 and 2009 at the glacial areas A and B.

3.2.6. Estimating a temporal glacial thickness change trend

For each glacial area on the Tibetan Plateau, a temporal linear trend is estimated if there are at least six average differences or epochs available, corresponding to at least six ICESat campaign tracks during the observed period 2003 – 2009. For example, Figure 3.4 shows the distribution of the average differences of the glacial areas A and B between 2003 and 2009. An annual glacial thickness change trend is estimated by linear adjustment using formula (3.9) (Teunissen, 2003).

$$\hat{x} = (A^T A)^{-1} A^T y \qquad (3.9)$$

Where,

$y = \left[\overline{\Delta h_1} \quad \overline{\Delta h_2} \quad \ldots \quad \overline{\Delta h_n}\right]^T$: the vector of the average elevation differences per epoch.

$x = \left[x_0 \quad v\right]$: the vector of parameters of the linear trend, offset x_0 and rate v.

$A = \begin{bmatrix} 1 & 1 & \dots & 1 \\ t_1 & t_2 & \dots & t_n \end{bmatrix}^T$: the design matrix, in which t_i denotes the i[th] epoch.

Note that n is required to be at least six epochs.

The rate *v* of a linear glacial thickness change is obtained by solving formula (3.9) and the root mean square error (RMSE), as standard deviation of residuals, is also computed, using formula (3.10) with the least-square residual vector $\hat{e} = y - A\hat{x}$. This value consists of a combination of possible data errors and mainly the non-validity of the linear regression model.

$$RMSE = \sqrt{\frac{\sum_{i=1}^{i=n} \hat{e}_i^2}{n}} \tag{3.10}$$

In addition, the propagated standard deviation σ_{vv} of the estimated velocity *v* is given in formula (3.11). This value is considered as the confidence interval for the estimated glacial thickness change.

$$Q_{\hat{x}\hat{x}} = \begin{bmatrix} \sigma^2_{x_0 x_0} & \sigma^2_{x_0 v} \\ \sigma^2_{v x_0} & \sigma^2_{vv} \end{bmatrix} = (A^T Q_{yy}^{-1} A)^{-1}, \text{ with } Q_{yy} = \begin{bmatrix} s_1^2 & 0 & 0 & 0 \\ 0 & s_2^2 & 0 & 0 \\ & & \dots & \\ 0 & 0 & 0 & s_n^2 \end{bmatrix} \tag{3.11}$$

Here, Q_{yy} denotes the variance matrix, in which s_i is the standard deviation of the i[th] average difference.

Continuing to the example of Figure 3.4, glacial area A has an elevation decrease of -1.66 ± 0.42 m a^{-1} and a RMSE of 3.46 m while glacial area B has an elevation increase of 0.50 ± 0.31 m a^{-1} and a RMSE of 3.37 m between 2003 and 2009.

3.3. Results

Following the method above, temporal glacial thickness change trends on the whole Tibetan Plateau between 2003 and 2009 are estimated for 15 different settings with respect to terrain slope and roughness. The results are shown in Table 3.2. It indicates that, as expected, the number of observed glacial areas and the RMSEs of differences estimated by the linear regression increase if the thresholds on slope S_0 and roughness R_0 are relaxed. In practice, the mean rates

of glacial thickness change trends on the whole Tibetan Plateau for the five settings from S11 to S15 (all with R_0 = 15 m) are quite similar. In addition, the number of trends having a RMSE of over 5 m significantly increases when ICESat footprints at slopes of over 20 deg are incorporated as well. A RMSE of over 5 m could correspond to a large fluctuation in glacial thickness or a bad fit of the linear trend model.

Table 3.2: Settings of terrain surface parameters for filtering ICESat footprints. Here S_0 and R_0 are terrain slope and roughness thresholds respectively. For each setting, N is the number of glacial areas observable with a given setting. The numbers $\bar{v}$ and $\overline{\sigma_{vv}}$ are the resulting overall rate and its propagated standard deviation of glacial thickness change while $\overline{RMSE}$ is the average of the root mean square errors (RMSEs) of the linear regression model. N_5 is the number of observed glacial areas having a RMSE of below 5 m.

Setting	S_0 (deg)	R_0 (m)	N	$\bar{v}$ (m a^{-1})	$\overline{\sigma_{vv}}$ (m a^{-1})	$\overline{RMSE}$ (m)	N_5
S1	10	5	33	-0.21	0.20	2.93	29
S2	15	5	38	-0.23	0.21	3.26	34
S3	20	5	43	-0.12	0.21	3.06	40
S4	25	5	49	0.01	0.23	3.34	43
S5	30	5	54	0.04	0.23	4.00	41
S6	10	10	37	-0.25	0.25	2.85	33
S7	15	10	55	-0.06	0.33	2.99	49
S8	20	10	76	-0.02	0.39	3.70	62
S9	25	10	98	0.13	0.44	4.29	68
S10	30	10	117	-0.04	0.45	5.40	67
S11	10	15	39	-0.21	0.26	2.89	36
S12	15	15	63	-0.15	0.40	3.05	58
S13	20	15	90	-0.17	0.47	4.02	67
S14	25	15	122	-0.21	0.56	4.89	64
S15	30	15	146	-0.21	0.61	5.92	57

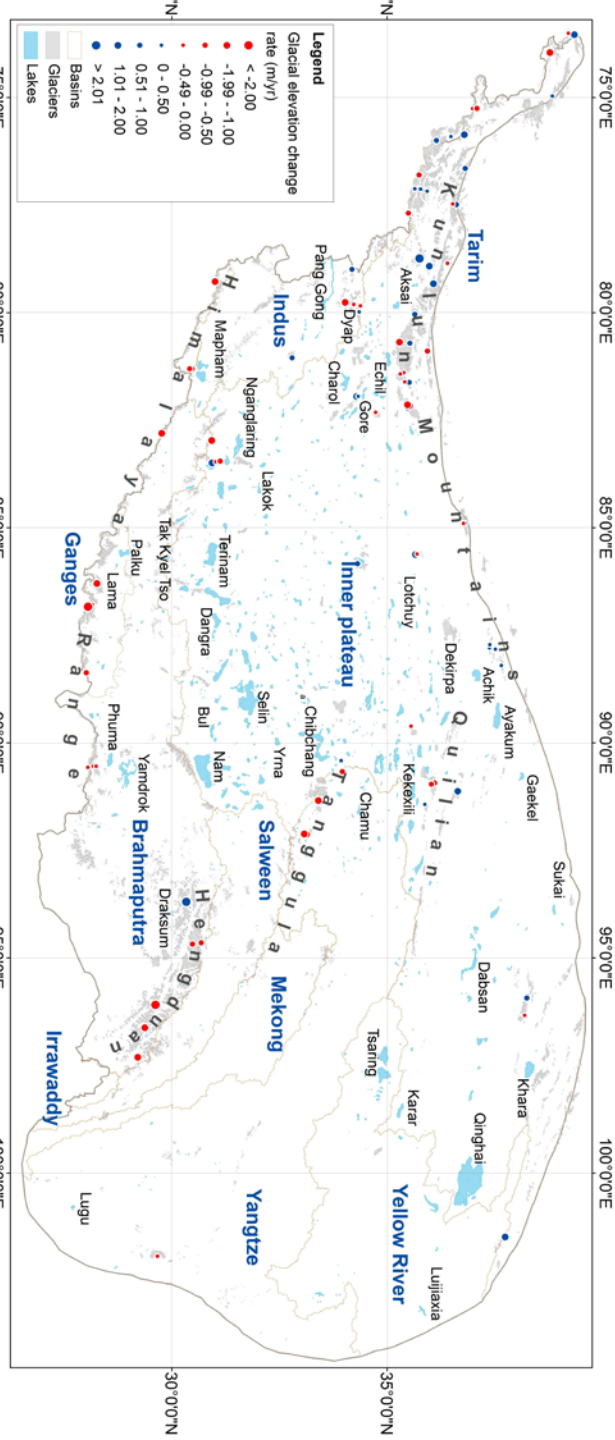

Figure 3.5: Glacial thickness change rates on the Tibetan Plateau between 2003 and 2009

In this section, we present the results of setting S13, where S_0 and R_0 equal 20 deg and 15 m, respectively, because in this case a maximum number of 67 areas are observed with RMSE $\leq$ 5 m. We assume that ICESat footprints selected for estimation of glacial thickness change given these settings are relatively appropriate given the steep and rough terrain of the Tibetan Plateau and given the quality of the SRTM DEM.

3.3.1. Overall glacial thickness changes: Tibetan Plateau and its basins

In case the thresholds S_0 = 20 deg for terrain slope and R_0 = 15 m for roughness are applied, the result indicates that 90 glacial areas on the whole Tibetan Plateau are sampled by enough ICESat footprints to estimate thickness change. Also, 67 RMSEs are below 5 m. For each glacial area, a temporal trend in glacial thickness is estimated, as shown in the Appendix A. In Figure 3.5, a glacial thickness change rate is symbolized by a red or blue disk at a representative location in each observed glacial area. Most of the observed glacial areas in the Himalaya, the Hengduan Mountains and the Tanggula Mountains experienced a serious decrease in glacial thickness. However, in most of the observed glacial areas in the western Kunlun Mountains in the north-west of the Tibetan Plateau, glaciers oriented toward the North were thickening while those oriented toward the South were thinning. In general, glacial thickness on the whole Tibetan Plateau decreased between 2003 and 2009 at a mean rate of -0.17 ± 0.47 m a^{-1}. This number is obtained by averaging all estimated rates v and their propagated standard deviations σ_{vv}, but note that the size, distribution and representativeness of the observed glacial areas are not taken into account.

The largest decrease in glacial thickness occurred at the Hengduan Mountains, compare Figure 3.6. The estimated rate equals -2.03 ± 0.73 m a^{-1} with a RMSE of 0.32 m. The observed glacial area consists of two GLIMS glaciers facing East. Although there are little discrepancies between the GLIMS glacier outlines and the Landsat 8 OLI/TIRS, captured on 13-Aug-2013, Figure 3.6 indicates that glaciers have retreated significantly between ~2002, the time corresponding to the GLIMS database, and 2013. On the other hand, the observed glacial area facing North at Western Mt. Kunlun had an elevation increase rate of 1.25 ± 0.51 m a^{-1} and a RMSE of 3.09 m, as illustrated in Figure 3.7. Overlaying the GLIMS glacier mask on the Landsat 8 OLI/TIRS image from 18-Sep-2013 indicates that in this area the glacier extent is relatively stable.

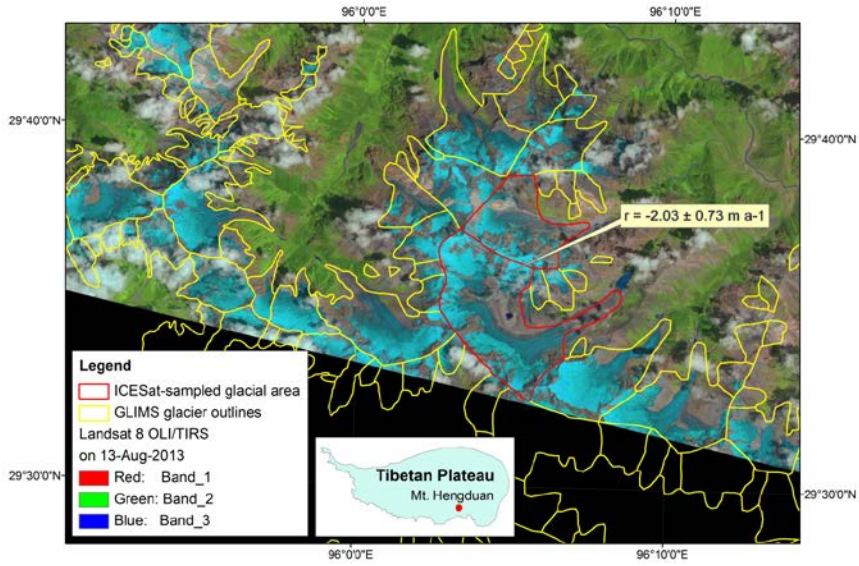

Figure 3.6: The maximal rate of glacial thickness decrease between 2003 and 2009 at the Mt. Hengduan. The figure is created by overlaying the GLIMS glacier outlines on the Landsat 8 OLI/TIRS image from 13-Aug-2013.

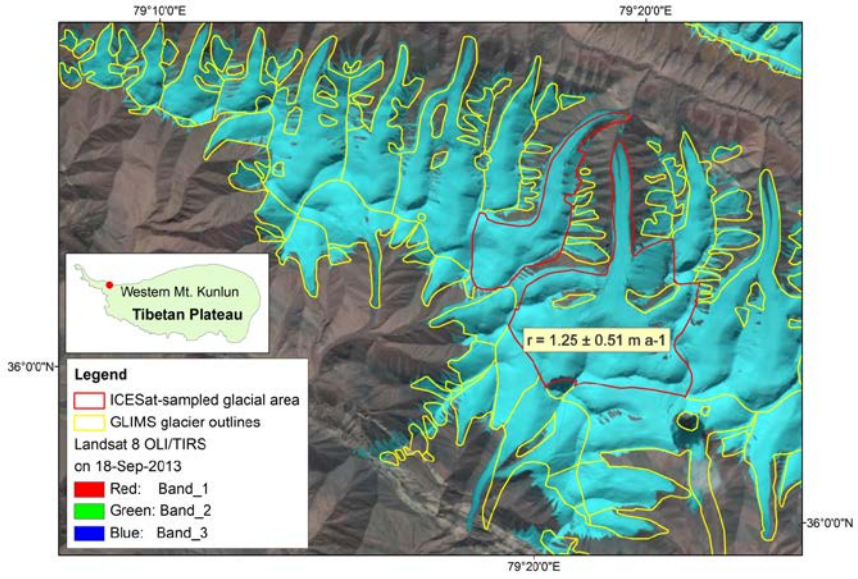

Figure 3.7: Strong glacial thickening between 2003 and 2009 at Western Mt. Kunlun. The figure is created by overlaying the GLIMS glacier outlines on the Landsat 8 OLI/TIRS image from 18-Sep-2013.

For each basin belonging to the Tibetan Plateau, a mean thinning or thickening rate $\overline{v_B} \pm \overline{\sigma_B}$ is estimated, as average of rates v and propagated standard deviations σ_{vv}. The result is shown in Table 3.3. In practice, the rate per basin is of course affected by the area of each glacier within the basin. However, in this study we only estimate trends representative of nearby-glacier groups. A next but far from trivial step would be to design an interpolation scheme taking the sparsely available trends as input and use them to estimate an overall trend while incorporating e.g. the relative location, orientation, and representativeness of each available trend. Here the area of glaciers is not taken into account when estimating overall glacial rates. The results show that mass loss due to glacier-thinning seems to take place in most of the basins, excluding Tarim Basin. Subsequently, lost or gained water volumes from glaciers by basin are approximately estimated, by multiplying the mean glacial thickness change rate with the total glacier area of each basin, as indicated in Table 3.3.

Table 3.3: Mean glacial thickness change rate per basin, where N is the number of observed glacial areas and the total glacier area is obtained from the GLIMS glacier mask. Lost or gained water volumes from glaciers are approximately estimated, by multiplying the mean glacial thickness change rate with the total glacier area of each basin.

Basin	Total glacier area (km^2)	N	$\overline{v_B} \pm \overline{\sigma_B}$ ($m\ a^{-1}$)	Water volume ($Gt\ a^{-1}$)
Brahmaputra	16 019	9	-0.56 ± 0.49	-8.97 ± 7.79
Ganges	4 033	8	-0.99 ± 0.47	-4.01 ± 1.90
Indus	2 409	5	-0.03 ± 0.34	-0.08 ± 0.82
Inner plateau	8 702	23	-0.16 ± 0.48	-1.39 ± 4.14
Salween	1 851	1	-0.78 ± 0.81	-1.44 ± 1.51
Tarim	20 996	39	0.21 ± 0.47	4.31 ± 9.79
Yangtze	2 012	5	-1.14 ± 0.46	-2.30 ± 0.93
Total	56 561	90	-0.17 ± 0.47	-9.62 ± 26.41

3.3.2. Impact of orientation on glacial thickness change

The results indicate that glacial thickness change indeed strongly depends on the relative position in a mountain range. Most glaciers at a North face increase in volume, although some decrease but in that case at a slower rate than its South-facing counterpart. In total, there are 15 pairs of observed glacial areas, i.e.

adjacent glacial areas located on opposite sides of the main mountain ridge, all listed in Table 3.4. Such situation is illustrated in Figure 3.8, showing the western Mt. Kunlun range. The temporal trends between 2003 and 2009 on the North-facing glacial area A equaled 0.69 ± 0.30 m a^{-1} while on its South-facing counterpart, glacial area B, the trend had opposite sign, equaling -1.02 ± 0.29 m a^{-1}. Similarly, the glacial thickness change rates at E, facing North, and F, facing Southeast were 0.58 ± 0.28 m a^{-1} and -0.29 ± 0.44 m a^{-1}, respectively. On the other hand, the glacial thickness on C, toward the Northeast, was estimated to decrease at a rate of 0.09 ± 0.30 m a^{-1} while glaciers in area D, toward the Southwest, thinned at a rate of -0.29 ± 0.20 m a^{-1}. A possible explanation is that South-facing glaciers receive much more solar radiation than North-facing glaciers because the Tibetan Plateau locates on the Northern Hemisphere and near the equator. Even glacial area C, oriented toward the Northeast, faces the sun more than areas A and E. Similarly, glacial area D, oriented toward the Southwest, is receiving less sunlight than glacial areas B and F.

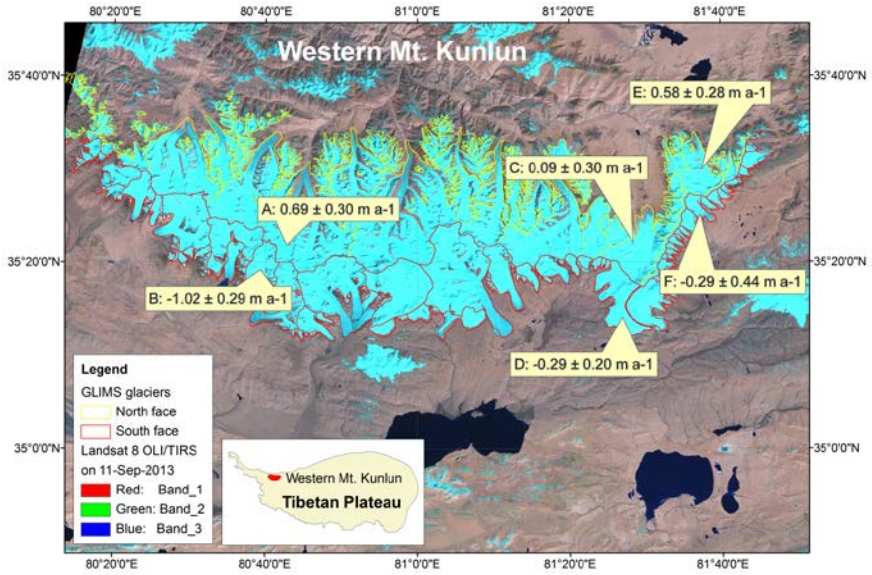

Figure 3.8: Different rates of glacial thickness changes between 2003 and 2009 at the North and South face of the Western Mt. Kunlun. The figure is created by overlaying the GLIMS glacier outlines on the Landsat 8 OLI/TIRS image from 11-Sep-2013, and adding the locations of observed glacial areas with thickness change rates.

Table 3.4: List of pairs of glacial areas that are adjacent, but located on opposite sides of the main mountain ridge. Here N_f is the total number of accepted footprints. Locations A, B, C, D, E and F are indicated in Figure 3.8.

	Lat.	Lon.	Basin	Ori.	N_f	$v \pm \sigma_{vv}$ (m a^{-1})	RMSE (m)
1	28.184	90.544	Brahmaputra	S	261	-0.09 ± 0.39	8.68
2	28.248	90.543	Brahmaputra	N	71	-0.14 ± 0.40	7.13
3	28.261	86.296	Ganges	S	323	-1.83 ± 0.37	3.40
4	28.336	86.302	Ganges	N	93	0.12 ± 0.25	4.64
5	30.415	81.306	Ganges	S	80	-0.90 ± 0.69	5.83
6	30.469	81.310	Ganges	N	99	-0.74 ± 0.54	3.40
7	30.936	83.494	In. plateau	E	83	1.63 ± 0.58	9.21
8	31.022	83.468	In. plateau	W	160	-0.46 ± 0.36	3.56
9	33.913	90.659	In. plateau	S	92	-0.47 ± 0.20	3.92
10	33.954	90.670	Yangtze	N	342	-0.60 ± 0.30	3.23
11	34.024	79.763	Indus	SW	79	-1.38 ± 0.43	2.73
12	34.053	79.788	Indus	E	185	-0.07 ± 0.20	1.51
13	34.288	81.946	In. plateau	S	106	1.23 ± 0.50	2.76
14	34.327	81.946	In. plateau	N	168	0.21 ± 0.47	2.25
15	35.284	80.685	In. plateau (B)	S	998	-1.02 ± 0.29	4.19
16	35.523	80.713	Tarim (A)	N	1320	0.69 ± 0.30	3.38
17	35.301	81.430	In. plateau (D)	SW	635	-0.29 ± 0.20	1.73
18	35.388	81.397	Tarim (C)	NE	633	-0.09 ± 0.30	1.44
19	35.410	81.612	Tarim (F)	SE	338	-0.44 ± 0.44	3.46
20	35.508	81.624	Tarim (E)	N	380	0.58 ± 0.28	1.79
21	35.470	82.143	In. plateau	S	92	-1.50 ± 0.79	4.41
22	35.516	82.162	Tarim	N	77	-1.02 ± 0.43	5.07
23	35.655	85.620	In. plateau	S	118	1.82 ± 0.48	5.08
24	35.696	85.613	In. plateau	N	257	-0.04 ± 0.24	2.85
25	35.774	77.130	Tarim	W	93	0.06 ± 0.57	4.74
26	35.812	77.148	Tarim	N	47	0.19 ± 0.57	3.16
27	36.024	90.962	Tarim	S	428	-0.80 ± 0.38	7.03
28	36.099	90.936	In. plateau	N	494	-0.55 ± 0.22	2.88
29	36.773	84.903	In. plateau	S	59	-0.13 ± 0.56	2.89
30	36.813	84.895	Tarim	N	52	0.03 ± 0.78	2.44

3.4. Discussion

In this section, we discuss the sensitivity of our results to the removal of ICESat footprints based on terrain surface criteria and the GLIMS glacier mask. First we discuss the impact of the terrain surface criteria for assessing the signal quality of the ICESat measurements. Second, the GLIMS glacier mask is static which has some effect on the estimation of glacial thickness change trend. Finally a comparison of our result to previous research is presented.

3.4.1. Exploring terrain surface criteria

Several large glaciers sampled by ICESat footprints were considered to assess appropriate terrain surface criteria. The following relations were notably studied while determining the thresholds for terrain slope and roughness: glacial elevation difference Δh vs slope S, roughness R and elevation h_{SRTM}, respectively; and slope S vs elevation h_{SRTM}. The results are illustrated here for one case study considering a glacier area at the Mt. Guala Mandhata I. The results indicate that glacial elevation differences Δh increase with terrain slope, as illustrated in Figure 3.9a. The existence of such a slope bias is already described in Slobbe et al. (2008). Large valley glaciers often have a surface roughness of below 20 m, see Figure 3.9b. Also a larger surface roughness will result in a positive bias in the estimated glacial thickness.

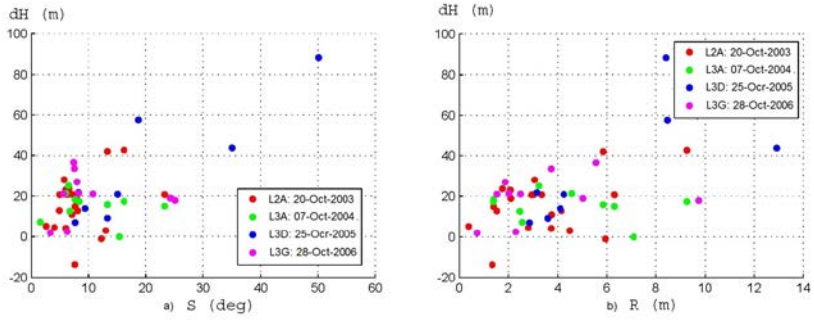

Figure 3.9: Relations between a) glacial elevation difference and slope and b) glacial elevation difference and roughness. Glacial elevation differences are between ICESat campaigns L2A, L3A, L3D and L3G and the SRTM DEM reference surface over a glacial area (No. 20 the Appendix A) at the Mt. Guala Mandhata I, belonging to the Ganges Basin.

The relaxation of the slope threshold results in an increase in the number of accepted ICESat track segments sampling a glacial area. This is illustrated in Figure 3.10 for an area in the Hengduan Mountains (No. 6 in the Appendix A). In Figure 3.10a, a number of 10 track segments was accepted, given a slope threshold of 15 deg. Based on these track segments, a trend was estimated with a RMSE of 4.18 m. In Figure 3.10b, the slope threshold was relaxed to 25 deg, resulting in a total number of 13 track segments. But the quality of the final trend (RMSE = 6.39 m) decreases with the increase of the number of track segments. These two examples show some of the impacts of the slope and roughness thresholds.

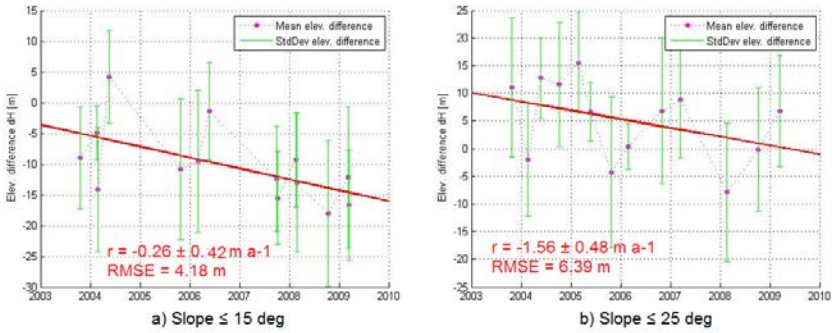

Figure 3.10: Estimations of glacial thickness change trends with varying slope S_0 thresholds: a) 15 deg, b) 25 deg at a glacial area (No. 6 in the Appendix A) in the Hengduan Mountains, belonging to the Brahmaputra Basin. In this example the roughness R_0 was kept fixed at 15 m.

One of the results of Kaab et al. (2012) and Neckel et al. (2014) were annual glacial thickness change trends for defined regions. These trends were directly estimated from all glacial elevation differences between ICESat elevations and the reference SRTM DEM on glacier areas, after removing footprints affected by clouds. This method ensures the availability of sufficient ICESat footprints to estimate trends in glacial thickness for relatively large regions. However, it ignores the impact of the high relief terrain characteristics of the Tibetan Plateau and surrounding mountain ranges. In addition, their definition of the sampled regions somehow smooths out significant signal, as it lumps together glaciers with different characteristics with respect to orography and orientation. Clearly

there is a difficult trade-off between using more elevations of less individual quality against using less elevations of better quality.

3.4.2. State of the GLIMS glacier mask

According to Shi et al. (2009), observations serving as input for the GLIMS glacier mask were obtained from 1978 to 2002, using aerial photographs, topographic maps and in situ measurements. Because of remoteness and harsh climatic conditions on the Tibetan Plateau, it is difficult to make field investigation, therefore the Chinese glacier inventory that was used to establish the GLIMS glacier mask took place at different periods. The inventory was organized per drainage basin. The inventory for example took place at Mt. Qilian in 1981, at the Inner Plateau in 1988, etc. Positional uncertainty is expressed as a distance of 20 m, i.e. a given location lies within a circle of 20 m radius from the true location. In addition, recent studies (Tian et al., 2014, Wei et al., 2014, Yao et al., 2012, Wang et al., 2011, Ye et al., 2009, Zhang Y. et al., 2008) report that the total glacier area on the Tibetan Plateau is shrinking. Therefore, in this study some ICESat footprints acquired between 2003 and 2009 will fall within the GLIMS glacier outlines but are not sampling a real glacier anymore. This will affect the mean elevation difference $\overline{\Delta h}_i$ at the ICESat acquisition time t_i. However, the number of such footprints within the same ICESat track segment is not large because the along track distance between consecutive footprints is approximately 170 m, and criteria on terrain surface are in place to remove uncertain footprints.

To further improve the glacial thickness change trends derived from ICESat/GLAS data, two techniques could be applied. First the glacier mask could be checked for each ICESat campaign using contemporary spectral (e.g. Landsat 8) or SAR data (e.g. Sentinel 1). Alternatively, classification techniques could be applied to the ICESat full waveform signals (GLA01 or GLA06 product) to verify if a ICESat signal is sampling snow, ice or rock (Molijn et al., 2011). Applying both types of analysis for the complete Tibetan Plateau is quite labor intensive however. Kaab et al. (2012) and Neckel et al. (2014) exploited the most cloud free Landsat scenes, acquired between 2003 and 2011 to delineate glacier outlines. However, it is difficult to match the acquisition time of ICESat campaigns with Landsat data for the full observed period for the whole Tibetan Plateau.

3.4.3. Glacial thickness changes for sub-regions

Our result considers annual glacial thickness change trends for relatively small areas. It is interesting to compare it with previous research (Neckel et al., 2014) and (Gardner et al., 2013). Neckel et al. (2014) grouped glaciers on the Tibetan Plateau into eight sub-regions, as illustrated in Figure 3.11. One of their results consists of annual glacial thickness change trends for each of these eight sub-regions. Accordingly we estimated glacial thickness change trends for the same eight sub-regions as well. For each sub-region, a mean glacial thickness change rate $\bar{v}_R \pm \bar{\sigma}_R$ is estimated as average of the glacial thickness change rates v and propagated standard deviations σ_{vv} of the observed glacial areas within the sub-region. The results are presented in Table 3.5 and compared to Neckel's Δh trends.

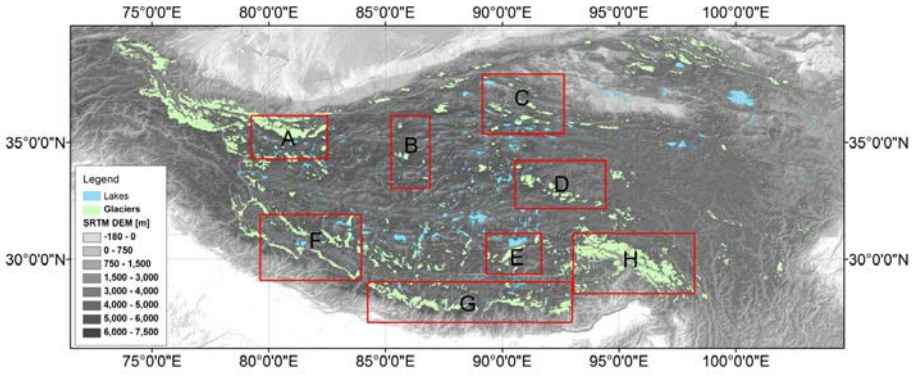

Figure 3.11: Sub-regions applied for monitoring glacial thickness change at the Tibetan Plateau, as described in (Neckel et al., 2014).

The comparison indicates that sub-regions (A, F, G, and H), relatively densely covered by glaciers, have a similar thickness change rate. Considering the other sub-regions, sub-region D has a somehow similar trend while rates in sub-regions B and C have a relative large disparity. The disparity between sub-regions B and C may be caused by i) the low number of observed glacial areas and ii) differences in orientation of the observed glacial areas: sub-region B consists of two South-facing glacial areas and one North-facing glacial area while sub-region C consists of three South-facing glacial areas and two North-facing glacial areas. At sub-region E, in case we set S_0 = 20 deg and R_0 = 15 m,

the number of ICESat footprints is not enough to estimate a temporal trend. We assume that the total number of observed glacial areas per sub-region and their orientation affect these mean glacial thickness change rates. That is, when the number of observed glacial areas is large enough and observed glacial areas located on opposite sides of the main mountain ridge are similarly equal, the mean glacial thickness change trend per sub-region is going to be more reliable.

Table 3.5: Mean glacial thickness change rates per sub-region, where N is the number of observed glacial areas within each sub-region.

Sub-region	Name	N	$\bar{v}_R \pm \bar{\sigma}_R$ (m a^{-1})	ΔH trend on-glaciers (m a^{-1}) (Neckel et al.)
A	Western Kunlun Mountains	20	0.16 ± 0.44	0.04 ± 0.29
B	Zangser Kangri and Songzhi Peak	3	0.86 ± 0.31	0.44 ± 0.26
C	Qilian Mountains and Eastern Kunlun Mountains	5	0.03 ± 0.47	-0.90 ± 0.28
D	Tanggula Mountains and Dongkemadi Ice Cap	6	-0.88 ± 0.41	-0.68 ±0.29
E	Western Nyainqentanglha range	0	NA	-0.23 ± 0.33
F	Gangdise Mountains	8	-0.60 ± 0.50	-0.44 ± 0.26
G	Central and Eastern Tibetan Himalaya	8	-0.70 ± 0.46	-0.78 ± 0.27
H	Eastern Nyainqentanglha and Hengduan Mountains	6	-0.67 ± 0.58	-0.81 ± 0.32

Generally our results are comparable to elevation change rates $\bar{v}_G \pm \bar{\sigma}_G$ estimated for high-mountain Asian glaciers by Gardner et al. (2013). Both results indicate that most of the glaciers in the Tibetan Plateau are thinning, except for western Mt. Kunlun, as shown in Table 3.6. The strongest glacier-thinning occurs in the Himalaya range and in the Hengduan mountains. The glacial thickness change rate in the western and inner plateau is near balanced or nearly equals zero. Inversely glaciers in the western Mt. Kunlun are thickening.

Table 3.6: Mean glacial thickness change rates per mountain region on the Tibetan Plateau, compared to the results of Gardner et al. (2013).

High mountain regions	$\bar{v}_R \pm \bar{\sigma}_R$ (m a^{-1})	$\bar{v}_G \pm \bar{\sigma}_G$ (m a^{-1}) (Gardner et al., 2013)
The Himalaya range	-0.81 ± 0.46	
- Western		-0.53 ± 0.13
- Central		-0.44 ± 0.20
- Eastern		-0.89 ± 0.13
The Hengduan mountains	-0.67 ± 0.58	-0.40 ± 0.41
The western and inner plateau	-0.05 ± 0.45	0.02 ± 0.14
The western Mt. Kunlun	0.20 ± 0.45	0.17 ± 0.15

3.4.4. Representativeness of an observed glacial area

A difficult question is to what extent the sparse estimates obtained by ICESat are representative for the full population of the Tibetan Plateau glaciers. This question cannot be answered here but we can assess which fraction of the glaciers is sampled. For this purpose we determine the ratio κ between glacial area sampled by ICESat footprints and the total glacial area, following formula (3.12).

$$\kappa = \frac{N * A_F}{A_G} \tag{3.12}$$

Here N is the total number of accepted ICESat footprints, A_F is the area covered by one ICESat footprint and A_G is the total sampled glacial area.

A glacial area can be considered to be well sampled if the total number of ICESat footprints sampling is large, while its total area is relatively small. An ICESat footprint with its diameter of 70 m occupies an area A_F of ~ 3,850 m^2. For example in Figure 3.3, glacial area A occupies 30.6 km^2 and is sampled by 108 accepted ICESat footprints. Therefore A's sample ratio equals 0.0136. Similarly, glacial area B occupies 8.5 km^2 and is sampled by 94 accepted ICESat footprints, so B's sample ratio is 0.0426. In this way the sample ratio for each of 90 observed glacial areas is determined, see the Appendix. Note that this ratio does not take the spatial and temporal distribution of the ICESat footprints into account, and therefore only provides a very rough indication on how well a glacial area is sampled.

Similarly, the sample ratio for all observed glacial areas on the whole Tibetan Plateau could be computed as well. As a result, the total area of 90 observed glacial areas for the whole Tibetan Plateau is 5831.5 km^2 and these glacial areas were sampled by a total number of 16,002 accepted ICESat footprints. Thus in this case the sample ratio equals 0.0106. Note that one location might be sampled by several ICESat footprints from different epochs. That is not taken into account in this first assessment.

3.5. Conclusions

By exploiting ICESat laser altimetry data, thickness change rates of 90 glacial areas on the whole Tibetan Plateau were estimated between 2003 and 2009. By considering terrain surface criteria slope and roughness, temporal glacial thickness change trends for the whole Tibetan Plateau were evaluated for 15 different settings. The results show that the settings of terrain slope and roughness equaling 20 deg and 15 m to remove uncertain ICESat footprints, respectively, are appropriate for the steep and rough Tibetan Plateau. In addition, the orientation of glaciers has been taken into account. The study indicated that most of the observed glacial areas in the Himalaya, the Hengduan Mountains and the Tanggula Mountains experienced a serious thinning while in most of the observed areas in the western Kunlun Mountains North-facing glaciers were thickening while South-facing glaciers were thinning. In addition, glacial thickness changes indeed strongly depend on the relative position in a mountain range. Most North-facing glaciers increase in thickness, although some decrease but in that case at a slower rate than its South-facing counterpart.

Chapter 4

ESTIMATING ANNUAL LAKE LEVEL TRENDS ON THE TIBETAN PLATEAU [3]

Changes in the water level of Tibetan lakes can be an important indicator for the water balance of the Tibetan Plateau, but were until now extremely difficult to monitor: performing continuous in situ measurements at a large number of lakes is not feasible because of their remoteness, while radar altimetry is only capable of monitoring large lakes. Between 2003 and 2009 the GLAS instrument on board of ICESat obtained world-wide elevation profiles during 18 one-month campaigns. Using the ICESat/GLAS data it is possible to obtain lake levels at decimeter accuracy. Available ICESat GLA14 data over the Tibetan lakes is selected by means of the MODIS land-water mask. As a result, lake level variations between 2003 and 2009 of 154 lakes with an area of over 1 km^2 could be observed. For these lakes, an analysis of annual water level trends is made, and then their yearly gained or lost water volumes are estimated. The resulting area averaged increase between 2003 and 2009 in water level over all observed Tibetan lakes is 0.20 meters per year (m a^{-1}). Most of the individual lakes considered in this study have little or no levels apparently documented, and so the ICESat data provide the first baseline measurements of water level in these lakes.

[3] Published as: Phan, V.H., Lindenbergh, R.C., Menenti, M.: ICESat derived elevation changes of Tibetan lakes between 2003 and 2009. *International Journal of Applied Earth Observation and Geoinformation*, 17, 12-22, 2012.

4.1. Introduction

Lake level changes can be considered one important indicator for the water balance of the Tibetan Plateau. This region contains thousands of lakes and is the origin of Asia's big rivers whose water levels are directly influenced by upstream glacial melt, snow melt, rain fall, but also by the upstream soil moisture conditions. Therefore observing the water level changes of the Tibetan Plateau is necessary. Unfortunately many of the lakes on the Tibetan Plateau are difficult to reach because of the remoteness and often harsh climatic conditions. It is only possible to a very limited extent to perform and maintain in situ measurements using, e.g. water-level gauges (Li et al., 2007). A solution to this problem is using remote sensing techniques provided that a technique is available with, first, sufficient coverage and spatial resolution, such that at least a considerable part of the lakes on the plateau is sampled and, second, sufficient temporal coverage, such that also lake level variations can be monitored at regular intervals (Alsdorf et al., 2007).

Since the 1990s, satellite radar altimetry has effectively been used for monitoring water surface elevation. In 1992, the TOPEX/Poseidon satellite was launched for measuring ocean surface topography. In addition, data from the radar altimeter on board the TOPEX/Poseidon satellite, with a footprint size of 5 km, has been used for monitoring inland water level variations. Practical studies were performed on big lakes all over the world such as Superior, Michigan and Huron lakes in America and Tanganyika, Malawi and Turkana lakes in Africa (Ponchaut and Cazennave, 1998), Chad Lake in the central Africa (Birkett, 2000), twelve big lakes in Africa (Mercier et al., 2002), a large Amazon Lake (Alsdorf et al., 2001), the Great Lakes in USA (Jekeli and Dumrongchai, 2003), six big lakes in China (Hwang et al., 2005), Dongting Lake in China (Zhang et al., 2006), etc. The TOPEX/Poseidon altimeter mission ran until 2005 and was followed by two other radar altimeter missions, Jason-1, launched in 2001 and Jason-2, in 2008. These two missions are still operational and have footprints of 5 km as well. In addition, the European Remote Sensing satellite, ERS-2, was launched in 1995. Similar to TOPEX/Poseidon, ERS-2 radar altimeter data with a footprint of 20 km has been used to monitor inland water level changes, particularly over big lakes all over the world. In 2002, ENVISAT was launched by the European Space Agency (ESA), carrying the RA2 altimeter with a footprint of 3.4 km. There are many researches using radar altimeter data from ERS-2 and Envisat on monitoring lake and river level variations. Some recent publications consider the Amazon basin (Da Silva et al., 2010), Kivu Lake in central Africa (Munyaneza et al., 2009), Louisiana wetlands in USA (Kim et al., 2009) and Izabal Lake in Guatemala (Medina et al., 2008). The typical relative

accuracy of radar altimetry over lakes is at the centimeter to decimeter level, and the revisit time varies between 10 and 35 days. The main problem with radar altimetry over small lakes is the footprint size. Only lakes passed by the satellite with an open water diameter equal to at least the double of 3.4 km, the footprint size of the RA2 ENVISAT radar altimeter (Frappart et al., 2006), are generally sampled without mixed pixels, that is without having signal parts resulting from reflections other than from the lake surface. It means that lakes should be much larger than one footprint to give altimeter measurements free of artifacts due to the surrounding terrain. Notably in the Tibetan Plateau there are many relatively small lakes that are difficult to sample by radar altimetry.

In January 2003, ICESat was launched for measuring ice sheet mass balance, cloud and aerosol heights, as well as land topography and vegetation structure. Up to now the GLAS instrument on board of ICESat is the only satellite laser altimetry instrument that provided elevation data all over the world. During its lifetime the GLAS instrument did not collect elevations continuously but only in designated campaigns. The available ICESat/GLAS-derived land surface elevations have a vertical accuracy at the decimeter level over flat terrain and a horizontal accuracy in the order of meters (Schutz, 2002; Schutz et al., 2005; Duong et al., 2008). Urban et al. (2008) recognized that the ICESat/GLAS data have potential for monitoring the level of inland water bodies. Each GLAS waveform was the result of the interaction of the emitted Gaussian pulse with the terrain surface within a ~70 m diameter footprint, much smaller than the radar footprints. This small footprint makes the ICESat/GLAS data advantageous in monitoring water level changes over relatively small lakes. ICESat only obtained measurements along track with an along track distance between consecutive footprints of 170 m. Although the ICESat 1,064 nm wavelength for assessing elevations at the ground or water level is strongly affected by clouds, the ICESat/GLAS data have potential to observe water level fluctuations of most lakes sampled by campaign tracks.

By using the ICESat GLA14 land surface elevation data, it will be possible to monitor lake level changes in the order of decimeters of a large number of these lakes at a temporal interval corresponding to the ICESat campaign dates. In practice this means that seasonal variations can be monitored. Because of the near-polar orbit of 94◦ inclination, distances across track between ICESat tracks over the Tibetan Plateau are in the order of 73 km. As a consequence, the GLA14 data is available all over the Tibetan Plateau but only at specific locations. A first exploration shows that there are 268 Tibetan lakes with an area of over 1 km^2 sampled by ICESat campaigns. As ICESat was repeating its tracks in an approximate sense, this implies that water level changes of a large fraction of these 268 lakes can be observed. In comparison, in literature only reports on

radar or in situ measurements on lake level changes for at most ten individual Tibetan lakes were found.

4.2. Methodology

In this section, we present how to exploit the ICESat GLA14 data with a combination of the MODIS land-water mask to estimate annual lake level trends on the whole Tibetan Plateau. The GLA14 data supports global land surface altimetry between 2003 and 2009, see Section 2.2.3. The 250 m MODIS land-water mask, also called MOD44W, represents land-water bodies, see Section 2.3.2. Figure 4.1 illustrates the tracks from the ICESat L2D campaign superimposed on the Tibetan lake layer, obtained from the MODIS land-water mask. Using an in polygon test, those ICESat/GLAS footprints are selected that fall completely within a lake boundary. Subsequently, the total number of Tibetan lakes with an area of over 1 km^2 sampled by at least one campaign equals 268. Therefore, a temporal lake level trend for each lake that is sufficiently sampled by GLA14 data is obtained in four steps: i) extract all footprints within a lake, ii) remove anomalies, iii) obtain mean lake levels, and iv) compute a rate of lake level change trend. Then, lake level variations were converted to water volume changes.

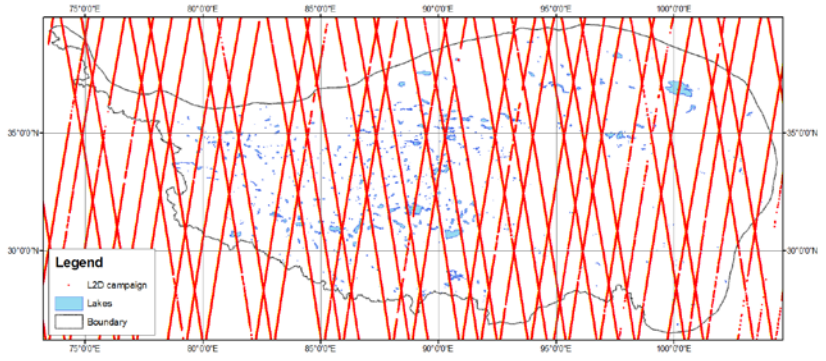

Figure 4.1: Tracks from the ICESat L2D campaign superimposed over Tibetan lakes obtained from the MODIS water-mask.

4.2.1. Estimating a temporal lake level trend

Firstly, for each ICESat-sampled lake all footprints from a campaign that fall completely within the lake are selected. Figure 4.2a illustrates the ICESat L3F

campaign over Paiku Lake. The elevations of the L3F campaign footprints within the lake are shown along track in Figure 4.2b. In exploring GLA14 elevations of the Tibetan lake surfaces, it was found that most campaigns are affected by anomalies. Based on the distribution of the elevations in Figure 4.2b, it is concluded that some anomalous elevations are present, also see Section 2.2.3.

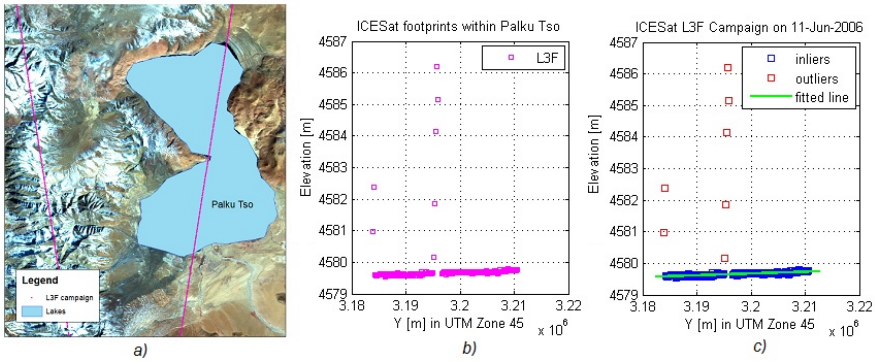

Figure 4.2: a) Tracks of the ICESat L3F campaign superimposed on Paiku Lake, derived from the MODIS land-water mask, b) Distribution of the ICESat L3F campaign elevations within Palku Lake in meters, and c) Line fitted with RANSAC.

Secondly, the RANdom SAmple Consensus algorithm, RANSAC (Fischler et al., 1981), is applied to remove outliers from the data table as follows. Each track segment of ICESat campaigns over one lake at the acquisition time is explored. Each point consists of an elevation and a y-coordinate corresponding to the distance along track over the lake. According to the RANSAC algorithm a line is fitted over and over again through a random pair of points belonging to the dataset. For the remaining points the distance to this line is determined. A point is considered an inlier if its distance to the fitted line stays within a predefined threshold. The line that maximizes the number of inliers is the final choice. In this research the threshold value to define a point as an outlier is chosen to be 15 cm, corresponding to the GLAS vertical accuracy (Schutz, 2002), where a 1^0 surface slope is assumed. Figure 4.2c shows the final line, and the corresponding outliers and inliers of the L3F campaign track over the Paiku Lake.

Thirdly, the mean elevation of the inliers is determined as the representative elevation of the lake surface at the corresponding UTC arrival time of the ICESat laser pulse. The representative elevation is only determined if there are at least four inliers and if moreover there are more inliers than outliers. The standard deviation of the inliers is calculated as well. As a result of the previous step, for each lake a set of mean elevations ordered by acquisition time between 2003 and 2009 is generated, as presented in Figure 4.3.

Finally, a linear temporal trend is estimated through the lake level elevations, resulting in a slope and a Root Mean Square Error, RMSE, see formulas (3.9), (3.10) and (3.11). The slope of the temporal trend indicates the rate of the lake level change per year while the RMSE, as a standard deviation of residuals, consists of a combination of possible data errors and mainly the inaccuracy of the linear regression model. The temporal trend is only calculated when a lake is sampled in at least 4 campaigns and if the observed period is at least 3 years. Figure 4.3 shows that the Paiku Lake level is trending down with a rate of -0.118 m a^{-1} and a RMSE of 0.258 m.

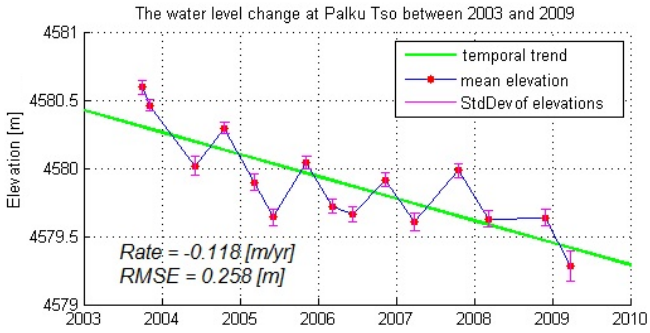

Figure 4.3: Distribution of the mean water level elevations and the annual trend of lake level changes between 2003 and 2009 at Paiku Lake.

4.2.2. Converting lake level trends to volume changes

A first estimation of lost or gained lake water volume can be determined by formula (4.1) below. A water volume change depends on both lake surface area and the rate of lake level change. The bigger a lake is, the more volume is lost or gained. It would be ideal if both lake area change and water level change would be considered in a joint analysis. Still the estimation of volume change based on a fixed lake area gives a reasonable first approximation.

$$V = v_L * A_L \quad (4.1)$$

Here V is the gained or lost water volume of a lake in $m^3\ a^{-1}$, v_L is the rate of a lake level variation in $m\ a^{-1}$, and A_L is the surface area of a lake in m^2.

4.3. Results

In this section, we first present the results of estimating annual lake level trends on the whole Tibetan Plateau. Then we compare lake level variations derived from ICESat laser altimetry data to radar altimetry data from the LEGOS centre. Case studies for this validation are Qinghai Lake and Selin Lake.

4.3.1. Annual lake level trends all over the Tibetan Plateau

As a result of the 4th step, for each of the 154 Tibetan lakes covered sufficiently by ICESat GLA14 land surface elevation data, a temporal water level trend has been calculated, given in Appendix B. Figure 4.4a shows a histogram of the estimated linear lake level trends between 2003 and 2009. Most of the observed lake levels are increasing. The result indicates that 67.53% of 154 lake levels are trending up between 0 and 0.4 m a^{-1} while 18.18% are trending down between 0 and 0.2 m a^{-1}. If the obtained lake level trends are averaged over the complete plateau relative to their area, a mean increase in lake level of 0.20 m a^{-1} is obtained, compare Table 4.1.

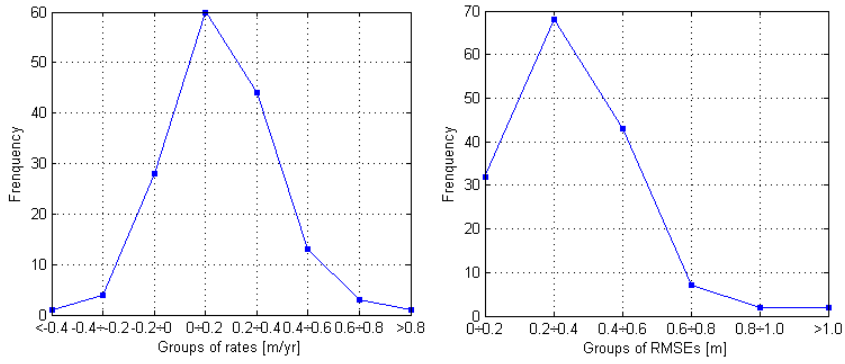

Figure 4.4: The histograms of a) rates of water level changes and b) RMSEs of estimated water levels of Tibetan lakes between 2003 and 2009.

Table 4.1: Water volume changes per basin. For each basin the number of sampled lakes, the total area of these lakes, the average volume change per year, the average elevation change, $\bar{v}$, per year and the RMSE, $\overline{RMSE}$, of this elevation change is indicated. From left to right results using a threshold of 15, 25 and 35 cm, respectively, are given.

Basin	Threshold = 15 cm					Threshold = 25 cm					Threshold = 35 cm				
	No. of lakes	Total area (km^2)	Volume change ($M\ m^3\ a^{-1}$)	$\bar{v}$ ($m\ a^{-1}$)	$\overline{RMSE}$ (m)	No. of lakes	Total area (km^2)	Volume change ($M\ m^3\ a^{-1}$)	$\bar{v}$ ($m\ a^{-1}$)	$\overline{RMSE}$ (m)	No. of lakes	Total area (km^2)	Volume change ($M\ m^3\ a^{-1}$)	$\bar{v}$ ($m\ a^{-1}$)	$\overline{RMSE}$ (m)
Inner plateau	106	15 124.56	4125.30	0.27	0.33	107	15 126.90	4 203.87	0.28	0.34	108	15 131.84	4 229.00	0.28	0.34
Yellow River	12	50 18.33	583.49	0.12	0.22	12	5 018.33	636.93	0.13	0.25	12	5 018.33	676.25	0.13	0.28
Yangtze	18	1 251.85	392.04	0.31	0.31	19	1 269.13	454.13	0.36	0.47	19	1 269.13	452.89	0.36	0.47
Indus	11	1 182.41	39.29	0.03	0.43	11	1 182.41	40.89	0.03	0.43	11	1 182.41	43.76	0.04	0.43
Ganges	2	280.32	-32.90	-0.12	0.26	2	280.32	-20.22	-0.07	0.34	2	280.32	-19.99	-0.07	0.34
Brahmaputra	5	963.71	-251.28	-0.26	0.47	5	963.71	-246.08	-0.26	0.53	5	963.71	-248.6	-0.26	0.5
Total	**154**	**23 821.18**	**4855.94**	**0.20**	**0.32**	**156**	**23 840.80**	**5 069.52**	**0.21**	**0.34**	**157**	**23 845.74**	**5 133.31**	**0.22**	**0.35**

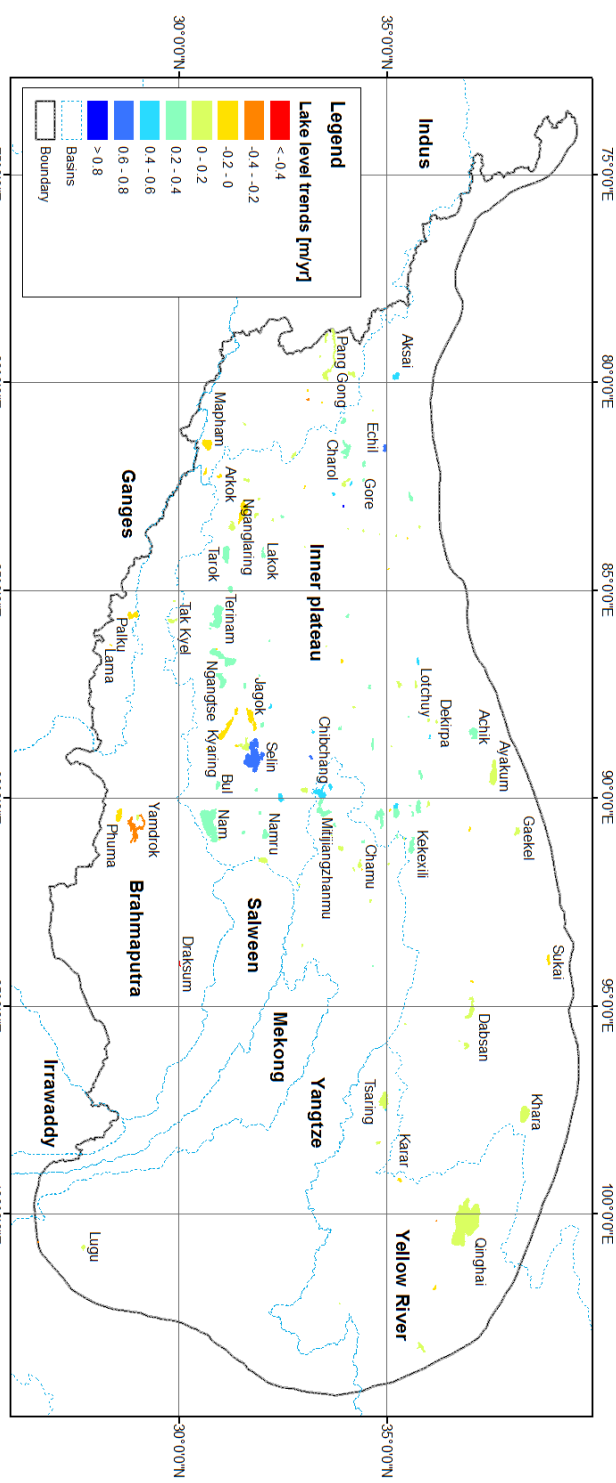

Figure 4.5: Rates of the lake level change trends on the Tibetan Plateau between 2003 and 2009.

More than 90% of the RMSEs of the lake level trends are between 0 and 0.60 m, as illustrated in Figure 4.4b. There are few lake level trends with a RMSE over 0.80 m. A large RMSE implies that a lake level variation is not linear or that input data is not fitting the model well because of notably a lack of campaigns and/or a lack of footprints in a lake.

The temporal lake level trends on the Tibetan Plateau between 2003 and 2009 are illustrated in Figure 4.5. Most of the lakes with a serious downwards trend are in the southern Tibetan Plateau and along the Himalaya mountain range and, vice versa, most of the lakes with a positive water level trend are in the inner Tibetan Plateau. Based on the different colors corresponding to different classes of lake level trends in the map, most of the lakes belonging to the Indus, Ganges, and Brahmaputra basins have a negative temporal water level trend while the lakes in the Yangtze and Yellow River basins mostly trend up. In the inner plateau, a few of the lakes have a negative water level trend between 0 and 0.20 m a^{-1} down, but most of the lakes have a positive water level trend.

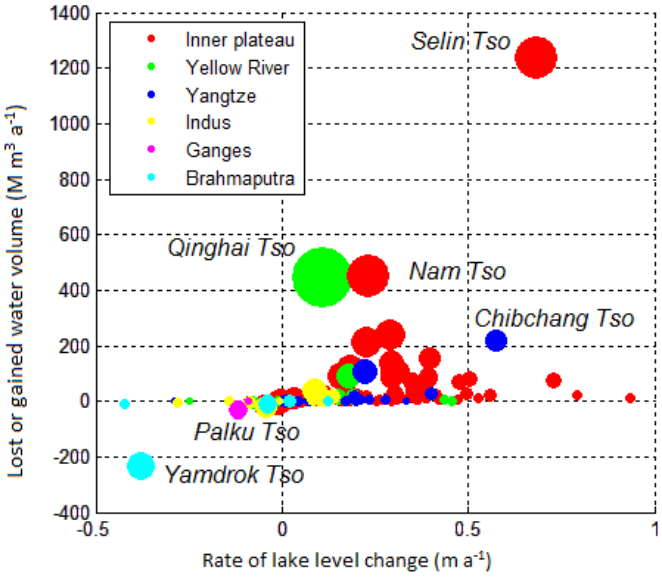

Figure 4.6: Distribution of gained or lost water volume colored by basin.

The distribution of water volume changes as derived from the lake level trends is shown in Figure 4.6. As expected, large lakes correspond to large volume changes, as even a relatively small lake level change over a wide area corresponds to a large volume change. The largest estimated volume change of about 1240 M m^3 a^{-1} comes from Selin Lake, a large lake that has a relatively large lake level change rate of +0.680 m a^{-1} as well. For each of the basins indicated in Figure 4.6, an average trend, $\overline{v}$, and RMSE, $\overline{RMSE}$, of the water level change per year is determined by taking the averages of the individual trends and RMSE values, weighted with respect to the area of each lake. The results, shown in Table 4.1, indicate that the sampled lakes in the Brahmaputra and Ganges basins, along the Himalaya mountain range, on average lost water, while conversely lakes in the inner plateau and in the Yellow River and Yangtze basins gained water.

4.3.2. Case studies: comparing GLAS results to LEGOS data

LEGOS/GOHS (Laboratoire d'Etudes en Geodesie et Oceanographie Spatiales, Equipe Geodesie, Oceanographie et Hydrologie Spatiales) is a French research laboratory that maintains a database of lake levels world wide, mainly based on radar altimetry data (Crétaux et al., 2011). The lake levels are based on merged TOPEX/Poseidon, Jason, ENVISAT and GFO data provided by ESA, NASA and CNES data centers. The database supports two lakes on the Tibetan Plateau, Qinghai Lake and Selin Lake. Below our results are compared to the LEGOS data for these two lakes. To estimate a comparable trend from the LEGOS database for the two lakes, we only considered LEGOS data between the start of ICESat's first campaign L1A and the end of the last campaign L2F, see Table 2.1. Standard deviations of individual lake levels were not taken into account in estimating the trend.

Qinghai Lake is the biggest lake on the Tibetan Plateau, with a total area of 4,166 km^2 and with an average water elevation of about 3,195 m. According to our results the lake level trend between 2003 and 2009 equals 0.11 m a^{-1} which would correspond to a gain in water volume of ~450 M m^3 a^{-1}. The LEGOS data result in a trend of 0.12 m a^{-1}, which is quite comparable.

Selin Lake, also called Garing Tso, is another big lake on the Plateau, occupying an area of ~1,820 km^2 area with an average water level height of 4,542 m. Based on the ICESat data an upward trend of 0.68 m a^{-1} is estimated, roughly corresponding to a yearly volume gain of about 1,240 M m^3 a^{-1}. The data in the LEGOS archive confirms this strong upward trend: the LEGOS trend for Selin Lake equals 0.71 m a^{-1}.

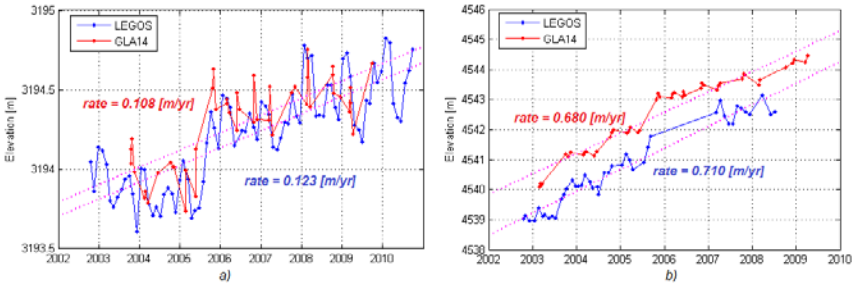

Figure 4.7: ICESat lake level variations compared to lake level data from the LEGOS archives for a) Qinghai Lake and b) Selin Lake.

GLAS and LEGOS lake elevations for Qinghai and Selin Lake are shown in Figure 4.7. Comparison of the graphs for both lakes indicates that not only the trend for both lakes is similar, but that also the variations in lake level are comparable. For example, for Qinghai Lake, the mean lake level after 2006 is several decimeters higher than before 2006 in both data sets, on the other hand the lake level of Selin Lake is for both data sets gradually increasing. Note that the absolute heights at Selin Lake from ICESat compared to LEGOS differ by about 1.30 m. For Qinghai Lake the difference in absolute height is only in the order of 0.10 m.

4.4. Discussion

In this chapter it is described how GLA14 elevations from the ICESat laser altimetry mission are used to obtain annual lake level variations for about 154 different lakes on the Tibetan Plateau between 2003 and 2009. In our opinion this research should be continued in two directions. First, current results should be improved and refined. Possibilities are indicated in Paragraphs 4.4.1 to 4.4.3 below. Second, the processes that potentially cause the lake level variations should, whenever possible, be linked to the results described here, as sketched in Paragraph 4.4.4.

It is also interesting to compare our results and methodology with the recent results and approach of Zhang et al. (2011) who also use ICESat/GLAS data to obtain elevation changes over Tibetan lakes. Our way of processing is quite different however. We used the 250 m MODIS land-water mask to select ICESat lake footprints while a 500 m MODIS snow cover product was used by Zhang et al. in which water is one of the classes. We use RANSAC to filter outlying

values, while Zhang et al. apply visual inspection and removal based on a standard deviation threshold. As a result we obtain lake level variations for 154 lakes, against 111 sampled lakes (Zhang et al., 2011). Also the way of presenting and validating the results is quite different. We group lakes based on the catchment they belong to, while Zhang et al. group lakes based on geographic locations and change tendencies in lake level. Zhang et al. could compare their results against some in situ gauge measurements for Nam Tso, why we could validate using radar altimetry data for Selin Lake and Qinghai Lake. The lake level rates resulting from both approaches seem quite comparable: over six of the bigger lakes (Gongmo, Nam, Phuma, Qinghai, Selin and Yamdrok) rates differ not more than 0.02 m a^{-1}, except for Phuma Lake where a larger difference of 0.10 m a^{-1} occurs.

4.4.1. Disadvantages of the supporting image data: the 250 m MODIS land-water mask and Landsat data

With a pixel size of 250 m, the spatial resolution of the MODIS land-water mask is relatively low, compared to the average size of a GLAS footprint of 70 m. The mask also contains errors affecting the shape of the lake polygon which will result in erroneously omitted and committed ICESat footprints. Note that the impact of these omission and commission errors is mitigated by the use of the RANSAC filtering. There are also cases where two different lake polygons are representing the same lake, e.g. Yamdrok Tso or Pang Gong Tso, and vice versa where different lakes are included in one lake polygon, e.g. Chibchang Tso and Mitijiangzhanmu Tso. The presence of some small seasonal lakes in the MODIS land water mask also affects the exploration of temporal lake level trends. In addition, the mask contains many small polygons representing parts of rivers. Here lake outlines were checked and river remains were removed with the support of Google Earth and one set of Landsat TM images. It would be most correct to always use image data acquired around the acquisition of the ICESat data to select GLA14 data from the lake surface. Still, the impact of such procedure would be small compared to the work involved, as most elevations considered now are already unambiguously representing a lake surface of a known lake.

4.4.2. Anomalies in the candidate ICESat lake elevations

Above it was described how RANSAC was used to remove GLA14 elevations that probably do not represent the lake surface. Anomalies corresponding to different surface characteristics are shown in Figure 2.4. Cases where ICESat `lake` data represents land instead of lake are mostly caused by errors in the MODIS land-water mask. These anomalies are identified by a distribution where some GLA14 elevations in a campaign differ by a few meters from the others in

the same campaign track as illustrated in Figure 2.4a. In addition, GLA14 elevations could be affected by clouds, waves, fog, or the return echoes are saturated, see Section 2.2.3. Further insights in these types of anomalies could be obtained by a more extensive study of the ICESat signals (Duong, 2010): signals affected by saturation or clouds can to a large extent be identified by GLAS quality flags. The relative return energy and the ICESat full waveform shape (GLA01 and GLA06 data) can be used as additional indicators if individual ICESat footprints were hitting land, but could also be used to distinguish between frozen and liquid water (Molijn et al., 2011). Nevertheless, in case of using only GLA14 data, anomalies in the data are all removed after processing by RANSAC.

4.4.3. Determining the threshold value in the RANSAC algorithm

RANSAC removes outliers using a threshold value of 15 cm. If this threshold value is set higher, a larger number of elevations are preserved. Increasing the threshold could be useful for lake surfaces experiencing a small roughness caused by e.g. waves. When the RANSAC threshold is increased to 35 cm, three additional lakes would be included. It turned out that the resulting lake level trends and RMSEs are similar for the three tested threshold values of 15 cm, 25 cm and 35 cm, as shown in the Appendix B. Accordingly, the average rates of lake level variations per basin are nearly the same for these three cases, as shown in Table 4.1.

4.4.4. Link to physical processes

An important next step is to link the results described in this study to the actual processes that cause the lake level variations. The graph of the lake levels of the glacier fed Palku Tso Lake, for example in Figure 4.3, indicates a strong seasonal influence. Each year during summer, the lake level increases by about 0.3 to 0.4 m, probably because of melt water from the northern slopes of the Himalaya. To obtain further insight in these processes, the lakes will have to be further characterized in future research. It should be considered that glacier-fed lakes are dominated by melt water from snow and ice while other lakes are mainly fed by rain, see Chapter 6. In addition it should be analyzed whether a lake is positioned in a closed basin or has river run-off, and it should be considered whether and how the different lakes are connected. The interpretation of Tibetan lake levels within the framework of a Limnological Information System, see e.g. (Tartari et al., 2008), could immediately contribute to the analysis of the hydrological system of the Tibetan Plateau as a whole. A combination of precipitation estimates with lake level variations could in some cases lead to constraints on upstream glacial mass balance variations (Bolch et al., 2010). Moreover lake level values could directly be used in hydrological

system modeling (Krause et al., 2010) and in the analysis of water loss through precipitation on one hand or agricultural water use on the other hand.

4.5. Conclusions

The results presented in this study indicate that lake level variations on the Tibetan Plateau between 2003 and 2009 can effectively be monitored using ICESat laser altimetry data. Validation of the results, against the by now traditional lake level variations based on radar altimetry, for two big lakes, Qinghai and Selin, indicates that the quality of the ICESat lake level variations is comparable to variations obtained by radar altimetry. This implies in practice that relative elevation changes in the order of a decimeter can be monitored at seasonal intervals. The big advantage of using GLA14 elevations is that now water level variations of 154 lakes spread all over the Tibetan Plateau could be obtained instead of water levels of not more than 10 large lakes using radar altimetry.

ICESat GLA14 data representing lake surface elevations were basically selected by using the MODIS water mask. For each of the lakes a temporal linear trend was determined. Consecutively these trends were applied to determine i) the average rate of lake level variation for each of the Tibetan basins and ii) the water volume on average gained or lost by each lake per year. The resulting lake level variations determined in this study can directly be applied to analyze the water balance of the Tibetan Plateau.

Chapter 5

ASSESSING SEASONAL LAKE LEVEL VARIATIONS USING ICESAT LASER ALTIMETRY [4]

Based on the ICESat campaign schedule, Tibetan lake levels derived from the GLA14 data are classified into three groups referenced to the Tibetan seasons: late dry, early wet, and early dry. For each lake sampled by sufficient ICESat campaigns, lake level trends could be estimated for lake levels in different seasons and different years, and seasonal lake level variations could be determined. The results indicate that most of the Southern Tibetan lakes loose water, while most other lakes on the Tibetan Plateau gain water, independent of the season from which lake levels were used for the trend determination. Observed seasonal lake level variations were much larger in the South than in the North and the West of the Tibetan Plateau. Based on the results, the Tibetan Plateau is divided into four sub-areas, according to the seasonal influence on the lake levels. The results confirm climatic trends as discussed in meteorological literature. Therefore, this analysis is expected to improve the understanding of the limnological processes on the Tibetan Plateau and their impacts on the surrounding regions.

[4] Published as: Phan, V.H., Lindenbergh, R.C., Menenti, M.: Seasonal trends in Tibetan lake level changes as observed by ICESat laser altimetry. *ISPRS Annals of the Photogrametry, Remote Sensing and Spatial Information Sciences*, 1 (7), 237-242, 2012.

5.1. Introduction

There are two different seasons in the Tibetan Plateau: the dry season, winter, and the wet or rainy season, summer. Most of the annual rainfall occurs between May and September, when the Tibetan Plateau is influenced by the Indian and East Asian monsoons (Zhisheng et al, 2001). According to Kang et al (2010), the Tibetan Plateau has been affected by significant warming for the last decades and will continue to warm in future. Tao et al. (2004) concluded that the South of the Tibetan Plateau becomes warmer and wetter with a clear increase in rainfall as well, while a part of the North turns warmer and drier. In addition, the central Tibetan Plateau is reported to become warmer and more humid as well, but here the increase in rainfall is insignificant. In general, climate and its changes are not the same for different sub-areas on the Tibetan Plateau.

Using the ICESat/GLAS data it is possible to accurately observe water level variations of Tibetan lakes, shown in Chapter 4 and (Zhang et al., 2011). In Chapter 4, annual water level trends between 2003 and 2009 for 154 Tibetan lakes over 1 km^2, obtained from the 250 m MODIS land-water mask, are estimated. It was concluded that most of the lakes with a clearly downward trend are in the South of the Tibetan Plateau and along the Himalaya range and, vice versa, most of the lakes with a positive water level trend are on the inner Tibetan Plateau. However, the ICESat data does not only enable the computation of annual lake level trends but also shows clearly seasonal differences. This study focuses on these seasonal differences. Subsequently, observing the seasonal changes in Tibetan lake levels could provide essential information to understand the characteristics of the Tibetan climate, its changes, and its impact on the surroundings.

5.2. Methodology

As a result of the estimation of annual lake level trends at the Tibetan Plateau between 2003 and 2009, for each ICESat-sampled lake there is a set of lake levels during the observed period, see Section 4.2.1. Each lake level is an average of elevations of ICESat/GLAS footprints completely within the lake at the arrival time of the laser pulse on the lake surface. According to the laser operational periods, compare Table 2.2, an observed lake was potentially sampled several times per year by the ICESat campaigns. Thus it is often possible to separately analyze trends in winter or summer lake levels and to assess the variations in lake level between consecutive seasons. This section

presents how to estimate such separate trends and how to obtain variations in lake level between seasons.

5.2.1. Estimating lake level trends per season

According to the ICESat/GLAS campaign schedule, for each lake the dataset of mean elevations is divided into 3 different seasonal groups: late dry, early wet and early dry, related to the Tibetan seasons as shown in Table 5.1. A trend between consecutive lake levels from one season is estimated by linear regression, see formulas (3.9), (3.10) and (3.11), if the lake level is sampled in that season in at least three different years. Subsequently, the slope of the trend indicates the rate of the lake level change in meters per year (m a^{-1}) while the RMSE (Root Mean Square Error) in meters, as a standard deviation of residuals, consists of a combination of possible data errors and mainly the inaccuracy of the linear regression model.

Table 5.1: Division of the ICESat/GLAS campaigns over the Tibetan seasons.

Tibetan season	Dry				Wet					Dry		
Month	1	2	3	4	5	6	7	8	9	10	11	12
Defined season			Late dry			Early wet				Early dry		
ICESat/GLAS campaigns			L1A, L2B, L3B, L3E, L3H, L3J, L2E			L2C, L3C, L3F				L2A, L3A, L3D, L2F, L3G, L3I, L3K, L2D,		

In this case, estimating a lake level trend based on only three campaigns can be applied because the mean elevations have relatively high confidence with a standard deviation of maximal 15 cm. In addition, potential useful information is lost if all trends based on three lake levels are removed. Therefore it is chosen to include these trends. Further confidence in individual elevation levels is also obtained by comparisons to in-situ data at Nam Lake (Zhang et al., 2011), or to

radar altimetry data at Qinghai Lake and Selin Lake, see Section 4.3.2. As an example, Figure 5.1 shows that the water level appears to decrease by 13.9 cm a year with a RMSE of 6.5 cm, if only water levels from the late dry season are used, while using only water levels from the early wet season and the early dry season results in trends of -17.8 ± 9.7 and -16.3 ± 8.7 cm/year, respectively. Therefore, for each Tibetan lake sampled by sufficient ICESat campaigns, at most three water level trends corresponding to the three defined seasons between 2003 and 2009 are obtained.

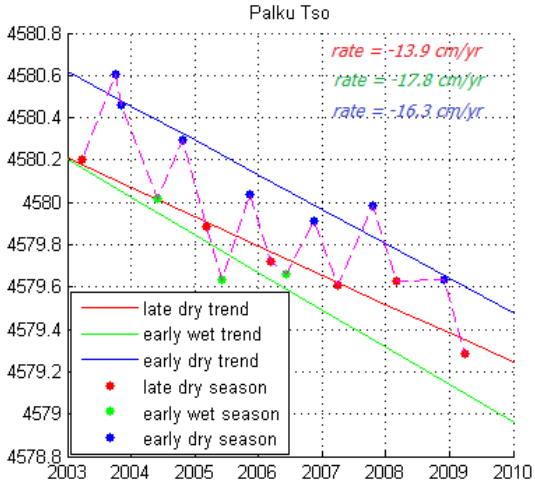

Figure 5.1: Seasonal water level trends between 2003 and 2009 at Palku Lake.

5.2.2. Obtaining seasonal lake level variations

According to Table 5.1, ICESat campaigns were classified in to 3 seasonal groups per year. For each ICESat-sampled lake, the set of mean elevations between 2003 and 2009 could be arranged into an array storing 21 seasonal values in sequence: late dry, early wet, early dry, and so on. It is noted that not all 21 defined seasons were covered by ICESat/GLAS data as ICESat only had 18 campaigns. Each of the at most 18 values represents a mean elevation of the lake surface corresponding to the defined season. If a lake was sampled by more than one ICESat track during any defined season, the average value of the mean elevations is assigned to an array element. For example, at the Palku Tso Lake as shown in Figure 5.1, the mean value of the two lake levels in the early dry season in 2003 is considered representative of the seasonal lake level. The array

of the seasonal Palku Tso lake level is shown in Table 5.2, where the 'not available – NA' value means that the lake surface was not sampled by ICESat during that defined season.

Table 5.2: The mean lake levels and lake level variations between defined seasons at Palku Lake between 2003 and 2009, where $\overline{H}_i$ is the mean lake level at the ith defined season.

i	ICESat Laser	Year	$\overline{H}_i$ (m)	Δ_1 (m)	Δ_2 (m)
1	L1A	2003	4579.90	0.63	
2			NA		
3	L2A		4580.53		NA
4	L2B	2004	NA	NA	
5	L2C		4580.02		
6	L3A		4580.30		-0.41
7	L3B	2005	4579.89	0.15	
8	L3C		4579.63		
9	L3D		4580.04		-0.32
10	L3E	2006	4579.72	0.19	
11	L3F		4579.66		
12	L3G		4579.91		-0.31
13	L3H	2007	4579.61	0.38	
14			NA		
15	L3I		4579.98		-0.36
16	L3J	2008	4579.63	0.01	
17			NA		
18	L3K, L2D		4579.64		-0.36
19	L2E	2009	4579.28	NA	
20			NA		
21	L2F		NA		
Mean elevation difference				**0.27**	**-0.35**

Based on the available lake levels, lake level differences between consecutive seasons could be obtained. Because there were only three campaigns L2C, L3C, and L3F in the early wet season, lake level differences with respect to these campaigns are not considered further. Thus two cases of lake level changes between consecutive seasons are considered. Firstly the difference between the late dry season and the consecutive early dry season in the same calendar year,

the Δ_1 column in Table 5.2, indicates the water level change during the monsoon. Secondly the difference between the early dry season and the late dry season of the next calendar year, the Δ_2 column in Table 5.2, indicates the water level change during the dry season. For example, the Palku Lake level increased by 15 cm during the monsoon in 2005 while it lost 32 cm during the dry season from 2005 to 2006, as shown in Table 5.2.

Accordingly a mean water level difference between the defined seasons is also obtained, by taking the average of all available differences. The $\overline{\Delta_1}$ value indicates the mean lake level change during the monsoon while $\overline{\Delta_2}$ indicates the mean lake level change during the dry season. For example at Palku Lake, as illustrated in Table 5.2, the water level increases on average by 27 cm during the monsoon while it has a mean decrement of 35 cm in the dry season between 2003 and 2009.

5.3. Results

In this section we first present the lake level trends estimated using lake levels from fixed seasons only for the whole Tibetan Plateau. Then, water level changes during winter and summer are shown. Finally, four case studies on the seasonal influence on lake levels are discussed, illustrating the spatial variety of the results.

5.3.1. Annual trends based on lake levels from fixed seasons

In total 121 trends based on late dry season lake levels, 42 trends based on early wet season lake levels and 123 trends based on early dry season lake levels could be obtained over the Tibetan Plateau. Most RMSEs of these trends were below 30 cm. Indeed, this held for 86% of the trends between late dry seasons, 88% of the trends based on early wet season lake levels and 57% of the trends resulting from early dry season lake levels.

In the early dry season, the temporal sampling was relatively wide spread, as lake levels could be obtained from the end of September to early December, as shown in Table 5.1. Actually most of the trends based on observations from one season only were quite similar to the trends estimated from all available lake levels simultaneously. This means that most of the observed lakes on the Southern Tibetan Plateau and along the Himalaya mountain ranges, belonging to the Brahmaputra, Ganges and Indus basins, had a serious downward water level trend while most of the observed lakes of the rest of the Tibetan Plateau had a

positive trend independent from which season was considered. In Figure 5.2 for the blue and red lakes trends estimated based on all available lake levels had the same sign as trends estimated based on lake levels from one fixed season, in contrast to the green and orange lakes, where these signs were opposite. The results indicate that such opposite signs occurred for 15.7 % of the number of lakes, if late dry season lake levels were used, see Figure 5.2.a, and for 10.6% of the number of lakes, if early dry season lake levels were used, see Figure 5.2.b.

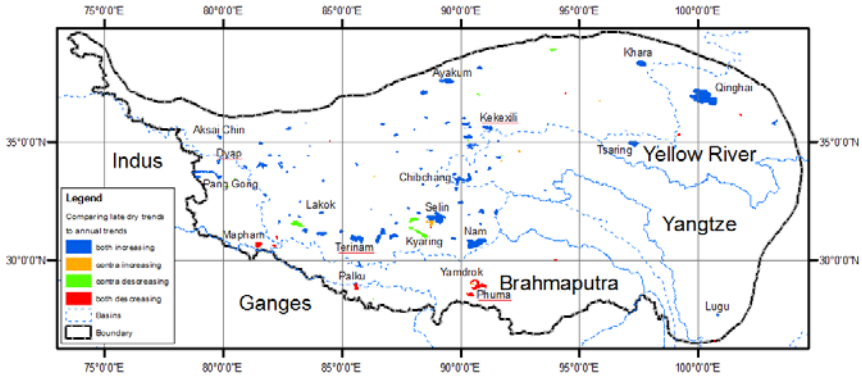

a)

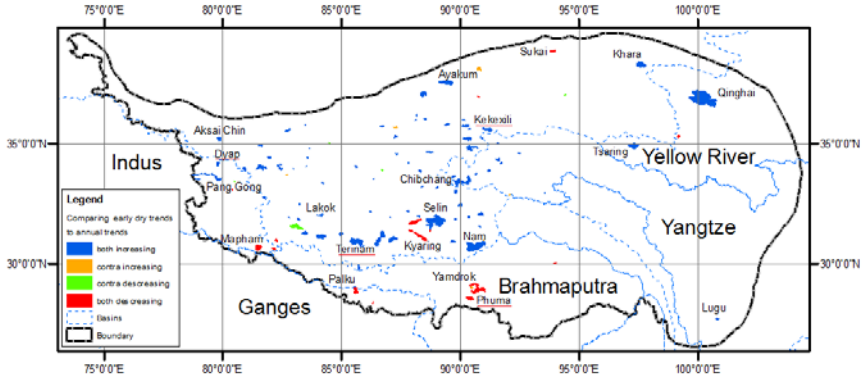

b)

Figure 5.2: Trends based on lake levels from a) the late dry season only, and b) the early dry season only, compared to trends estimated from all available lake levels for a given lake.

5.3.2. Lake level changes during the monsoon and the dry season

After calculating average lake level differences between two defined seasons, the observed lakes were classified into five groups and colored as represented in Figures 5.3. Lakes colored green varied maximal only +/- 15 cm in the indicated season. Red and orange colored lakes lose water during a season, while blue and cyan lakes significantly gained water level.

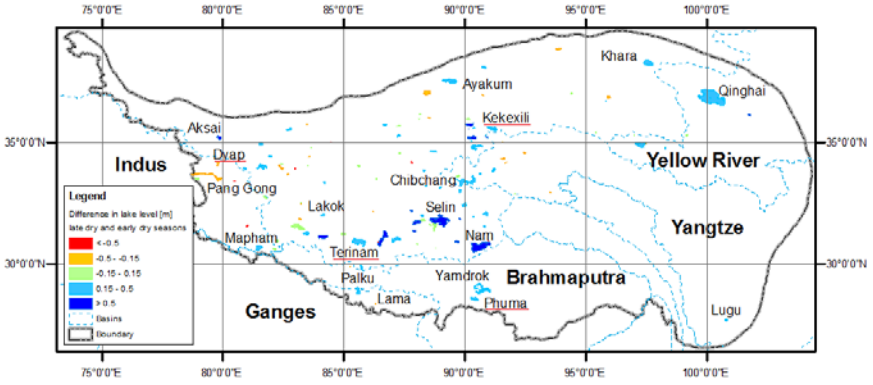

a)

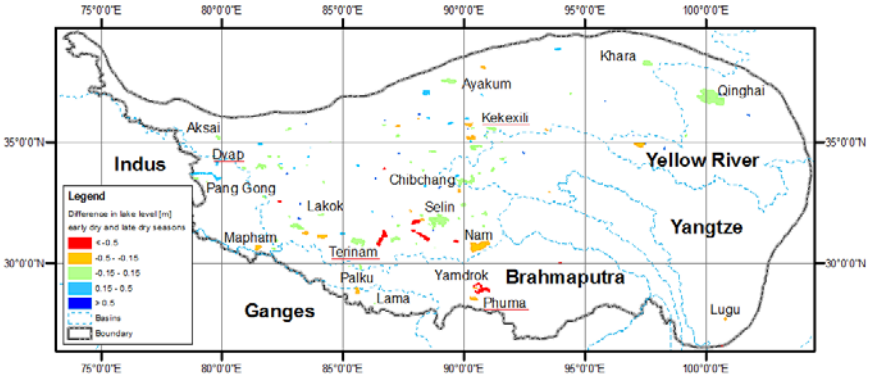

b)

Figure 5.3: Mean lake level changes during a) the monsoon and b) the dry season on the Tibetan Plateau between 2003 and 2009

As a result, the $\overline{\Delta_1}$ values of 125 lakes on the Tibetan Plateau can be obtained, indicating the mean lake level changes during the monsoon between 2003 and 2009, as shown in Figure 5.3a. The result shows that water level increased in the 51.2% of the 125 lakes while it decreased in the 24% of these lake levels. In addition 24.8% of these lakes were considered to have constant water levels. Most of the blue and cyan lakes having a water level increment were located on the East and South of the Tibetan Plateau, while some but less red and orange lakes also occurred in the North of the Tibetan Plateau, belonging to the Indus basin, and sparsely from the Northeast to the Northwest of the Tibetan Plateau, as illustrated in Figure 5.3a. Moreover the Southern Tibetan lakes had an obvious water level increment and these differences gradually decreased from the South to the North and the Northwest of the Tibetan Plateau.

In addition, the mean lake level change between 2003 and 2009 during the dry season, corresponding to the $\overline{\Delta_2}$ values, are illustrated in Figure 5.3b. The results show that 46.4% of the 138 observed lake level changes were in the range of +/- 15 cm. Furthermore, 22.4% decreased more while 31.2% had an increase over 15 cm. In addition, a strong water level decrement occurred in the Southern Tibetan Plateau while lake levels in the central Tibetan Plateau were nearly constant as shown in Figure 5.3b. A quick drainage took place at a few lakes in the inner plateau. The lakes having a significant water level increment were in the Western Tibetan Plateau and belonged to the Indus basin. In addition a few increasing lakes were located in the Northern Tibetan Plateau. Moreover, most of the red and orange lakes in Figure 5.3a, having a water level decrement during the monsoon, changed into green, cyan or blue lakes in Figure 5.3b, being nearly constant or having a water level increment during the dry season.

5.3.3. Case studies

Based on the trends estimated from lake levels of one season only and the lake level changes during a season, patterns in the distribution of the results could be determined. Accordingly the Tibetan Plateau is divided into four sub-areas where lakes have similar characteristics. The first group of lakes is in the South of the Tibetan Plateau and belongs to the Brahmaputra, Ganges and Indus basins, e.g. Lugu Lake, Phuma Lake, Yamdrok Lake, Palku Lake, Mapham Lake, etc. The second group is in the South and belongs to the inner plateau, e.g. Selin Lake, Terinam Lake, Lakok Lake, etc. The third group is in the center and upwards to the North, e.g. Qinghai Lake, Khara Lake, Kekexili Lake, Ayakum Lake, Charol Lake, Aksai Lake, etc. Finally the fourth group is in the West and belongs to the Indus basin, e.g. Pang Gong Lake, Dyap Lake, etc.

Firstly in the South of the Tibetan Plateau and belonging to the Brahmaputra, Ganges and Indus basins, most of the observed lakes have a downward trend, independent if all lake levels simultaneously, or lake levels from one defined season only are used for the trend estimation. However the lakes always have much higher lake levels in the early dry season than in the late dry season. The lake levels increase clearly during the start of monsoon and decrease quickly during the dry season as illustrated for the Phuma Lake in Figure 5.4a. These lakes seem strongly affected by the annual Indian and Asian monsoons.

Secondly in the South of the Tibetan Plateau and belonging to the inner plateau, most of the observed lakes gain water on average. Nevertheless, the lake level change during the monsoon is much larger than that during the Tibetan dry season. The lake levels are nearly constant or decrease only a little in the dry season. The Terinam Lake could be representative for this sub-area, compare Figure 5.4b. This sub-area seems also influenced by the annual monsoons.

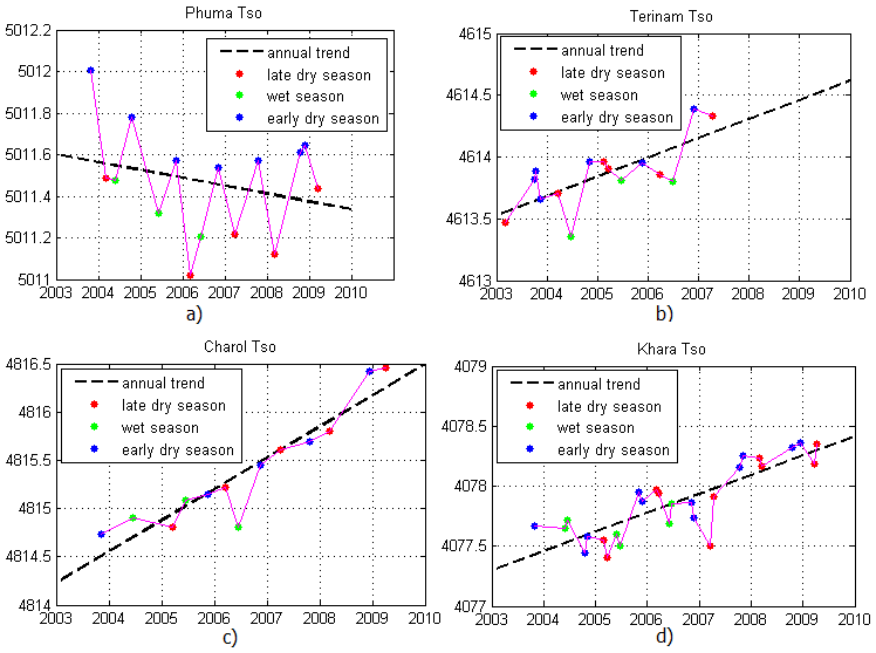

Figure 5.4: Typical seasonal lake level variations at selected lakes in sub-areas on the Tibetan Plateau between 2003 and 2009: a) Phuma Lake, b) Terinam Lake, c) Kekexili Lake and d) Dyap Lake.

Thirdly in the center and upwards to the North of the Tibetan Plateau, most of the lakes have the same tendency as the second group. Their seasonal lake level trends are mostly positive and their water levels increase after the annual rainfalls. However the lake level changes during the monsoon are smaller and gradually decrease from the Southeast to the Northwest. The Kekexili Lake as shown in Figure 5.4c is considered typical for this sub-area. Nevertheless this sub-area contains few lakes having the same characteristics as the lakes discussed in the following.

Finally in the West of the Tibetan Plateau and belonging to the Indus basin, most of the lakes have a small upward lake level trend, independent from how the trend was estimated. On average these lakes lose water during the monsoon, while they gain water during the dry season. Dyap Lake is chosen as an example for this sub-area, see Figure 5.4.d.

5.4. Discussion

As described in the results above, the seasonal trends and inter-seasonal water level variations of the observed lakes between 2003 and 2009 are confirming the climatic trend on the Tibetan Plateau mentioned in recent research. Lake levels in the South of the Tibetan Plateau clearly increase between roughly March and June, probably corresponding to a large amount of precipitation caused annually by the Indian and South Asian monsoons (Kang et al., 2010). Inversely most of the lake levels in the West and the North decrease little in the wet or summer season while they increase little or are nearly changeless in the dry or winter season. This confirms the claims on temperature and humidity (Tao et al., 2011) stating that the West and North of the Tibetan Plateau turn warmer and drier. Moreover, precipitation in the wet season gradually decreases from the Southeast to the Northwest of the Tibetan Plateau (Tao et al., 2004; Kang et al., 2010). In addition, Frauenfeld et al. (2005) concluded that temperature in the Western plateau is cooler than that in the Eastern plateau. These characteristics could affect the lake levels to make the average differences during the monsoon progressively decrease from the Southeast to the Northwest.

5.5. Conclusions

The ICESat/GLAS data cannot only be used to monitor water level variations and to estimate linear annual trends, but can also be used to assess seasonal lake level effects on the Tibetan Plateau. The lakes observed by sufficient ICESat/GLAS observations are analyzed in two ways, first according to trends

obtained from observations in fixed seasons only, and, second, based on the changes in lake level during or between fixed seasons. The results show that in most cases it does not matter much if all available lake levels are used to estimate an annual trend compared to using only lake levels from a fixed season. This means that most of the Southern Tibetan lakes had a serious downward trend while most of the lakes on the Inner Plateau gained water on average between 2003 and 2009. Seasonal influences were more obvious in the South than in the Northwest. The seasonal variations gradually decreased from the Southeast to the Northwest of the Tibetan Plateau. These characteristics corresponded with the trends in precipitation, temperature and humidity documented in recent researches in climatic change at the Tibetan Plateau.

Chapter 6

IDENTIFYING GEOMETRIC LINKS BETWEEN GLACIERS AND LAKES ON THE TIBETAN PLATEAU [(5)]

This chapter exploits different remote sensing products to determine which glaciers drain into which lakes on the Tibetan Plateau. The main products consist of the CAREERI glacier mask, the 250 m MODIS land-water mask, and the HydroSHEDS river network and drainage basins. The land-water mask gives the locations of Tibetan lakes. The glacier mask gives the outlines of glaciers in the Tibetan Plateau. The river network provides information on the direction of surface runoff, while the drainage basin data describes the catchment areas on the Tibetan Plateau. Using a drainage network analysis, all drainage links between glaciers and lakes are determined. This analysis also helps to differentiate between lakes with and without outlet. In addition, the notion of geometric dependency of a lake on glacial runoff is defined as the ratio between the total area of glaciers draining into a lake and the area of the lake catchment. As a result, geometric dependencies for all ~900 sufficiently large Tibetan lakes are determined. The results show that 25.3% of the total glacier area directly drains into one of 244 Tibetan lakes.

[(5)] Published as: Phan, V.H., Lindenbergh, R.C., Menenti, M.: Geometric dependency of Tibetan lakes on glacial runoff. *Hydrology and Earth System Sciences*, 17, 4061-4077, 2013.

6.1. Introduction

Recent research indicates that glaciers at individual regions on the Tibetan Plateau and surroundings are shrinking and thinning during the last decades. A lot of data sources and methods have been applied for these studies. Firstly these glacial shrinkages were analyzed from topographic maps, in situ measurements, and/or optical remotely sensed images during the observed periods (Tian et al., 2014; Wei et al., 2014; Yao et al., 2012; Sorg et al., 2012; Wang et al., 2011; Bolch et al., 2010; Ye et al., 2009; Zhang et al., 2008). Secondly Gardelle et al. (2012) compared two digital elevation models between 1999 and 2008 and revealed that ice thinning and ablation is occurring at high rates in the central Karakoram and the Himalaya mountain ranges. Thirdly Quincey et al. (2009) used satellite radar interferometry and feature tracking to quantify glacier velocities between 1992 and 2002 in the Everest region. Finally Kaab et al. (2012), Gardner et al. (2013), Neckel et al. (2014), and Phan et al. (2014), exploited ICESat laser altimetry between 2003 and 2009 to estimate rates of glacial thickness change trends.

In addition to monitoring glacier changes, researchers have also studied lake level fluctuations on the Tibetan Plateau. As described in recent reports (Zhang et al., 2011; Phan et al., 2012a; Wang et al., 2013), studies estimated roughly 150 water level trends of Tibetan lakes sampled by the ICESat/GLAS campaigns between 2003 and 2009. The results indicated that the water level of most lakes on the southern Tibetan Plateau and along the Himalaya mountain range shows a serious downwards trend. Lakes with a positive water level trend during the observed period are mostly located on the inner plateau. Phan et al. (2012b) showed that seasonal variations in lake levels differ considerably for different parts of the Tibetan Plateau. In addition, Zhang et al. (2013) correlated water mass increases derived from GRACE data to positive lake level trends.

Glacial runoff is only one component contributing to the water levels of the lakes on the Tibetan Plateau. Water levels are also affected by rainfall, snow melt, underground water, evaporation and lake water runoff. Hydrological models can be used to estimate the amount of glacial melt water flowing into a lake. At the moment, it is only possible to establish these hydrological models for selected basins, simply because the necessary measurements are not available for most of the Tibetan Plateau. As demonstrated in this study, however, it is possible to determine all geometric links between Tibetan lakes and glaciers. This enables us to determine to what level each lake is geometrically dependent on glacial runoff. This work will constrain the modeling of hydrological processes and will also provide an indirect way to monitor the state of the Tibetan glaciers, as

monitoring lake levels is easier than monitoring glacial changes in a high-relief environment. We believe that a regional approach, like this work, is needed to start understanding the spatial variations in glacial mass changes that are reported in current literature.

6.2. Methodology

In this study, main data sources consist of the CAREERI glacier mask, the 250 m MODIS land-water mask, and the HydroSHEDS hydrographic data, see Section 2.3.1, 2.3.3, and 2.3.4, respectively. The Tibetan lake layer obtained from the MODIS land-water mask represents ~900 lakes with an area of over 1 km^2. The CAREERI glacier mask gives the glacier outlines at the Tibetan Plateau. The HydroSHEDS hydrographic data provides information on the direction of surface flow, and shapes and areas of drainage basins on the Tibetan Plateau. Figure 6.1 illustrates input data sources used in this study.

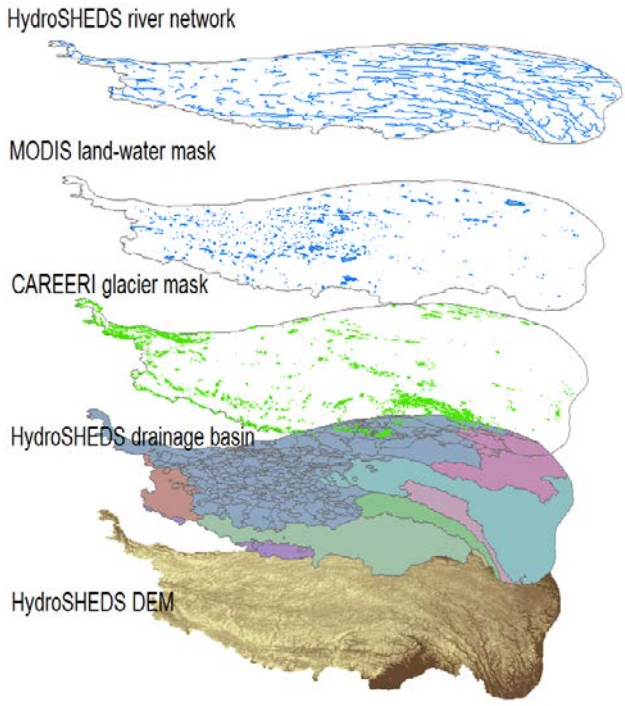

Figure 6.1: The input data consisting of the CAREERI glacier mask, the MODIS land-water mask, and the HydroSHEDS river network and drainage basins.

Exploiting these data to determine geometric dependency of Tibetan lakes on glacial runoff consists of the three following steps. Firstly we define geospatial notions such as lake-catchment, lake-outlet, connection between glacier and lake, etc. Then, it is shown how to determine connections between glaciers and lakes. Finally, indicators for the geometric dependency of a Tibetan lake on glaciers and methods for the computation of this dependency are described.

6.2.1. Determining the catchment of a Tibetan lake

A catchment, also known as drainage basin or watershed, is defined as the area where the surface water from rain and melting snow or ice converges to a single point or outlet, where the water joins another water body such as a lake, river or ocean (DeBarry, 2004). In a closed catchment, also called endorheic basin, surface flow is trapped in a lake or depression without outlet. Water typically leaves the basin by evaporation. As surface water contains some salt that is left behind after evaporation, such sink lakes, e.g. Nam Tso, are typically salty. Figure 6.2 illustrates the Kekexili catchment. All surface runoff from this closed catchment (described by the purple boundary) converges to Kekexili Lake, a sink lake. Each catchment is surrounded by a geographical barrier, typically a mountain ridge.

Catchments drain into other catchments in a hierarchical pattern, with smaller catchments, also called sub-catchments, combining to larger catchments. Depending on the application scale, a sub-catchment can be determined accordingly. If there is one river that leaves a certain lake with an outlet, that lake is an upstream lake. The sub-catchment for such a lake is part of a bigger catchment. An example for this is the Yinma Lake catchment. As shown in Figure 6.2, the Yinma Lake catchment is a sub-catchment of the Kekexili Lake catchment.

6.2.2. Identifying connections between glaciers and lakes

Based on the river network, an oriented route of river segments can be determined, running from one node to another. Determining the connection between a glacier and a lake means finding a route from an origin (where the glacier drains into the river network) to the outlet of a lake catchment. In most cases, the origin of the glacier-melt drainage coincides with the from-node of a river segment, as illustrated in Figure 6.2. A node of the river network is also used to represent the outlet of a lake catchment, as illustrated in Figure 6.4. A connection between lakes as an oriented route from the outlet of a lake catchment to the outlet of another lake catchment is described. To determine

these glacier-lake and lake-lake connections, we have designed and built a module in a GIS environment that executes the four procedures below.

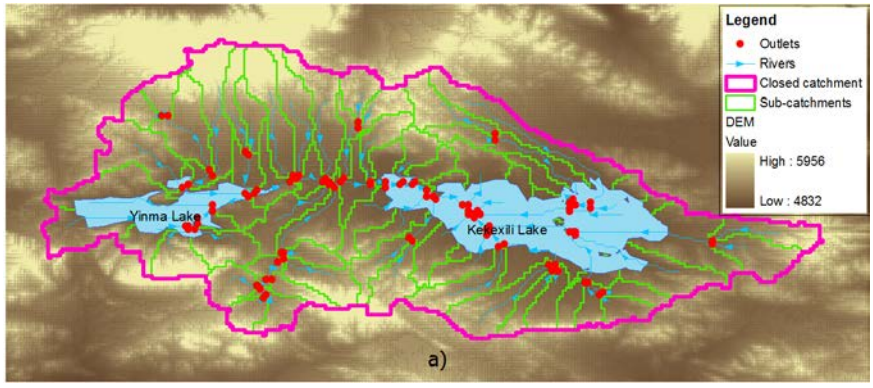

a)

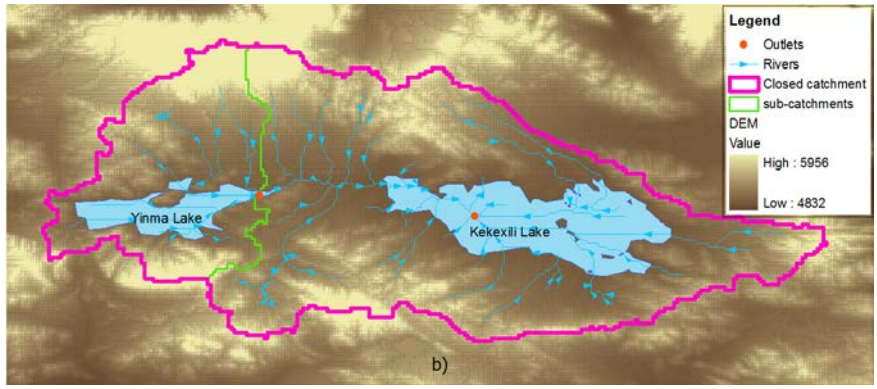

b)

Figure 6.2: a) Catchments represented by at least 100 upstream cells draining into a river segment based on the HydroSHEDS DEM data at 15 arc-second resolution, and b) The Yinma Lake sub-catchment as part of the Kekexili Lake closed catchment.

i) *Determining which catchment a glacier belongs to.* Because of the geographical characteristics of catchment boundaries, each glacier only belongs to one catchment. However, due to discrepancies between the

GLIMS glacier outlines and the HydroSHEDS catchments, glaciers can appear to belong to more than one catchment. If this is the case, the glacier is assumed to belong to that catchment that contains the largest part of the glacier. For example, in Figure 6.3, the two glaciers G_1 and G_2 are assumed to belong to catchment Cat_1.

ii) *Estimating the origin of the glacier-melt drainage.* In reality, meltwater from a glacier directly drains into the outlet of one catchment, through surface runoff or surface streams. In the glacier mask, each glacier is digitized as an undivided polygon. It still has to be estimated in which of possible several adjacent catchments the melt water will drain indirectly only through catchment boundaries and hierarchy of nodes. It is assumed that each glacier only drains to one river, following an oriented route of river segments. In this study, the source of this route is assumed to be the from-node of that river segment that is nearest to the glacial outline. For each catchment, the distances from each glacier to each from-node are computed, where a distance between a polygon and a point is determined as the minimum distance from the point to a vertex of the polygon. Figure 6.3 shows the distances from glaciers G_1 and G_2 to nodes A and B. The from-node with minimum distance to the glacier is considered the source of the drainage route. A distance threshold is used to restrict the number of potential from-nodes. In Figure 6.3, the distance from glacier G_1 to from-node A is smaller than the distance to from-node B, so from-node A is assumed to be the origin of the G_1 glacier-melt drainage. Similarly, d_{2B} is the smallest distance of d_{2A}, d_{2B}, and d_{2C}, so from-node B is considered the origin of the G_2 glacier-melt drainage although in reality glacier G_2 may also drain its glacier-melt water via from-node C.

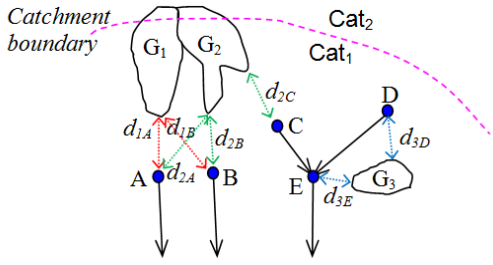

Figure 6.3: Glaciers G_1 and G_2 belonging to catchment Cat_1 and from-nodes A, B and E corresponding to origins of the glacier-melt drainage of glaciers G_1, G_2 and G_3.

iii) *Identifying the outlet of a lake catchment.* The outlet of each lake has to be inside the lake region. If all incident river segments stream toward the outlet inside a lake, that lake is the sink of a closed catchment. In Figure 6.4a and 6.4c, point A and point H are the outlets of closed catchments, and are therefore sinks. If even one river segment leaves a lake and drains into another lake or river, the lake is an upstream lake. In Figure 6.4b and 6.4c, point C and point F are outlets of their sub-catchments.

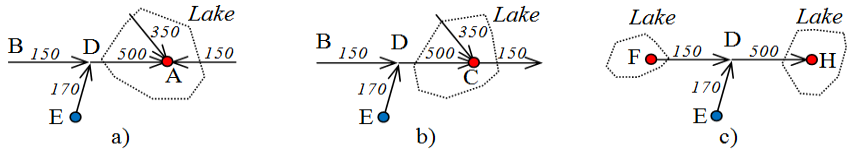

Figure 6.4: The sinks A and H of closed catchments and the outlets C and F of sub-catchments.

iv) *Indicating the oriented route of river segments from a source to a destination.* Each river segment is an oriented vector. At each node of the river network, the number of river segments leaving the node can be zero or one, as illustrated in Figure 6.4. Therefore, the oriented route from a source (glacier or lake outlet) to a destination can be determined using the following procedure. First, the river segment whose from-node coincides with the source begins the route. If the to-node of that river segment coincides with the from-node of another river segment, that river segment is added to the route. This process is repeated until the to-node of a river segment coincides with the destination. In Figure 6.4a, for example, a route is mapped from source E to destination A. The route includes two segments (ED and DA), making point D the point of conjunction. Similarly, the route from F to H in Figure 6.4c consists of two segments (FD and DH).

The module outputs GIS shapefiles in polyline vector format, with each polyline representing an oriented route from a source to a destination. The route's attributes consist of the identification codes of the source and the destination. The module determines either a connection between a glacier attributed with a glacial code and a lake with a lake code or a connection between two lakes, each with its own lake code. Figure 6.5 shows the result of the module for the Kekexili catchment.

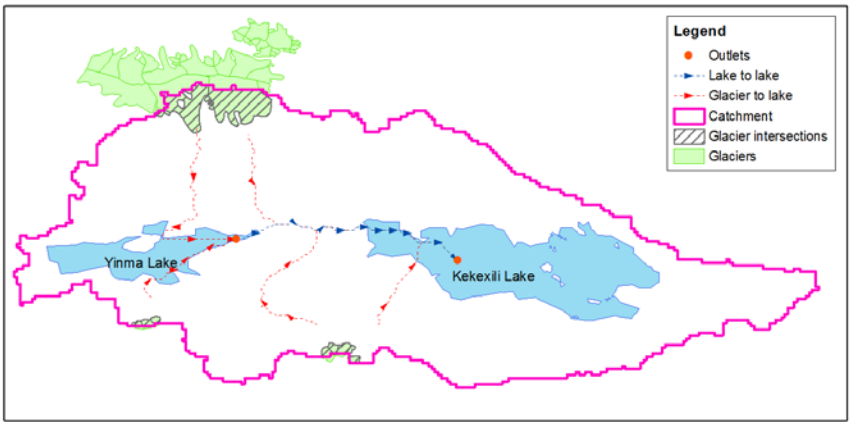

Figure 6.5: Determination of the glaciers belonging to the Kekexili catchment, the runoff connections from glaciers to Yinma Lake and Kekexili Lake, and the flow from Yinma Lake to Kekexili Lake.

6.2.3. Calculating the area of a lake catchment

Based on the HydroSHEDS drainage basin data, it is concluded that most of the catchments inside the inner Tibetan Plateau are closed catchments. Lake catchments that are not closed belong to the catchments of one of the major rivers: Brahmaputra, Ganges, Indus, Irrawaddy, Mekong, Salween, Yangtze, or the Yellow River. Because HydroSHEDS only includes the shapes and areas of closed catchments or big river catchments, this study needed to explicitly determine the areas (A_C) of lake sub-catchments, as follows.

a) Computing the area of a lake sub-catchment

The HydroSHEDS river data provides the number of upstream grid cells of each river segment, as illustrated in Figure 6.4. From this, the area of each lake catchment can be calculated as the product of grid cell size and total number of upstream grid cells of all river segments converging on the outlet of the lake. For each sub-catchment, the following steps have to be performed.

i) *Obtaining the total number of upstream grid cells*. For each lake, an outlet is determined by the module described above. Then, the total number of upstream grid cells is determined, by adding up the upstream grid cells derived from river segments draining into the outlet of the lake. In Figure 6.4, for example, the total number of upstream grid cells flowing into an outlet is 1,000 cells for sink A, 500 cells for sink H, 850

cells for outlet C, and zero for outlet F. In the case of outlet F, the area of the lake catchment was calculated manually using ArcHydro, as mentioned in the discussion section below. For instance, the total number of grid cells representing the Yinma Lake catchment, as illustrated in Figure 6.2b, is 3,775.

ii) *Calculating grid cell size in meters.* Grid cell size, including width and height, varies regularly depending on latitude. Grid cell size is approximated using the 'haversine' formula (Sinnott, 1984) which takes this dependency into account, see formula (3.4).

The Tibetan lake catchments may occupy large areas. The latitude of the outlet of the lake sub-catchment is used to compute a grid cell size for the entire lake sub-catchment. For example, the outlet of the Yinma Lake catchment is located at 35.62 degree latitude. Therefore, its average grid cell size is estimated at 0.3766 x 0.6433 km. This results in an estimated area of approximately 658.7 km^2. Alternatively, the Yinma Lake catchment area can be derived from its geospatial boundary, as illustrated in Figure 6.2b. This method also shows the area of the Yinma Lake catchment to be 658.7 km^2.

b) Obtaining the area of a closed lake catchment

The area of closed Tibetan lake catchments can be determined by three methods.

i) Taken directly from the attributes of the HydroSHEDS drainage basin data. For example, HydroSHEDS reports the Kekexili Lake catchment area as 2,636.5 km^2.

ii) Calculated from grid cell size and total number of upstream grid cells. Similar to the computation of the area of the Yinma Lake sub-catchment above, the average grid cell size for the Kekexili Lake catchment is 0.3767 x 0.6433 km. The total number of grid cells in the Kekexili Lake catchment is 15,100 cells. Therefore, the area of the Kekexili Lake catchment is approximately 2,635.3 km^2.

iii) Calculated from its geospatial boundary. The Kekexili Lake catchment occupies an area of 2,636.8 km^2.

The small differences in area derived from method two are caused by using one representative grid cell size. Bigger catchment areas actually include a range of grid sizes, depending on latitude. For highest accuracy, the rest of the paper derives the area of each closed catchment of a Tibetan lake directly from the drainage basin data.

6.2.4. Computing the total area of glaciers draining into a lake

Based on the distribution of the Tibetan glaciers, it is obvious that part of the glacial melt water flows to some of the Tibetan lakes. A lake can collect glacial melt water directly from glaciers or indirectly via upstream lakes. For each lake, we therefore distinguish the total area of directly contributing glaciers (A_{GD}) and the total area of upstream glaciers (A_{GU}) draining into it.

$$A_{GD} = \sum_{i=1}^{n} A_i \tag{6.1}$$

$$A_{GU} = \sum_{i=1}^{n} A_i + \sum_{j=1}^{m} A_{GDj} \tag{6.2}$$

Where A_i is the area of the i^{th} glacier directly draining into the lake, and A_{GDj} is the total area of glaciers contributing directly to the j^{th} upstream lake flowing to the lake.

For example, 41.9 km^2 of glaciers drain directly into Yinma Lake and 50.1 km^2 into Kekexili Lake, as shown in Figure 6.5. Because Yinma Lake is the only lake upstream of Kekexili Lake, the total area of upstream glaciers of Kekexili Lake equals 92 km^2.

6.2.5. Defining the geometric dependency of a lake on glacial runoff

An indicator for the dependency of a lake on glacier runoff is the ratio between the area in the catchment occupied by glaciers and the lake catchment area itself. If the ratio equals zero, the lake catchment does not contain any glaciers, meaning that the lake is not fed by glaciers at all. If the indicator is close to one, the lake catchment is almost fully covered by glaciers. The indicator R_D indicates the geometric dependency of that lake on glaciers draining directly into it. The indicator R_U represents the geometric dependency of the lake on any upstream glaciers.

$$R_D = \frac{A_{GD}}{A_C} \tag{6.3}$$

$$R_U = \frac{A_{GU}}{A_C} \tag{6.4}$$

Continuing the above example, R_D for Yinma Lake equals 0.064, while R_D for Kekexili Lake equals 0.019. Since no glacier-fed lakes drain into Yinma Lake, R_U equals R_D for Yinma Lake. As Yinma Lake is upstream of Kekexili Lake, R_U for Kekexili Lake is 0.035.

6.3. Results

After defining the geospatial objects and coding the procedures introduced above, we computed R_D and R_U, representing the geometric dependency of a Tibetan lake on glaciers, for all the lakes on the Tibetan Plateau with an area over 1 km^2. The result shows that 244 Tibetan lakes are directly fed by glaciers while 266 lakes have at least one upstream glacier, possibly buffered by an upstream lake. In addition, we include three case studies, studying the glacial dependency of three lakes: the Aksai Chin Lake in the Northwestern Kunlun Mountain, the Nam Tso Lake 100 km North of Lhasa and the Yamdrok Lake in the South of Tibet.

6.3.1. Lakes with glacial runoff at the Tibetan Plateau

a) Classification of lakes with or without outlet

The Tibetan Plateau contains 891 lakes over 1 km^2, occupying a total area of approximately 38,800 km^2. 150 of those lakes have an area of over 50 km^2. In Table 6.1, the Tibetan lakes are divided into lakes with an outlet (upstream lakes) and without an outlet (sinks). As it turns out, over two third of the Tibetan lake water is contained in sinks. On average, these endorheic lakes are four to five times bigger than lakes with an outlet. In total, there are 96 sinks with an area of over 50 km^2, 86 of which are located in the region called the inner plateau.

Table 6.1: Tibetan lakes with and without outlet.

Catchment	Upstream lakes	Total area of upstream lakes (km^2)	Endorheic lakes	Total area of sink lakes (km^2)
Brahmaputra	78	1 535.3	3	53.6
Ganges	14	78.5	2	330.1
Indus	28	1 333.5	5	212.7
Irrawaddy	0	0	0	0

Mekong	3	15.3	1	17.7
Salween	16	253.4	0	0
Yangtze	87	965.4	13	1 157.9
Yellow River	56	2 165.6	2	4 170.1
Inner plateau	323	5 949.0	260	20 560.7
Total	605	12 296.0	286	26 502.8

b) Geometric dependency of Tibetan lakes on direct glacier runoff

Based on the spatial distribution of glaciers and catchments, the glacier area per catchment is shown in Table 6.2. In this study, we only consider the major catchments of the Tibetan Plateau. According to Table 6.2, 25.3% of the total glacier area drains directly into 244 lakes. These lakes consist of 133 upstream lakes and 111 sinks. Thus, 74.7% of the total glacial area on the Tibetan Plateau directly drains into rivers, notably Brahmaputra, Ganges, Indus, Mekong, Yangtze, and Yellow River. On the inner plateau, 37.4% of the glacier area drains directly into 160 lakes, mostly situated in the north and the northwest of the inner plateau. Within the Brahmaputra River catchment, 11.1% of glacier area drains directly into its 33 lakes. The remaining glacier area, approximately 14,000 km^2, eventually drains into the Brahmaputra River which passes through China, India and Bangladesh. Similarly, 96.6% of glaciers attributed to the Mekong catchment, approximately 316 km^2, eventually drain into the Mekong river, supporting fresh water for China, Myanmar, Laos, Thailand, Cambodia and Vietnam.

Subsequently, we determined R_D, the geometric dependency of a lake on direct glacial runoff, for all Tibetan lakes. R_D values are symbolized by red disks in Figure 6.6. We then grouped Tibetan lakes by their R_D, as shown in Figure 6.7. Most of the lakes have an R_D below 0.005, corresponding to 75% of 244 lakes with at least one glacier draining directly into it. Our calculations also found eight lakes with an R_D over 0.5. These eight lakes are all relatively small, each occupying approximately 2 km^2. They are predictably located near glaciers and spread along mountain ranges in the southern and western Tibetan Plateau. Table 6.3 shows a list of the top ten lakes ranked by total area of directly contributing glaciers.

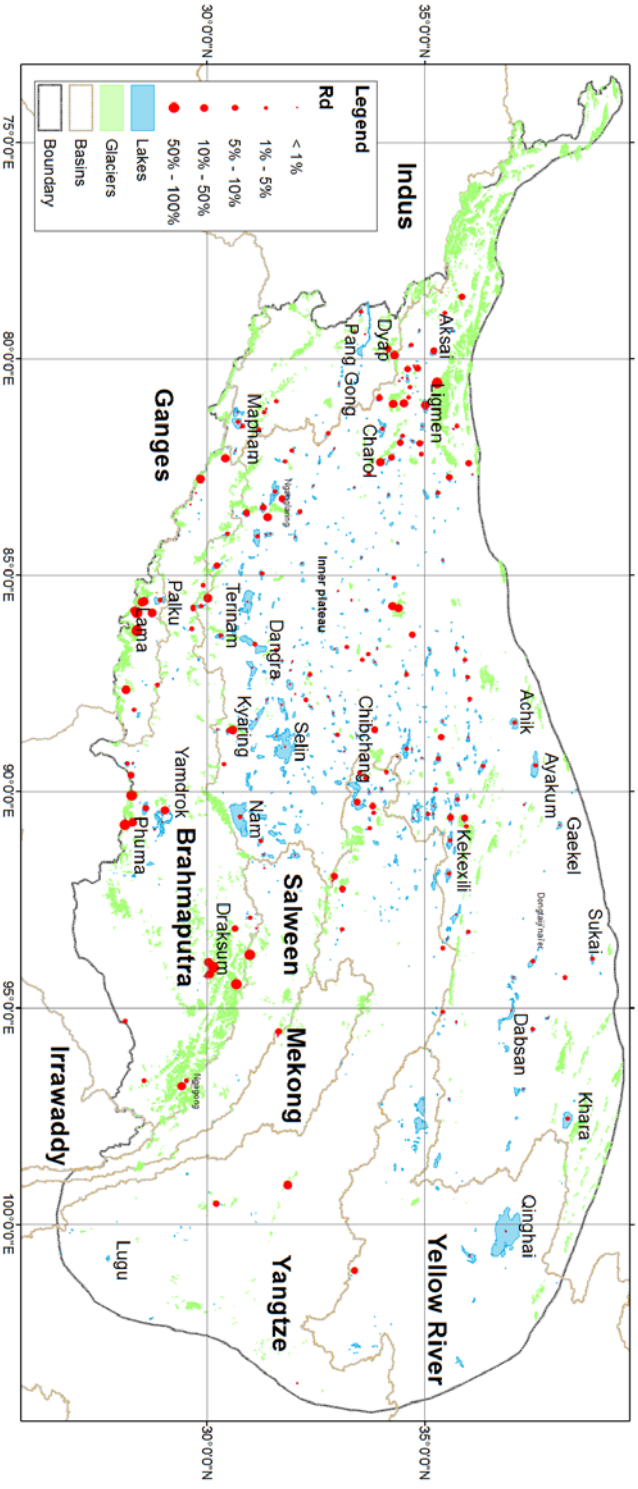

Figure 6.6: The geometric dependency of Tibetan lakes on direct glacial runoff (R_D).

Table 6.2: Glacier area per basin on the Tibetan Plateau. Here, N is the number of directly glacier-fed lakes, A_{Total} is the total area of glaciers with direct runoff into a lake and R_{Total} is the ratio between A_{Total} and the total glacier area.

Basin name	Basin area (km^2)	Total glacier area (km^2)	N	A_{Total} (km^2)	R_{Total} (%)
Brahmaputra	344,528	15,677	33	1,748.2	11.1
Ganges	39,772	3,636	10	355.5	9.8
Indus	101,428	2,430	14	727.9	30.0
Irrawaddy	4,227	32	0	0.0	0.0
Mekong	86,392	327	2	11.0	3.4
Salween	108,266	1,893	4	53.4	2.8
Yangtze	484,317	2,432	18	520.0	21.4
Yellow River	263,928	297	3	167.1	56.4
Inner plateau	1,098,382	26,512	160	9,909.7	37.4
Total	2,531,240	53,236	244	13,492.8	25.3

Table 6.3: Top ten lakes with the largest total area of directly contributing glaciers. Here, A_C is the area of the lake catchment, A_{GD} is the total area of glaciers directly draining into the lake, and R_D is the geometric dependency of the lake on direct glacial runoff.

No.	Lake name	Lat.	Lon.	A_C (km^2)	A_{GD} (km^2)	R_D
1	Dongtaiji'nai'er	37.496	93.935	34,148	691.5	0.020
2	Aksai	35.208	79.828	7,993	672.8	0.084
3	Ligmen	35.028	81.082	2,727	518.7	0.190
4	Ngagong	29.413	96.817	1,290	484.6	0.376
5	Ayakum Kul	37.546	89.373	24,147	383.7	0.016
6	Nam	30.718	90.646	10,741	334.5	0.031
7	Draksum	30.026	93.997	1,722	307.2	0.178
8	Nganglaring	31.540	83.101	12,464	291.2	0.023
9	Achik	37.067	88.431	13,263	280.8	0.021
10	Dabsan	36.978	95.205	109,629	242.7	0.002

c) Geometric dependency of Tibetan lakes on upstream glaciers

In addition to being directly fed by glaciers, a Tibetan lake can also be fed indirectly by glaciers, through upstream lakes. That is why we also determined R_U for the 266 lakes, to show the geometric dependency of Tibetan lakes on upstream glaciers. Figure 6.7 also shows the result of grouping the Tibetan lakes according to their R_U. About 75% of the 266 lakes with at least one upstream glacier correspond have an R_U of under 0.005. We also found 9 sinks and 13 lakes with runoff that are only indirectly fed by glaciers.

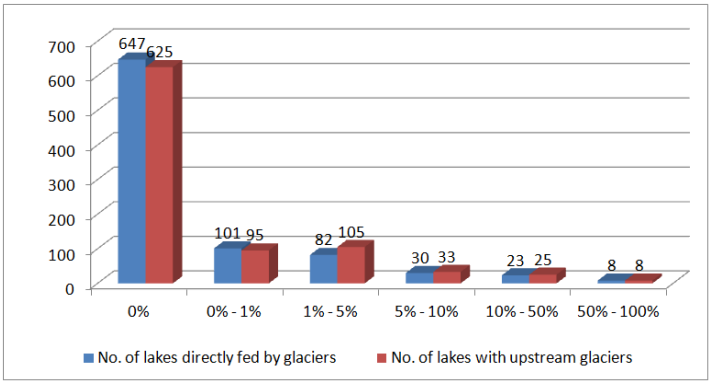

Figure 6.7: Tibetan lakes grouped by their level (%) of geometric dependencies R_D and R_U on glacial runoff.

6.3.2. Case studies

The case studies below show the situation in the catchments of three lakes: Aksai Chin Lake, Nam Tso Lake and Yamdrok Lake. The Aksai Chin Lake closed catchment contains a small lake with highest geometric dependency on direct glacial runoff. The geospatial properties of this lake are characteristic for Tibetan lakes with high R_D values. The Nam Tso Lake closed catchment is included as a case study since it has been a pilot for many studies on lake water level change and water balance. Nam Tso Lake mostly depends on directly contributing glaciers situated in the Nyainqentanglha Mountains. Finally, the Yamdrok Lake sub-catchment is surrounded by snow-capped mountains, but Yamdrok Lake depends much more on indirect glacial runoff via upstream lakes rather than from direct glacial runoff.

a) Aksai Chin Lake closed catchment

Aksai Chin Lake is a sink on the Aksai Chin plateau. The lake is located at 35.208 N, 79.828 E in the south of the Kunlun Mountains. The Aksai Chin plateau is a vast high-altitude desert at an average elevation of 5,500 m. Aksai Chin Lake is fed by Aksai River and many other streams, as illustrated in Figure 6.8. The Aksai Chin Lake closed catchment occupies an area of about 8,000 km^2. A_{GD}, the total area of glaciers draining directly into Aksai Chin Lake, equals 673 km^2. There is only one small lake upstream of Aksai Chin Lake. A_{GU}, the total area of the glaciers upstream Aksai Chin Lake, is approximately 769 km^2. Accordingly, its R_D value is 0.084 while its R_U value is 0.096. We conclude that the dependency of Aksai Chin Lake on glacial runoff is mostly direct, i.e. almost not tempered by intermediate lakes.

The maximum R_D value we found in this study, 0.816, belongs to a relatively small lake in Aksai Chin Lake catchment, occupying only 2 km^2. It is located at 35.293 N, 80.572 E at an altitude of approximately 5,500 m in the Kunlun Mountains, as shown in Figure 6.9. This lake is the only lake draining into Aksai Chin Lake that receives glacial runoff. Its sub-catchment occupies an area of about 118 km^2, of which approximately 96 km^2 is covered by glaciers. The lake is almost fully fed by glacial melt-water. The geographic properties of this lake are representative for lakes with an R_D value of over 0.5.

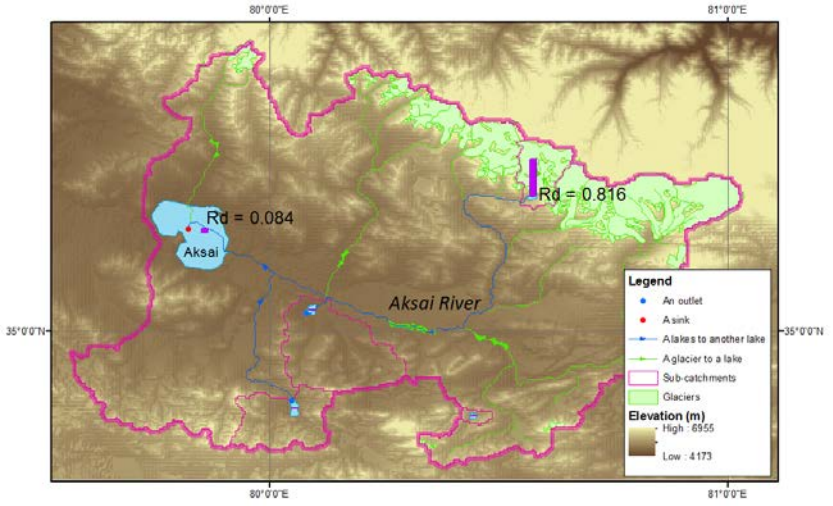

Figure 6.8: The maximum R_D value occurs at a small lake belonging to the Aksai Chin Lake closed catchment.

b) Nam Tso closed catchment

Nam Tso Lake, also called Nam Tso or Nam Co, is the largest salt lake on the Tibetan Plateau. The lake is located at 30.718 N, 90.646 E at an elevation of 4,718 m and occupies a surface area of about 1,960 km^2, as shown in Figure 6.9. Nam Tso is a sink at the foot of the Nyainqentanglha Mountains and is mostly fed by glaciers from these mountains. While Nam Tso has two small upstream lakes, no glacier drains into these smaller lakes. The Nam Tso closed catchment occupies an area of 10,741 km^2 while the total area of direct glaciers draining into Nam Tso is calculated as 334.5 km^2. This makes it one of the top ten lakes directly fed by glaciers, as shown in Table 6.3. This gives it an R_D value of 0.031, which indicates that over 3% of the Nam Tso catchment is covered by glaciers. This R_D value can be considered relatively high, and shows a relatively high dependency of Nam Tso on glacial runoff.

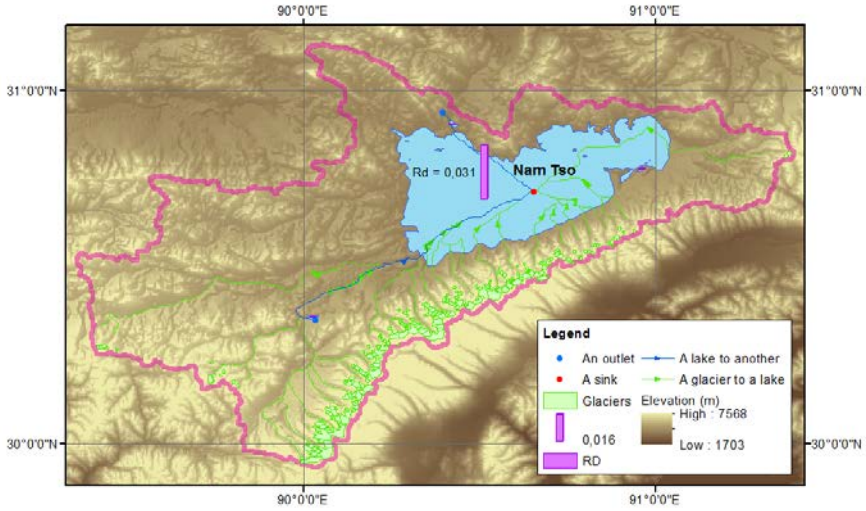

Figure 6.9: Geometric dependency of Nam Tso Lake on glacial runoff.

According to Krause et al. (2010), the sum of all water inflow to Nam Tso Lake resulted in an increase of the lake volume by 33.5 km^3 for the period between November 1961 and October 2010. This study computed the mean total annual inflow of water from glaciers into Nam Tso as 7.12 $km^3\ yr^{-1}$ during the observed period, and indicated that this glacial meltwater is the largest contributor to the increased lake water volume. This was corroborated by analysis of satellite laser

altimetry data from between 2003 and 2009, which show that Nam Tso has a positive lake level trend of +23 cm yr^{-1} (Phan et al., 2012a) or +25 cm yr^{-1} (Zhang et al., 2011). At the same time, Bolch et al. (2010) reported that the glaciers from the Nyainqentanglha Mountains draining into the Nam Tso catchment were shrinking during the period 2001–2009, based on analysis of optical data from Hexagon KH-9 and Landsat MSS (both 1976), Metric Camera (1984), and Landsat TM/ETM+ (1991, 2001, 2005, 2009).

Nam Tso is exceptional among the many lakes on the Tibetan Plateau because it is relatively well studied. In our opinion, our analysis of Nam Tso indicates the potential of the approach of this study. By correlating the geometric dependency of Nam Tso Lake on glacial runoff to other papers on water level, we can link glacial shrinkage and lake level increase. The possible significance of these links should be studied further for a large number of lakes.

c) Yamdrok Lake sub-catchment

Yamdrok Lake, also called Yamzho Yumco, is one of the largest lakes on the Tibetan Plateau. The lake is fan-shaped and occupies an area of ~640 km^2. It is located at 28.979 N, 90.717 E at an elevation of about 4,440 m on the north side of Mt. Qomolangma. The lake is fed by numerous small streams. The outlet stream of the Yamdrok Lake sub-catchment is at the far western end of the lake, as shown in Figure 6.10. The Yamdrok Lake sub-catchment, derived from the HydroSHEDS drainage basin data, occupies an area of 9,940 km^2 and belongs to the major catchment of Brahmaputra River. Although surrounded by many snow-capped mountains, Yamdrok Lake is only directly fed by a few glaciers occupying a total area of only 21 km^2. Therefore, Yamdrok Lake's R_D only equals 0.002. The total area of glaciers upstream of Yamdrok Lake, however, is 255 km^2, and this gives Yamdrok Lake a relatively high R_U of 0.026. This means that Yamdrok Lake depends more on glacial runoff from upstream lakes than on direct glacial runoff.

The geometric links also indicate that three nearby lakes, Bagyu, Gongmo and Phuma, flow into Yamdrok Lake, as shown in Figure 6.9. Although no glacier directly feeds it, Bagyu Lake depends on glacial runoff through a nearby small lake with an R_D of 0.004, giving Bagyu Lake an R_U of 0.004. Yamdrok Lake has a high dependency on glacial runoff from Gongma Lake and Phuma Lake.

Gongmo Lake is another of the lakes upstream of Yamdrok Lake. The lake occupies an area of about 40 km^2. It is located near the western end of Yamdrok Lake, at an altitude of 4,500 m. The Gongmo Lake sub-catchment occupies an area of 620 km^2, with 77.7 km^2 of the area covered by glaciers. Therefore, the

dependency of Gongmo Lake on direct glaciers is high, with an R_D value of 0.125.

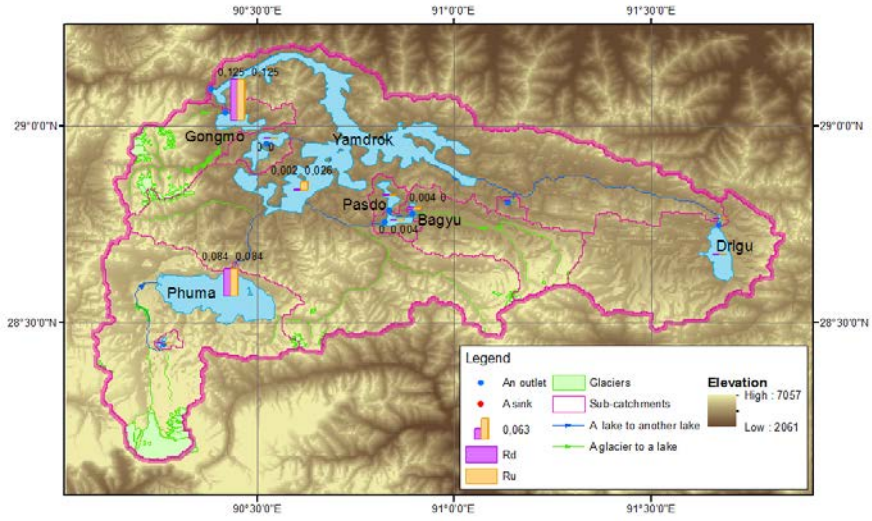

Figure 6.10: Geometric dependency of Yamdrok Lake sub-catchment lakes on glacial runoff.

Phuma Lake, also called Puma Yumco, is a big upstream lake draining into Yamdrok Lake, as shown in Figure 6.10. Phuma Lake occupies an area of about 285 km^2, at an elevation of 5,030 m. The lake is directly fed by glacier-melt water from surrounding mountains. The area of the Phuma Lake sub-catchment equals about 1 815 km^2. Our analysis indicates that the total area of glaciers draining directly into Phuma Lake is about 153 km^2 indicating Phuma Lake also depends highly on direct glacial runoff, corresponding to an R_D value of 0.084.

6.4. Discussion

In this discussion chapter, two topics are considered. First, we discuss how the geometric links we quantified between glaciers and lakes are expected to contribute to further understanding of the hydrological mass balance of the Tibetan Plateau. The second part gives more details on several technical aspects,

such as input data, computation times and the non-standard processing steps that were necessary to arrive at the results presented above.

6.4.1. The hydrological interpretation of geometric dependency on glacial runoff

Because of the high relief of the Tibetan Plateau, elevation dominates the hydrological processes that influence mass balance. This high relief also makes it more difficult to assess the state of mass balance from remote sensing data, when compared to monitoring the mass balance of the relatively flat Greenland and Antarctica ice sheets (Radic and Hock, 2011). Recent work, however, showed two things: how to gather information on water level variations for many Tibetan lakes (Zhang et al., 2011; Phan et al., 2012a), and how to collect data on glacier mass changes on the borders of the Tibetan Plateau (Kaab et al., 2012). It was also shown that lake levels vary per season and per location (Phan et al., 2012b), in a way that is not directly understandable without further information. State-of-the-art modeling results of the hydrological mass balance of the Tibetan Plateau relies on an underlying grid of surface runoff with a grid size in the order of 5 km (Immerzeel et al., 2010).

The first goal in establishing and quantifying geometric links between glaciers and lakes is to obtain direct insight into the dependency of the different lakes on direct and indirect glacial runoff. Although glaciers may also lose mass due to sublimation and evaporation, a major part of the mass loss is due to melting. This meltwater will drain away via streams that may end in one of the ~900 Tibetan lakes. Groundwater flow on the Tibetan Plateau is also largely dominated by elevation differences, and a large part of the groundwater flow will also end up in lakes. Estimating discharge due to melting has already successfully been attempted at smaller scale. Krause et al. (2010), for example, used a degree day factor approach to estimate the mean total annual inflow of glacier meltwater into the Nam Tso Lake at 7.12 $km^3 a^{-1}$ during the period between 1961 and 2010. Similarly, Zhou et al. (2010) also used a degree day model to study how changes in air temperature and precipitation from 2007 to 2008 affected glacier runoff from Zhadang glacier runoff in the Nam Tso Lake basin. To quantify each lake's potential inflow of glacier-melt water, we determine the R_D (geometric dependency of a lake on direct glacial inflow). Clearly, glaciers buffered by an upstream lake may also have impact on a downstream lake's water balance, but only in an indirect way. Therefore, we distinguish between direct and indirect inflow by determining a separate R_U value (geometric dependency of a lake on both direct and indirect glacial inflow). Further research is expected to show to what extent the difference in dependency on glacier-melt water can explain differences in lake level variations.

A second goal of the work in this study is to facilitate and further constrain future hydrological modeling efforts. This work shows in detail how to create a surface runoff grid for the Tibetan Plateau, including lakes, rivers and glaciers, at a resolution of an unprecedented ~400 m. Combining this hydrological model with existing and new empirical results on the mass balance of lakes and glaciers is expected to result in new and more accurate hydrological mass balance predictions.

6.4.2. Details on computing the geometric dependency of lakes on glacial runoff

a) Reliability of the results

In this paragraph, we discuss how the results presented in this study depend on the quality of the different data sets and on the processing.

i) *The MODIS land-water mask.* The MODIS MOD44W 250m land-water mask was produced using over 8 years of Terra MODIS spectral data, over 6 years of Aqua MODIS spectral data and Shuttle Radar Topography Mission (SRTM) elevation data (GLCF, 2012). With a pixel size of 250 m, the spatial resolution of the MODIS land-water mask is relatively low. Besides, the mask also contains errors affecting the shape of the lake polygons. For example, there are cases where two different lake polygons represent the same lake, e.g. Yamdrok Tso or Pang Gong Tso, and, vice versa, where different lakes are included in one lake polygon, e.g. Chibchang Tso and Mitijiangzhanmu Tso. Except for permanent lakes, the MODIS land-water mask also contains some small seasonal lakes. In addition, the mask contains many small polygons representing parts of rivers.

The Tibetan lake layer, used in this study, was derived from the MODIS land-water mask. It is stored in shapefile format and is the product of a previous study (Phan et al., 2012a). All lake outlines were checked and river remains were removed with the support of Google Earth and one set of Landsat TM data. The Landsat TM image data used as reference acquired in 2002 and 2003 which corresponds to the acquisition of the data used for the MODIS land-water mask. We believe that the number of remaining errors in the lake mask is quite small, also because most elevations considered now are already unambiguously representing a lake surface of a known lake, compare also Phan et al. (2012a).

ii) The HydroSHEDS river data derived from SRTM. SRTM data are used to generate the HydroSHEDS data sets at 3 arc second resolution (approximately 90 m at equator). With a pixel size of ~90 m, the SRTM data represent a digital topographic map of the Earth's land surface. Note that at 90 m resolution it is possible that some river channels running in for example a canyon are not well represented. This may in some cases result in incorrect channel representations in derived products, such as the HydroSHEDS product. The SRTM data has an absolute horizontal accuracy of below 20 m and a relative vertical accuracy of less than 10 m (Bamler, 1999; Zandbergen, 2008). The HydroSHEDS data sets including stream networks, watershed boundaries, drainage directions and ancillary data layers such as flow accumulations, distances and river topology information are derived from SRTM DEM, basically using an eight-direction (D8) flow model (O'Callaghan and Mark, 1984). The D8 method estimates surface flow in gridded digital terrain models from systematically 8 possible directions from a candidate pixel to one of its eight neighbors. This method works well when the direction of steepest descent is well-defined. Errors in the elevation data and lack of relief may therefore result in wrong channel locations, or even in locally wrong flow directions. The level of detail of these hydrologic data sets depends on the minimum number of accumulation upstream pixels that is used to create a stream or a river segment.

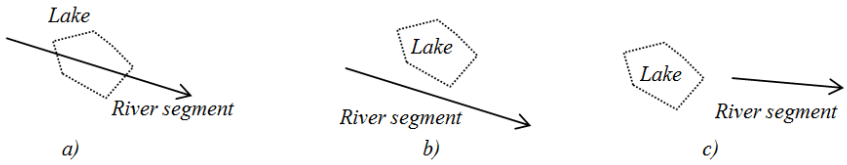

Figure 6.11: Description of the low resolution of the HydroSHEDS rivers superimposed over the MODIS lakes: a) the river segment crossing over the lake while b) and c) the river segment outside the lake.

Based on the river network and the location of a lake, the outlet of each lake catchment is defined as a point inside the lake region. If river segments all stream to the intersection point inside the lake polygon, the lake has no outflow. The intersection point is considered a sink of a closed catchment. If one river segment has the from-node inside and the to-node outside a

lake, the lake has an outflow. The from-node of the river segment is considered the outlet of a lake sub-catchment. By applying this rule, we could identify the outlets of most of the 891 Tibetan lakes. The outlets of some lakes are not automatically determined due to the low resolution of the river network, as described in Figure 6.11. These lakes were marked and checked manually. If glaciers occur in the lake's catchment, we manually created a detailed drainage network of the lake's area in ArcHydro, as described in the following section b.

The low resolution of SRTM has for example affected the connection between Chibchang Tso Lake and Mitijiangzhanmu Tso Lake (Appendix D). In reality, these lakes are connected by a small channel, as shown in Figure 6.12. However, the HydroSHEDS catchment data, derived from SRTM, represent Chibchang Tso Lake and Mitijiangzhanmu Tso Lake as sinks in two separate closed catchments. The mean altitude of Mitijiangzhanmu Tso is 4,938.1 m while the mean altitude of Chibchang Tso is 4,933.4 m, according to SRTM. It is quite possible that in reality these two lakes connect only during part of the year. It should be further investigated.

Figure 6.12: Effect of the low resolution of SRTM in the separation of Chibchang Tso and Mitijiangzhanmu Tso into two closed catchments derived from the HydoSHEDS drainage basins when overlaid on Google Earth.

iii) The flat outlets. Also the height differences between linked lakes have been evaluated to further identify possible suspicious cases. In total, there are 311 pairs of linked lakes. For 16 pairs, the difference in mean elevation is only below 1 m. They all represent connections between two nearby lakes inside the same closed catchment. Besides, the mean elevation of a lake is also affected by the lake shape. For example, at the Jagok Tso Lake catchment, Chagut Tso at a mean attitude of 4,558.6 m directly drains into Jagok Tso at a mean altitude of 4,557.2 m and Kyaring Tso at a mean altitude of 4,656.0 m directly drains into Chikut Tso at a mean attitude of 4 654.6 m before draining into Jagok Tso (Appendix D).

The HydroSHEDS river network is susceptible to various errors, foremost in flat regions, including lake surfaces. In fact, river segments inside a lake polygon are still oriented. This can affect the location of the outlet of a lake. Furthermore, the vertical error of SRTM can influence the orientation of a river segment. Of the 311 pairs, there are 99 ones in which the difference in mean elevation between two linked lakes is less than 20 m. It is noticed that 33 of such 99 pairs are directly dominated by glaciers. Thus, if some of the links orient inversely by the elevation error, the corresponding indicator values (R_U) of geometric dependency of the linked lakes are affected.

iv) The seasonal variations. In this study, we use the Tibetan lake layer, as produced for a previous study in which Phan et al. (2012a) removed small seasonal lakes or empty depressions from the MODIS land-water mask. However, as a result of the drainage network analysis, we also found 140 sinks without permanent lake, according to the MODIS land-water mask. Most of them are in the northern Tibetan Plateau. It is possible that these sinks correspond to seasonal lakes that may be empty in winter and with water in summer by rainfall and snow melt.

v) The deformations in the glacier mask. Recent studies report that the total glacier area on the Tibetan Plateau is shrinking. This affects the indicator values R_D and R_U because the total area of glaciers directly and indirectly draining into a lake changes. In this study, the area of each glacier, derived from the CAREERI glacier mask, is determined based on both remote sensing and in-situ data from 1978 to 2002. Thus, the indicator values R_D and R_U represent the geometric dependency of the Tibetan lakes on glacial runoff in 2002. Therefore, in order to determine the indicator values R_D and R_U in later years, the rates of retreat in glaciers can be used to re-compute the area of each glacier. These rates are reported in recent literatures for individual regions on the Tibetan Plateau. For example, Wang et al. (2011) estimated a retreat in glacier area of 21.7% in the Middle Qilian Mountain

Region from 1956 to 2003. Thus, the area of each glacier in this region can decline 4.6% in 2012. Subsequently, the indicator values R_D and R_U at the lakes dominated by glaciers in this region have a reduction of 4.6% in 2012 as well.

b) Manually calculating the area of lake sub-catchments using ArcHydro

As mentioned in section 6.1.3, the area of a lake sub-catchment is the product of its grid cell size and the total number of grid cells draining into its outlet. Due to the limited resolution of the HydroSHEDS river network, the outlet of a lake sub-catchment can be just one of several sources of a river network, e.g. outlet F in Figure 6.4c. In this particular case, the total number of grid cells cannot be determined automatically from the HydroSHEDS data. However, the area of a lake sub-catchment can also be calculated based on its geometric shape. The ArcHydro extension of ArcGIS supports manual outlining of catchments from a digital elevation model.

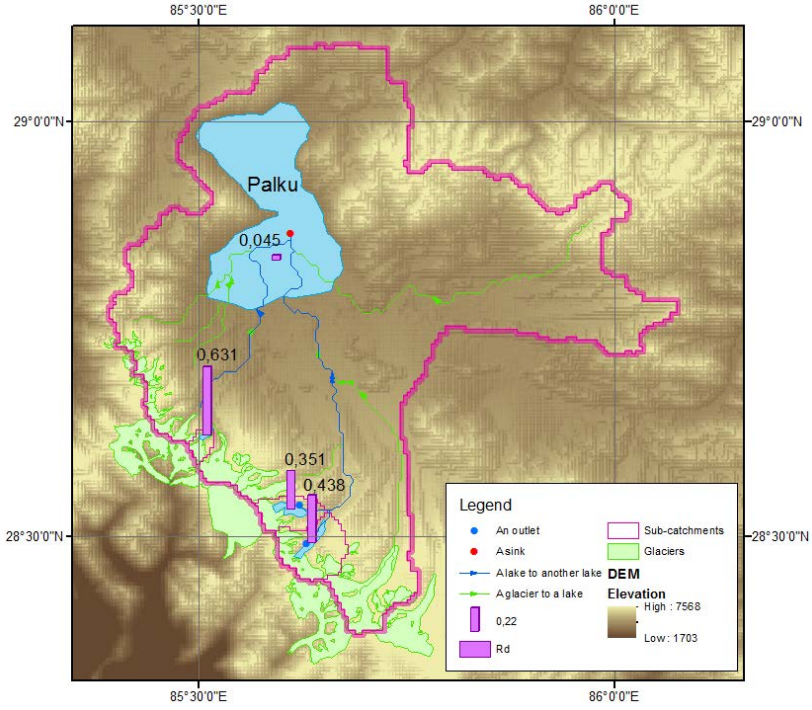

Figure 6.13: The lake sub-catchments, belonging to the Palku Lake closed catchment, are manually created, using ArcHydro.

Based on the HydroSHEDS DEM data at 15 arc-second resolution (USGS, 2012), lake sub-catchments were outlined manually using the ArcHydro tools for these cases. We found 19 such lakes directly fed by glaciers. First, we clipped the terrain data for the 19 lake regions from the HydroSHEDS DEM. Second, we created small catchments by following the ArcHydro user guide. For this purpose, a threshold of 30 upstream drainage grid cells is used to define a river segment, to improve the level of detail of the river network. This threshold also means that this manual outlining will only produce catchments with an area of at least 30 grid cells. Subsequently, for each lake, we determined the lake sub-catchment by merging the small catchments draining into its outlet, as illustrated in Figure 6.2. Finally, the catchment area was obtained directly from its geometric shape. As an example, the geometric shapes of the three small lake sub-catchments in the south of the Palku Lake basin are shown in Figure 6.13.

c) Dividing the Tibetan Plateau into parts for speeding up computations

The Tibetan Plateau is large, so it takes a long time to run the drainage network analysis module and determine connections between glaciers and lakes. When the module was run on a desktop with a 3.2GHz CPU and 2GB RAM or on a laptop with a 2.2 GHz Core 2 Duo CPU and 4 GB RAM, it took 4 or 5 days to process the data for the whole Tibetan Plateau. Sometimes the process stopped altogether. Although the river network is organized per catchment, a large amount of PC memory is required to find a route of river segments for each glacier. This holds especially for the major catchment of Brahmaputra River, which occupies a large area and has a densely spread river network. To complicate calculations, most of the glaciers inside the Brahmaputra major catchment do not drain into the outlet of any lake catchment. To more efficiently calculate the total area of directly contributing glaciers draining into each lake on the whole plateau, we divided the plateau into sub-areas, grouping some closed catchments on the inner plateau. As a consequence, we had to run the module several times to manually determine connections between glaciers and lakes. In addition, for each major river catchment we created several virtual outlets in the river network to reduce computation time. Then we used the module to make connections between the virtual outlets, the way it is also used to make connections between lakes. Finally, we found the connections between glaciers and lakes in each major catchment by combining routes from glaciers to outlets and between outlets.

6.5. Conclusions

In this study, we calculate for each lake with an area of over 1 km^2 on the Tibetan Plateau (891 in total) how much it is geometrically dependent on glacial runoff. The results show that 244 of these lakes receive direct runoff from glaciers while another 22 lakes only obtain glacier-melt water buffered by upstream lakes. The ratio between the total area of glaciers draining into a lake and the area of its catchment (R_D) represents the dependency of a lake on glacial runoff. Geometric connections between glaciers and lakes are determined based on drainage network analysis. From this, the total area of directly contributing glaciers or the total area of upstream glaciers draining into a lake is computed. This geometric dependency is a first proxy for the actual dependency of a lake on glacial runoff. Our results clearly list which lakes are more or less dependent on glacial runoff and therefore indicate which lakes are expected to be strongly affected by the predicted further shrinkage of the glaciers on the Tibetan Plateau.

Based on analyzing the geometric connections between glaciers and lakes, it is concluded that 74.7% of the total glacial area, approximately 40,000 km^2, directly drains into rivers originating at the Tibetan Plateau and terminating in sea. Notably, a glacial area of approximately 14,000 km^2 directly drains into Brahmaputra River which passes through China, India and Bangladesh. Of the 244 lakes that receive direct runoff from glaciers, 111 lakes are within closed basins while the remaining 133 lakes flow to upper branches of Asia's big rivers. These conclusions show that our results could be used to estimate the contribution of Tibetan glaciers to future sea-level rise.

Chapter 7

CONCLUSIONS

In this chapter the achievements of this thesis are reviewed by summarizing the answers to the research question stated in Chapter 1, and then recommendations for possible future work are given.

7.1. Achievements

The main research question started in Chapter 1 was '*How to monitor changes in glacier thickness and lake levels on the Tibetan Plateau exploiting ICESat laser altimetry?*'. Different aspects of this research question were considered in Chapter 2 to 6. The achievements of this research are summarized here by considering the different sub-objectives identified in Chapter 1.

i) How to exploit ICESat laser altimetry and additional data for obtaining lake levels in the Tibetan Plateau?

   Using the ICESat GLA14 land surface elevation data in combination with the MODIS land-water mask, water level variations of 154 lakes spread all over the Tibetan Plateau could be obtained. The GLA14 elevations representing lake surface elevations were basically selected by using the lake outlines, derived from the MODIS land-water mask. For each ICESat sampled lake, anomalies in observed surface elevations due to e.g. clouds, saturation or surface characteristics, were removed using the RANSAC algorithm. Then the mean elevations corresponding to the ICESat acquisition times were determined. They were representative for lake levels during the observed period. Subsequently, a temporal lake level trend was estimated by linear regression. The results indicated that most of the lakes with a serious downwards trend are in the southern Tibetan Plateau and along the Himalaya mountain range and, vice versa, most of the lakes with a positive water level trend between 2003 and 2009 are in the inner Tibetan Plateau.

   The ICESat laser altimetry data could not only be used to monitor water level variations and to estimate the linear annual trends, but also to obtain seasonal water level trends and inter-seasonal water level variations of the Tibetan lakes. For each lake sampled by sufficient ICESat campaigns, the GLA14 elevations were grouped into three seasons following the ICESat acquisition schedule: late dry season, wet season, and early dry season. Yearly trends were estimated using lake levels in the same season and different years and results were compared to trends obtained from using all lake levels simultaneously. In addition, lake level changes per season were assessed. The results indicated that seasonal influences were similar to their annual trends between 2003 and 2009. Seasonal influences were more obvious in the South of the Tibetan Plateau than those in the Northwest. The seasonal influence on lake level gradually decreased from the Southeast to the Northwest of the Tibetan Plateau. These results

correspond to trends in precipitation, temperature and humidity as documented in recent research on climatic change at the Tibetan Plateau.

ii) How to exploit ICESat laser altimetry and additional data for estimating trends in glacial thinning or thickening in the Tibetan Plateau?

By exploiting ICESat GLA14 land surface elevation data in combination with the SRTM DEM and the GLIMS glacier mask, trends in the estimated thickness of 90 glacial areas on the whole Tibetan Plateau were estimated between 2003 and 2009. Here, the approach for estimating glacial thickness was to estimate the difference between the GLA14 elevation and the reference SRTM DEM. By considering where ICESat measurements sampled glaciers, ICESat-sampled nearby glaciers having similar orientation were grouped into observed glacial areas. Accordingly the GLA14 elevations on these glacial areas were selected. For each glacial area, uncertain GLAS elevations were removed, based on criteria that were also used for lakes, while in addition, also the terrain slope and roughness were considered. In the final chosen setting notably only measurements over terrain with slope $< 20^0$ and roughness < 15 m were maintained. Subsequently, the mean elevation difference between the remaining GLA14 elevations and the SRTM DEM, corresponding to each ICESat acquisition time, was determined. It was assumed representative of the mean glacial thickness at the time of ICESat sampling. Based on these mean differences, a temporal trend of glacier thinning or thickening between 2003 and 2009 was estimated. The results indicated that most of the observed glacial areas at the Tibetan Plateau experienced a serious thinning, except the North-facing glaciers of the western Kunlun Mountains. Moreover, glacial thickness changes indeed strongly depend on the relative position in a mountain range. Conversely most North-facing glaciers increased in thickness, although some decreased but in that case at a slower rate than its South-facing counterpart.

However, the results were sensible to the removal of ICESat footprints based on terrain surface criteria and the GLIMS glacier mask. Firstly the impact of the terrain surface criteria for assessing the signal quality of the ICESat measurements was considered. By applying filtering criteria on terrain slope and roughness at ICESat footprints on several large glaciers, the results indicated that the elevation differences increase with terrain slope while large valley glaciers often have a surface roughness of below 20 m. Moreover, it is assumed that the accumulation zone of a mountain glacier on the Tibetan Plateau is steep. Therefore it was expected that the remaining ICESat footprints would be inside the glacier ablation zone and

the elevation differences at ICESat sampled locations with gentle slope. Secondly, the GLIMS glacier mask is static which has some effect on the estimation of a glacial thickness change trend. The GLIMS glacier mask was established using image data acquired from 1978 to 2002 while ICESat sampled glacial areas between 2003 and 2009. Thus, maybe some ICESat footprints fell within the GLIMS glacier outlines but were not sampling a real glacier anymore at the time of their acquisition. Nevertheless, the number of such footprints within the same ICESat track is not large because the along track distance between consecutive footprints is approximately 170 m, and criteria on terrain surface are in place to remove uncertain footprints.

iii) How to validate trends in lake levels and glacial thickness change derived from ICESat laser altimetry?

The lake level changes, derived from the ICESat GLA14 land surface elevation data, could be validated using radar altimetry and in situ measurements at large Tibetan lakes. In this research, we compared our results in the water level variations to radar altimetry results for two large lakes, Qinghai and Seilin. The radar altimetry data for these two lakes were obtained from the Laboratoire d'Etudes en Geodesie et Oceanographie Spatiales, Equipe Geodesie, Oceanographie et Hydrologie Spatiales (LEGOS). The comparison indicated that not only the mean trend for both lakes was similar, but that also the variations in lake level were comparable.

The glacial thickness changes, derived from the GLA14 elevations, were observed for relatively small glacial areas sparsely distributed over the Tibetan Plateau. Nevertheless, it is interesting to compare them with previous research, (Neckel et al., 2014) and (Gardner et al., 2013). A comparison to Neckel's glacial thickness change rates of eight sub-regions indicated that four sub-regions, relatively densely covered by glaciers, had a similar thickness change rate, one sub-region had a somehow similar rate while two sub-regions had a relative large disparity. This disparity could be caused by the low number of observed glacial areas and differences in orientation of the observed glacial areas. For the last sub-region, there were not enough ICESat footprints for our method to estimate a temporal trend. In a comparison to Gardner's glacier elevation changes, both results indicated that most of the glaciers in the Tibetan Plateau were thinning between 2003 and 2009, except for western Mt. Kunlun. The strongest glacier-thinning occurred in the Himalaya range and in the Hengduan mountains. Glacial thickness changes were

near balance in the western and inner plateau. Inversely glaciers in the western Mt. Kunlun were thickening.

iv) How to link changes in glaciers and lakes on the Tibetan Plateau?

Geometric links between glaciers and lakes on the Tibetan Plateau were determined by applying a surface flow network analysis in catchments with both a lake and a glacier. The surface flow network was based on the HydroSHEDS product which was derived from the SRTM digital elevation model data, but needed corrections at several locations. The results indicated that 25.3% of the glaciers release their melt water directly to 244 lakes. Moreover, the ratio between the total area of glaciers draining into a lake and the area of its catchment was introduced as a proxy for the dependency of a lake on glacial runoff. The results clearly listed which lakes are more or less dependent on glacial runoff and therefore indicated which lakes are expected to be strongly affected by the shrinkage of the glaciers on the Tibetan Plateau.

v) Is any relationship observable between changes in glacier thickness and lake levels at the Tibetan Plateau?

The results indicated that the ICESat sampled glaciers and lakes on the Tibetan Plateau were observed sparsely. Figure 7.1 presents rates of the change in glacier thickness and lake levels between 2003 and 2009 on the Tibetan Plateau, derived from the ICESat laser altimetry.

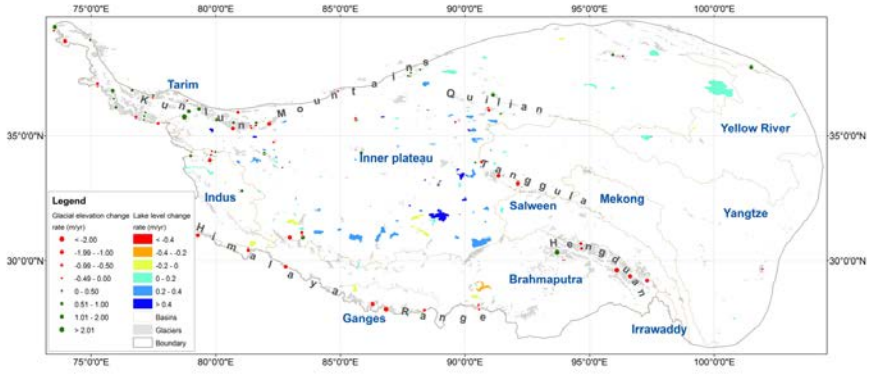

Figure 7.1: Rates of the change in glacier thickness and lake levels between 2003 and 2009 on the Tibetan Plateau.

There were a limited number of lake catchments in which both glaciers and the lake were sampled by enough ICESat campaigns. Based on the geometric links between glaciers and lakes, the relationship between changes in glacier thickness and lake levels is in principle observable. As a first example, Figure 7.2 shows that glacier melt water from the location on the South face of the Mt. Western Kunlun flows to Aksai Lake. The estimated rate of glacial thinning is -1.02 ± 0.29 m a^{-1} while the lake level is going up at a rate of +0.5 m a^{-1} between 2003 and 2009. Moreover, the geometric dependency of Aksai Lake on directly glacial runoff R_D is 0.084 while its geometric dependency on upstream glacial runoff R_U is 0.096.

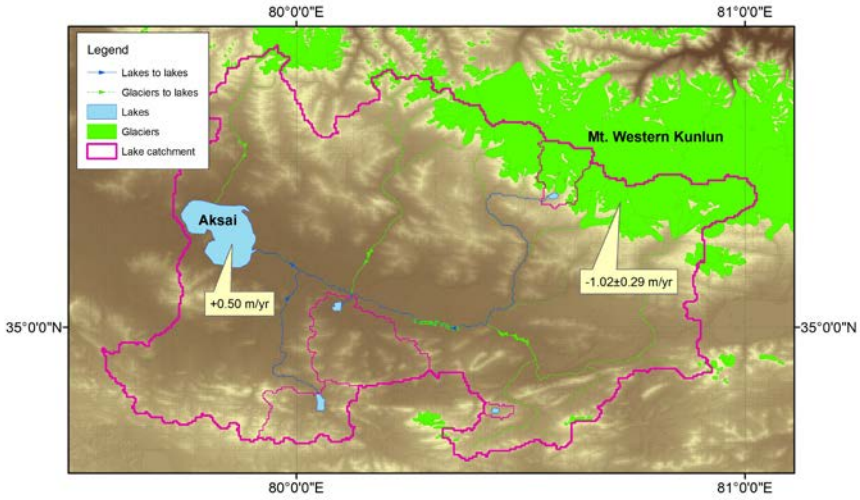

Figure 7.2: Rates of the glacier thinning and the lake level increase between 2003 and 2009 at the Aksai Lake catchment.

In general, the geometric dependency of Tibetan lakes on glacial runoff is only a simple representation of a potential relationship between changes in glacier thickness and lake levels. It is difficult to estimate how much glacial thinning or thickening relates to lake level change. However, both changes in glacier thickness and lake levels directly correspond to water volume changes in glaciers and lakes. Accordingly, lake level and glacial thickness changes could be converted to water volume changes. An analysis of spatial patterns in water volume changes in glacial areas and lakes could be performed to determine a

possible correlation. This correlation is expected to reveal the relationship between changes in glacier thickness and lake levels all over the Tibetan Plateau. However, glacial areas and lakes were sparsely sampled by ICESat on the Tibetan Plateau. Therefore, converting glacial thickness and lake level changes into water volume changes on the whole Tibetan Plateau could be complicated. Nevertheless, this correlation can be performed using additional data from future satellite missions in further research.

7.2. Recommendations

In this research, it is described how ICESat GLA14 land surface elevation data are used to obtain changes in glacier thickness and lake levels on the Tibetan Plateau between 2003 and 2009. In my opinion this research should be continued in two directions. First, current results should be improved and refined. Possibilities are indicated in section 7.2.1. Second, the hydrologic processes that potentially cause the water flow variations in the Tibetan Plateau should be linked to the results described here, as sketched in section 7.2.2.

7.2.1. Data processing

- Improving the quality of the lake mask

  This research used the 250 m MODIS land-water mask to represent lake outlines on the Tibetan Plateau. The mask represents land-water bodies in the period between 2000 and 2002. Currently this product is the land-water mask with the highest available resolution. Except permanent lakes, the mask represents many small parts of rivers and empty small holes. In addition, it also contains errors affecting the shape of the lake polygons. In this work, Landsat imagery was used to check the existence of lakes, but spectral data was not used to update the shape of the lake boundaries. Therefore, Landsat imagery acquired between 2000 and 2002 could be used to improve the lake outlines. This can decrease the number of uncertain ICESat footprints located inside sampled lakes.

- Updating the glacier inventory

  The GLIMS glacier mask was used in this research to represent glacier outlines on the Tibetan Plateau. The observations serving as input for the glacier mask were obtained from 1978 to 2002, using aerial photographs, topographic maps and in situ measurements. The glacier mask was established per drainage basin and was constructed in different periods.

On the other hand, recent research reported that the total glacier area on the Tibetan Plateau is shrinking during last decades. Therefore, some ICESat footprints acquired between 2003 and 2009 that fell within the GLIMS glacier outlines may not be sampling a real glacier anymore. Landsat 7 imagery could be used to verify glacier outlines around 2002 while Landsat 8 imagery, and possibly also Sentinel-2 data, could be extracted to assess the recent state of glaciers. In addition, if a specific glacier is known to be retreating, it may be possible to predict the state of the glacier outline at the moment of an ICESat acquisition.

- Using the raw ICESat full waveform signal

  Classification techniques could be applied to the raw ICESat full waveform signals to determine which reflecting surface an ICESat signal is sampling, such as vegetation, lake, snow, glacier or rock. The ICESat GLA01 and GLA06 products provide the global altimetry data at Level-1A and Level-1B, respectively, including the transmitted and received waveform from the altimeter. Applying this analysis for the complete Tibetan Plateau is quite labor intensive, however, the information in the full waveform signal could assist in verifying if an ICESat footprint is located completely within a lake or a glacier.

7.2.2. Upcoming missions

- Cryosat-2 mission

  In 2010 the Cryosat-2 satellite was launched with the Synthetic aperture Interferometric Radar ALtimeter (SIRAL) onboard. The Cryosat-2 mission first acquires accurate measurements of the thickness of floating sea ice and second surveys the surface of ice sheets accurately enough to detect small changes. This altimeter is operated in three modes: Low Resolution (LR), Synthetic Aperture Radar (SAR), and Synthetic Aperture Radar Interferometry (SARIn). Notably it should be mentioned that SarIN mode is meant for high-relief terrain and is operational over the Tibetan Plateau. Cryosat-2 has certainly potential for monitoring lake levels of several tenths of lakes at the Tibetan plateau. Extracting glacial changes is very difficult, as relief results in complex Cryosat-2 waveform responses.

- ICESat-2 mission

  Following on the NASA ICESat mission's success, the ICESat-2 mission has been developed and scheduled for launch in 2017. It will observe ice-sheet elevation change, sea-ice, and vegetation canopy height. The laser altimeter designed using micro-pulses and multi-beams will improve both the cross-track and along-track sampling and the estimation of elevations in sloping and rough terrain. This improvement in configuration may be advantageous for monitoring changes in glacier thickness and lake levels on the Tibetan Plateau. Nevertheless, the ATLAS instrument on board of ICESat-2 will emit green laser pulses, and thus it will be a challenge to exploit its measurements to monitor lake levels on the Tibetan Plateau.

7.3. Further research

Given the current results on glacial and lake level changes, the next steps towards understanding the hydrologic processes and the water balance of the Tibetan Plateau could be as follows.

- An analysis of spatial patterns in the rate of glacier thickness change and rate of lake level change to determine the correlation between glacier change and lake level change all over the Tibetan Plateau. Links between glaciers and lakes already existing in Chapter 6 could be used as an input for this analysis.

- In addition, possible explanations for spatial variations in glacial and lake level trends could be found by linking those to results from other recent research on albedo, temperature, precipitation, and evaporation variations on the Tibetan Plateau.

Bibliography

Alsdorf, D., Birkett, C., Dunne, T., Melack, J., Hess, L.: *Water level changes in a Lake Amazon lake measured with spaceborne radar interferometry and altimetry*. Geophysical Research Letters, 28, 2671 – 2674, 2001.

Alsdorf, D.E., Rodriguez, E., Lettenmaier, D.P.: *Measuring surface water from space.* Reviews of Geophysics, 45 (2), RG 2002, 2007.

Bamler, R.: *The SRTM mission – A world-wide 30m resolution DEM from SAR interferometry in 11 days*. Proceedings of the 47th PhotogrammetricWeek '99, Wichmann Verlag, Heidelberg, Germany, 145 – 154, 1999.

Bhatt, C. M., Srinivasa Rao, G., Begum, A., Manjusree, P., Sharma, S. V. S. P., Prasanna, L., Bhanumurthy, V.: *Satellite images for extraction of flood disaster footprints and assessing the disaster impact: Brahmaputra floods of June–July 2012, Assam, India.* Current Science, 104 (12), 1692 – 1700, 2013.

Birkett, C.M.: *Synergistic remote sensing of Lake Chad: variability of basin inundation.* Remote Sensing of Environment, 72, 218 – 236, 2000.

Bolch, T., Yao, T., Kang, S., Buchroithner,M. F., Scherer, D., Maussion, F., Huintjes, E., and Schneider, C.: *A glacier inventory for the western Nyainqentanglha Range and the Nam Co Basin, Tibet, and glacier changes 1976 – 2009*. The Cryosphere, 4, 419 – 433, doi:10.5194/tc-4-419-2010, 2010.

Carroll, M., Townshend, J., DiMiceli, C., Noojipady, P., Sohlberg, R.: *A New Global Raster Water Mask at 250 Meter Resolution.* International Journal of Digital Earth, 2 (4), http://glcf.umd.edu/data/watermask/, 2009.

Crétaux, J.F., Jelinski, W., Calmant, S., Kouraev, A., Vuglinski, V., Bergé Nguyen, M., Gennero, M.C., Nino, F., Abarca Del Rio, R., Cazenave, A., Maisongrande, P.: SOLS: *A Lake database to monitor in Near Real Time water level and storage variations from remote sensing data*. Advances in Space Research, doi:10.1016/j.asr.2011.01.004, 2011.

Da Silva, J.S., Calmant, S., Seyler, F., Filho, O.C.R., Cochonneau, G., Mansur, W.J.: *Water levels in the Amazon basin derived from the ERS-2 and ENVISAT radar altimetry missions.* Remote Sensing of Environment, 114, 2160 – 2181, 2010.

DeBarry, P. A.: *Watersheds: Processes, Assessment and Management*. John Wiley & Sons, Chapter 1, 2004.

Duong, H., Pfeifer, N., Lindenbergh, R.C: *Full waveform analysis: ICESat laser data for land cover classification.* In proceedings: ISPRS Mid0term Symposium, Remote Sensing: From pixel to process, Enschdede, The Netherlands, 31 – 35, 2006.

Duong, H., Lindenbergh, R., Pfeifer, N., Vosselman, G.: *Single and two epoch analysis of ICESat full waveform data over forested areas.* International Journal of Remote Sensing, 29, 1453 – 1473, 2008.

Duong, H.: *Processing and Application of ICESat Large Footprint Full Waveform Laser Range Data.* PhD Thesis, Delft University of Technology, The Netherlands, 2010.

Fischler, A.M., Bolles, C.R.: *Random Sample Consensus: A paradigm for model fitting with applications to image analysis and automated cartography.* Communication of the ACM, 24, 381 – 395, 1981.

Frappart, F., Calmant, S., Cauhopé, M., Seyler, F., Cazenave, A.: *Preliminary results of ENVISAT RA-2 derived water levels validation over the Amazon basin.* International Journal of Remote Sensing, 100 (2), 252 – 264, 2006.

Frauenfeld, O.W., Zhang, T., Setteze, M.C.: *Climate change and variability using European Centre for Medium-Range Weather Forecasts reanalysis (ERA-40) temperatures on the Tibetan plateau*. Journal of Geophysical Researsch, 110, doi:10.1029/2004JD005230, 2005.

Gardelle, J., Berthier, E., and Arnaud, Y.: *Slight mass gain of Karakoram glaciers in the early twenty-first century*. Nature Geoscience, 5, 322 – 325, doi:10.1038/NGEO1450, 2012.

Gardner, A.S., Moholdt, G., Cogley, J.G., Wouters, B., Arendt, A.A., Wahr, J., Berthier, E., Hock, R., Pfeffer, W.T., Kaser, G., Ligtenberg, S.R.M., Bolch, T., Sharp, M.J., Hagen, J.O., van den Broeke, M.R., Paul, F.: *A Reconciled Estimate of Glacier Contributions to Sea Level Rise: 2003 to 2009.* Science, 340 (852), 857 – 857, doi:10.1126/science.1234532, 2013.

Hwang, C., Peng, M.F., Ning, J., Luo, J., Sui, C.H.: *Lake level variations in China from Topex/Poseidon altimetry: data quality assessment and links to precipitation and ENSO.* Geophysical Journal International, 161, 1 – 11, 2005.

Immerzeel, W.W., Van Beek, L.P.H., Bierkens, M.F.P.: *Climate change will affect the Asian water towers.* Science, 328, 1382 – 1385, 2010.

Jarvis, A., H.I. Reuter, A. Nelson, E. Guevara: *Hole-filled SRTM for the globe Version 4.* The CGIAR-CSI SRTM 90m Database, http://srtm.csi.cgiar.org/, 2008.

Jekeli, C., Dumrongchai, P.: *On monitoring a vertical datum with satellite altimetry and water-level gause data on large lakes.* Journal of Geodesy, 77, 447 – 453, 2003.

Kaab, A., Berthier, E., Nuth, C., Gardelle, J., and Arnaud, Y.: *Contrasting patterns of early twenty-first-century glacier mass change in the Himalayas.* Nature, 488, 495 – 498, 2012.

Kang, S., Xu, Y., You, Q., Flugel, W.A., Pepin, N., Yao, T.: *Review of climate and cryospheric change in the Tibetan plateau.* Environmental Research Letters, 5, doi:10.1088/1748-9326/5/1/015101, 2010.

Kim, J.W., Lu, Z., Lee, H., Shum, C.K., Swarzenski, C.M., Doyle, T.W., Baek, S.H.: *Integrated analysis of PALSAR/Radarsat-1 InSAR and ENVISAT altimeter data for mapping of absolute water level changes in Louisiana wetlands.* Remote Sensing of Environment, 113, 2356 – 2365, 2009.

Krause, P., Biskop, S., Helmschrot, J., Flügel, W.A., Kang, S., Gao, T.: *Hydrological system analysis and modelling of the Nam Co basin in Tibet.* Advances in Geosciences, 27, 29 – 36, doi:10.5194/adgeo-27-29-2010, 2010.

Kropacek, J., Neckel, N., Bauder, A.: *Estimation of volume changes of mountain glaciers from ICESat data: an example from the Aletsch Glacier, Swiss Alps.* The Cryosphere Discussion, 7, 3261 – 3291, 2013.

Lay, D.C.: *Linear Algebra and its applications (3rd Edition)*. Addison Wesley, Chapter 6, 2002.

Lehner, B., Verdin, K., Jarvis, A.: *New global hydrography derived from spaceborne elevation data*. EOS, Transactions, American Geophysical Union, 89, 93 – 94, 2008.

Li, X. (submitter): *GLIMS Glacier Database.* Boulder, Colorado USA: National Snow and Ice Data Center, http://dx.doi.org/10.7265/N5V98602, 2003.

Li, X., Xu, H., Sun, Y., Zhang, D., Yang, Z.: *Lake-level change and water balance analysis at Lake Qinghai, West China during recent decades.* Water Resources Management, 21 (9), 1505–1516, 2007.

Long, S., Fatoyinbo, T.E., Policelli, F.: *Flood extent mapping for Namibia using change detection and thresholding with SAR.* Environmental Research Letters, 9, doi:10.1088/1748-9326/9/3/035002, 2014.

Medina, C.E., Gomez-Enri, J., Alonso, J.J., Villares, P.: *Water level fluctuations derived from ENVISAT radar altimeter (RA-2) and in-situ measurements in a subtropical waterbody: Lake Izabal (Guatemala).* Remote Sensing of Environment, 112, 3604 – 3617, 2008.

Mercier, F., Cazenave, A., Maheu, C.: *Inter annual lake level fluctuations (1993 – 1999) in Africa from Topex/Poseidon: connections with ocean – atmosphere interactions over the Indian Ocean.* Global and Planetary Changes, 32, 141 – 163, 2002.

Molijn, R., Lindenbergh, R., Gunter, B.: *ICESat laser full waveform analysis for the classification of land cover types over the cryosphere.* International Journal of Remote Sensing, 32 (23), 8799 – 8822, 2011.

Munyaneza, O., Wali, U.G., Uhlenbrook, S., Maskey, S., Mlotha, M.J.: *Water level monitoring using radar remote sensing data: application to Lake Kivu, central Africa.* Physics and Chemistry of the Earth, 34, 722 – 728, 2009.

Neckel, N., Kropacek, J., Bolch, T., Hochschild, V.: *Glacier mass changes on the Tibetan Plateau 2003-2009 derived from ICESat laser altimetry measurements.* Environment Research Letters, 9, http://iopscience.iop.org/1748-9326/9/1/014009, 2014.

O'Callaghan, J. F. and Mark, D. M.: *The extraction of drainage networks from digital elevation data.* Computer Vision, Graphics, and Image Processing, 28, 323 – 344, 1984.

Parkinson, C.L., Ward, A., King, M.D.: *Earth Science Reference Handbook.* National Aeronautics and Space Administration, 2006.

Pavlis, N.K., Holmes, S.A., Kenyon, S.C., Factor, J.K.: *An Earth Gravitational Model to Degree 2160: EGM2008.* The 2008 General Assembly of the European Geosciences Union, Vienna, Austria, April 13 – 18, 2008.

Ponchaut, F., Cazennave, A.: *Continental lake level variations from Topex/Poseidon (1993 – 1996).* Earth and Planetary Science, 326, 13 – 20, 1998.

Quincey, D.J., Luckman, A., Benn, D.: *Quantification of Everest region glacier velocities between 1992 and 2002, using satellite radar interferometry and feature tracking.* Journal of Glaciology, 55 (192), 596 – 606, 2009.

Radic, V. and Hock, R.: *Regionally differentiated contribution of mountain glaciers and ice caps to future sea-level rise.* Nature Geoscience, 4, 91 – 94, 2011.

Schutz, B.E.: *Laser footprint location (geolocation) and surface profiles – Technical report of Geoscience Laser Altimeter System (GLAS).* Center for Space Research, The University of Texas at Austin, 2002.

Schutz, B.E., Zwally, H.J., Shuman, C.A., Hancock, D., DiMarzio, J. P.: *Overview of the ICESat Mission.* Geophysical Research Letters, 32, doi:10.1029/2005GL024009, 2005.

Shi, Y., Liu C., Kang, E.: *The glacier Inventory of China.* Annals of Glaciology, 50 (53), 1 – 4, 2009.

Shi, J., Menenti, M., Lindenbergh, R.C.: *Parameterization of Surface Roughness Based on ICESat/GLAS Full Waveforms: A Case Study on the Tibetan Plateau.* Journal of Hydrometeorology, 14 (4), 1278 – 1292, http://dx.doi.org/10.1175/JHM-D-12-0130.1, 2013.

Sinnott, R.W.: *Virtues of the Haversine.* Sky and Telescope, 68 (2), page 159, 1984.

Slobbe, D.C., Lindenbergh, R.C., Ditmar, P.: *Estimation of volume change rates of Greenland's ice sheet from ICESat data using overlapping footprints.* Remote Sensing of Environment, 112 (12), 4204 – 4213, 2008.

Sorg, A., Bolch, T., Stoffel, M., Solomina, O., and Beniston, M.: *Climate change impacts on glaciers and runoff in Tien Shan (Central Asia).* Nature Climate Change, 2, 725 – 731, 2012.

Tao, N., Longxun, C., Zijiang, Z.: *The characteristics of climate change over the Tibetan plateau in the last 40 years and the detection of climatic jumps.* Advances in Atmospheric Sciences, 21 (2), 193 – 203, 2004.

Tartari, G., Salerno, F., Buraschi E., Bruccoleri, G., Smiraglia, C.: *Lake surface area variations in the North-Eastern sector of Sagarmatha National Park (Nepal) at the end of the 20th Century by comparison of historical maps.* Journal of Limnology, 67 (2), 139 – 154, 2008.

Teunissen, P.J.G.: *Adjustment theory: an introduction.* VSSD, Chapter 2, 2003.

Tian, H., Yang, T., Liu, Q.: *Climate change and glacier area shrinkage in the Qilian mountains, China, from 1956 to 2010.* Annals of Glaciology, 55 (66), 187 – 197, 2014.

Urban, T.J., Schutz, B.E., Neuenschwander, A.L.: *A survey of ICESat coastal altimetry applications: continental coast, open ocean island, and inland river.* Journal of Terrestrial, Atmospheric, and Oceanic Sciences, 19, 1 – 2, 2008.

Verdin, K.L., Godt, J.W., Funk, C., Pedreros, D., Worstell, B., Verdin, J.: *Development of a global slope dataset for estimation of landslide occurrence resulting from earthquakes.* Colorado: U.S. Geological Survey, Open-File Report 2007 – 1188, 2007.

Wang, P., Li, Z., Gao, W.: *Rapid shrinking of glaciers in the Middle Qilian Mountain region of Northwest China during the last ~50 years.* Journal of Earth Science, 22, 539 – 548, 2011.

Wang, X., Gong, P., Zhao, Y., Xu, Y., Chang, X., Niu, Z.,Luo, Z., Huang, H., Sun, F., and Li, X.: *Water-level changes in China's large lakes determined from ICESat/GLAS data.* Remote Sensing of Environment, 132, 131 – 144, 2013.

Wei, J., Liu, S., Gou, W., Yao, X., Xu, J., Bao, W., Jiang, Z.: *Surface-area changes of glaciers in the Tibetan Plateau interior area since the 1970s using recent Landsat images and historical maps.* Annals of Glaciology, 55 (56), 213 – 222, 2014.

Xu, J.C., Shrestha, A., Vaidya, R., Eriksson, M., Hewitt, K.: *The melting Himalayas: regional challenges and local impacts of climate change on mountain ecosystems and livelihoods.* ICIMOD Technical Paper, Kathmandu: ICIMOD, 2007.

Yao, T., Thompson, L., Yang, W., Yu, W., Gao, Y., Gou, X., Yang, X., Duan, K., Zhao, H., Xu, B., Pu, J., Lu, A., Xiang, Y., Kattel, D. B., and Joswiak, D.: *Different glacier status with atmospheric circulations in Tibetan Plateau and surroundings*. Nature Climate Change, 2, 663 – 667, 2012.

Ye, Q., Zhong, Z., Kang, S., Stein, A., Wei, Q., Liu, J.: *Monitoring glacier and supra-glacier lakes from space in Mt. Qomolangma Region of the Himalayas on the Tibetan plateau in China.* Journal of Mountain and Science, 6, 211 – 220, 2009.

Zandbergen, P.: *Applications of Shuttle Radar Topography Mission Elevation Data.* Geography Compass, 2 (5), 1404 – 1431, 2008.

Zhang, J., Xu, K., Yang, Y., Qi, L., Hayashi, S., Wantanabe, M.: *Measuring water storage fluctuations in Lake Dongting, China, by Topex/Poseidon satellite altimetry.* Environmental Monitoring and Assessment, 115, 25 – 37, 2006.

Zhang, G., Yao, T., Xie, H., Kang, S., and Lei, Y.: *Increased mass over the Tibetan Plateau: From lakes or glaciers?* Geophysical Research Letters, 40, 2125 – 2130, doi:10.1002/grl.50462, 2013.

Zhang, G.Q., Xie, H.J., Kang, S.C., Yi, D.H., Ackley, S.F.: *Monitoring lake level changes on the Tibetan Plateau using ICESat altimetry data (2003-2009).* Remote Sensing of Environment, 115, 1733 – 1742, 2011.

Zhang, Y., Liu, S., Xu, J., Shangguan, D.: *Glacier change and glacier runoff variation in the Tuotuo River basin, the source region of Yangtze River in western China.* Environmental Geology, 56, 59 – 68, 2008.

Zhisheng, A., Kutzbach J.E., Prell W.L., Porter S.C.: *Evolution of Asian monsoons and phased uplift of the Himalaya – Tibetan plateau since Late Miocene times.* Nature, 411, 62 – 66, 2001.

Zhou, S. Q., Kang, S. C., Gao, T. G., and Zhang, G. S.: *Response of Zhadang Glacier runoff in Nam Co Basin, Tibet, to changes in air temperature and precipitation form*. Chinese Science Bulletin, 55, 2103 – 2110, 2010.

Zwally, H., Schutz, R., Bentley, C., Bufton, J., Herring, T., Minster, J., Spinhirne, J., Thomas, R.: *GLAS/ICESat L2 Global Land Surface Altimetry Data*. Boulder, Colorado USA: National Snow and Ice Data Center, 2011.

Websites

GLAS: Geoscience Laser Altimeter System. Last visiting on April 2014. Link: http://glas.gsfc.nasa.gov/

GLIMS: Global Land Ice Measurements from Space. Last visiting on April 2014. Link: http://www.glims.org/

HydroSHEDS: USGS – Hydrological data and maps based on Shuttle Elevation Derivatives at multiple Scales. Last visiting on April 2014. Link: http://hydrosheds.cr.usgs.gov/index.php

NASA: National Aeronautics and Space Administration - ICESat. Last visiting on April 2014. Link: http://icesat.gsfc.nasa.gov/icesat/

NSIDC: National Snow and Ice Data Center. Last visiting on April 2014. Link: https://nsidc.org/data/icesat/

USGS: United State Geological Survey – The Water Cycle. Last visiting on April 2014. Link: http://water.usgs.gov/edu/watercycle.html

Yale: Environment 360 of Yale Education. Last visiting on April 2014. Link: http://e360.yale.edu/content/images/0710-breashears-kyetrak-comp.html

Publications

Phan, V.H., Lindenberg, R.C., Menenti, M.: *ICESat derived elevation changes of Tibetan lakes between 2003 and 2009*. International Journal of Applied Earth Observation and Geoinformatics, 17, 12 – 22, 2012.

Phan, V. H., Lindenbergh, R. C., and Menenti, M.: *Seasonal trends in Tibetan lake level changes as observed by ICESat laser altimetry.* ISPRS – International Annals of the Photogrammetry, Remote Sensing and Spatial Information Sciences, 1, 237 – 242, 2012.

Phan, V.H., Lindenbergh, R.C., Menenti, M.: *Determining geometric links between glaciers and lakes on the Tibetan Plateau.* Proceedings of the International Workshop on Terrestrial Water Cycle Observation and Modeling from Space: Innovation and Reliability of Data Products, Beijing, China, 26 – 30 April, 2013.

Phan, V.H, Lindenbergh, R.C., Menenti, M.: *Geometric dependency of Tibetan lakes on glacier runoff.* Hydrology and Earth System Sciences, 17, 4061 – 4077, 2013.

Song, C., Huang B., Richards, K., Ke, L., Phan, V.H.: *Accelerated lake expansion on the Tibetan Plateau in the 2000s: Induced by glacial melting or other processes.* Water Resurces Research, doi:10.1002/2013WR014724, 2014.

Phan, V.H., Lindenbergh, R.C., Menenti, M.: *Orientation dependent glacial changes at the Tibetan Plateau derived from 2003 – 2009 ICESat laser altimetry*. The Cryosphere Discussion, 8, 2425 – 2463, doi:10.5194/tcd-8-2425-2014, 2014.

Appendix A

Table A: Rates of glacial thickness changes on the Tibetan Plateau between 2003 and 2009

	Glacial area				S ≤ 15 deg and R ≤ 15 m					S ≤ 20 deg and R ≤ 15 m					S ≤ 25 deg and R ≤ 15 m				
No.	Lat.	Lon.	Orient.	Basin	N	$\dot{V}$ (m/yr)	s_{vv} (m/yr)	RMSE (m)	k	N	$\dot{V}$ (m/yr)	s_{vv} (m/yr)	RMSE (m)	k	N	$\dot{V}$ (m/yr)	s_{vv} (m/yr)	RMSE (m)	k
1	28.2483	90.5435	N	Brahmaputra						71	-0.14	0.40	7.13	0.0080	111	0.70	0.40	6.12	0.0124
2	30.3370	93.6944	N	Brahmaputra						75	2.38	0.38	6.37	0.0034	98	2.30	0.56	8.08	0.0045
3	30.3640	93.9454	N	Brahmaputra											63	0.32	1.00	7.83	0.0038
4	28.0525	90.5693	NE	Brahmaputra						63	-0.48	0.61	3.76	0.0094	82	-0.67	0.59	7.12	0.0122
5	29.2107	97.3078	NE	Brahmaputra						73	-1.06	0.73	7.91	0.0087	87	-3.04	0.65	5.82	0.0104
6	29.3733	96.6197	NE	Brahmaputra	128	-0.26	0.42	4.18	0.0024	181	-1.56	0.49	6.12	0.0033	187	-1.56	0.48	6.39	0.0034
7	29.7669	82.8037	NE	Brahmaputra	248	-1.04	0.31	2.51	0.0138	262	-1.09	0.33	2.33	0.0146	273	-1.10	0.40	2.38	0.0152
8	27.9793	92.7260	E	Brahmaputra											86	0.26	0.76	7.31	0.0040
9	29.6202	96.0862	E	Brahmaputra						76	-2.03	0.73	0.32	0.0043	102	-2.68	0.81	1.82	0.0057
10	30.3395	93.1502	E	Brahmaputra											75	0.94	0.65	5.96	0.0181
11	30.3670	93.8065	E	Brahmaputra											52	0.39	0.93	6.06	0.0037
12	30.6042	95.2404	E	Brahmaputra											62	-0.44	0.70	3.27	0.0104
13	30.1126	90.2632	SE	Brahmaputra											54	0.30	0.86	5.95	0.0185
14	30.1705	90.2812	SE	Brahmaputra											58	-2.86	0.50	6.67	0.0183
15	30.4785	94.6782	SE	Brahmaputra	369	-0.81	0.28	4.83	0.0030	444	-0.97	0.32	4.44	0.0036	557	-1.24	0.44	3.94	0.0045
16	28.1838	90.5439	S	Brahmaputra	195	-0.72	0.36	6.80	0.0142	261	-0.09	0.39	8.68	0.0190	309	0.12	0.43	9.15	0.0226
17	28.0152	88.3758	N	Ganges						61	-0.95	0.81	2.63	0.0239	88	-2.11	0.69	3.15	0.0345
18	28.0554	86.8359	N	Ganges	189	-1.77	0.32	4.77	0.0091	239	-2.09	0.36	7.61	0.0115	328	-1.23	0.42	9.64	0.0157
19	28.3360	86.3018	N	Ganges	84	-0.06	0.20	2.12	0.0117	93	0.12	0.25	4.64	0.0129	103	0.01	0.25	3.09	0.0143
20	30.4692	81.3096	N	Ganges	94	-0.71	0.52	3.63	0.0212	99	-0.74	0.54	3.40	0.0223	108	-0.53	0.46	3.25	0.0243
21	31.0027	79.2772	N	Ganges	207	-1.61	0.20	4.95	0.0139	236	-1.39	0.23	4.87	0.0158	250	-1.37	0.31	5.00	0.0168
22	28.6863	85.4509	NE	Ganges											70	-0.39	0.36	6.90	0.0117
23	28.1540	86.7890	E	Ganges						74	-0.17	0.52	2.97	0.0110	99	-0.36	0.52	4.28	0.0147

	Glacial area				S ≤ 15 deg and R ≤ 15 m					S ≤ 20 deg and R ≤ 15 m					S ≤ 25 deg and R ≤ 15 m				
No.	Lat.	Lon.	Orient.	Basin	N	V (m/yr)	s_{vv} (m/yr)	RMSE (m)	k	N	V (m/yr)	s_{vv} (m/yr)	RMSE (m)	k	N	V (m/yr)	s_{vv} (m/yr)	RMSE (m)	k
24	28.2613	86.2958	S	Ganges	261	-2.01	0.30	3.91	0.0228	323	-1.83	0.37	3.40	0.0283	361	-1.82	0.40	3.41	0.0316
25	30.4152	81.3064	S	Ganges	75	-0.38	0.68	5.91	0.0260	80	-0.90	0.69	5.83	0.0278	82	-0.94	0.70	5.81	0.0285
26	31.1669	79.3033	NW	Ganges											72	1.19	0.69	9.28	0.0418
27	34.1788	78.9947	N	Indus						77	0.74	0.35	2.12	0.0280	109	1.43	0.40	3.26	0.0396
28	32.7876	81.0514	E	Indus	60	-0.69	0.51	3.01	0.0111	128	0.65	0.71	4.86	0.0237	169	0.13	0.72	5.11	0.0313
29	34.0527	79.7882	E	Indus	178	-0.05	0.19	1.59	0.0761	185	-0.07	0.20	1.51	0.0791	191	0.03	0.20	2.77	0.0817
30	34.2232	79.8126	S	Indus	106	-0.11	0.01	1.67	0.1105	106	-0.11	0.01	1.67	0.1105	106	-0.11	0.01	1.67	0.1105
31	34.0245	79.7631	SW	Indus	63	-0.85	0.39	2.20	0.0186	79	-1.38	0.43	2.73	0.0234	87	-1.47	0.47	3.22	0.0257
32	31.1226	83.4559	N	Inner plateau	58	-1.31	0.50	2.55	0.0117	68	-0.71	0.47	3.61	0.0138	74	-0.69	0.48	2.77	0.0150
33	33.9313	90.4148	N	Inner plateau	49	0.38	0.38	2.69	0.0154	63	0.48	0.46	3.17	0.0198	68	0.62	0.49	4.24	0.0213
34	34.3265	81.9460	N	Inner plateau	150	0.25	0.38	3.07	0.0355	168	0.21	0.47	2.25	0.0398	193	0.55	0.49	3.64	0.0457
35	34.5128	80.7636	N	Inner plateau											79	-1.77	0.89	6.89	0.0428
36	35.6960	85.6129	N	Inner plateau	220	-0.34	0.24	0.98	0.0167	257	-0.04	0.24	2.85	0.0195	284	0.09	0.25	5.08	0.0216
37	36.0994	90.9355	N	Inner plateau	444	-0.41	0.20	2.62	0.0090	494	-0.55	0.22	2.88	0.0100	531	-0.48	0.25	2.73	0.0107
38	30.9295	82.9716	NE	Inner plateau	48	-1.38	1.15	3.90	0.0064	74	-1.13	0.82	4.28	0.0099	97	-1.59	0.69	5.86	0.0130
39	33.6898	82.4899	NE	Inner plateau											68	-2.43	1.35	4.81	0.0236
40	34.3768	79.8450	NE	Inner plateau	138	0.16	0.39	3.38	0.0161	210	-0.03	0.46	1.85	0.0246	245	0.17	0.51	2.06	0.0287
41	30.6121	86.4643	E	Inner plateau						46	-4.38	0.98	5.99	0.0042	60	-1.94	0.99	5.89	0.0054
42	30.9359	83.4939	E	Inner plateau	55	0.43	0.78	6.44	0.0181	83	1.63	0.58	9.21	0.0273	93	2.12	0.76	7.79	0.0306
43	33.3058	91.3293	SE	Inner plateau											62	-3.15	1.18	4.60	0.0321
44	33.4696	86.7921	SE	Inner plateau											53	-1.37	0.81	5.38	0.0226
45	35.4881	82.1995	SE	Inner plateau	58	0.91	0.83	2.54	0.0140	100	1.01	0.87	5.04	0.0242	132	2.45	0.67	7.54	0.0320
46	35.5528	89.6168	SE	Inner plateau	161	0.12	0.40	3.03	0.0176	192	-0.06	0.61	4.45	0.0210	212	-0.48	0.69	4.40	0.0232
47	35.8736	91.4318	SE	Inner plateau	46	1.01	0.45	3.49	0.0184	85	0.18	0.61	3.67	0.0340	101	-0.13	0.59	4.28	0.0404
48	33.9128	90.6589	S	Inner plateau	57	-0.59	0.20	3.16	0.0269	92	-0.47	0.20	3.92	0.0433	105	-0.05	0.20	4.74	0.0495
49	34.2879	81.9455	S	Inner plateau	63	1.54	0.49	2.56	0.0188	106	1.23	0.49	2.76	0.0316	116	1.23	0.49	2.83	0.0346
50	35.2841	80.6850	S	Inner plateau	815	-1.41	0.27	4.65	0.0078	998	-1.02	0.29	4.19	0.0096	1150	-0.84	0.30	4.08	0.0111
51	35.4700	82.1430	S	Inner plateau	67	1.18	1.13	2.67	0.0198	92	-1.50	0.79	4.41	0.0271	118	-1.30	0.66	5.56	0.0348
52	35.6549	85.6200	S	Inner plateau	55	2.01	0.63	3.82	0.0046	118	1.82	0.48	5.08	0.0100	159	1.69	0.54	5.34	0.0134
53	36.7727	84.9026	S	Inner plateau						59	-0.13	0.56	2.89	0.0246	80	0.13	0.62	5.10	0.0333

	Glacial area				S ≤ 15 deg and R ≤ 15 m					S ≤ 20 deg and R ≤ 15 m					S ≤ 25 deg and R ≤ 15 m				
No.	Lat.	Lon.	Orient.	Basin	N	V (m/yr)	s_{vv} (m/yr)	RMSE (m)	k	N	V (m/yr)	s_{vv} (m/yr)	RMSE (m)	k	N	V (m/yr)	s_{vv} (m/yr)	RMSE (m)	k
54	34.3105	85.8384	SW	Inner plateau	284	0.60	0.17	2.27	0.0358	310	0.81	0.20	2.66	0.0391	322	0.76	0.20	3.37	0.0406
55	35.3008	81.4300	SW	Inner plateau	574	-0.26	0.19	1.71	0.0270	635	-0.29	0.20	1.73	0.0298	661	-0.31	0.20	1.93	0.0311
56	31.0217	83.4683	W	Inner plateau	139	-0.14	0.28	3.80	0.0113	160	-0.46	0.36	3.56	0.0130	189	-0.59	0.46	4.31	0.0153
57	34.7324	82.3218	W	Inner plateau	245	-0.70	0.30	1.71	0.0165	294	-0.39	0.34	2.72	0.0198	311	-0.50	0.39	3.07	0.0210
58	33.4831	86.7867	NW	Inner plateau											51	1.17	0.99	2.79	0.0318
59	34.3519	79.9857	NW	Inner plateau	226	0.21	0.22	2.58	0.0319	242	0.11	0.25	3.69	0.0342	266	0.31	0.25	8.13	0.0375
60	34.3766	85.8347	NW	Inner plateau											74	-0.57	0.72	3.62	0.0169
61	33.5516	94.7536	N	Mekong											74	-1.01	0.48	6.18	0.0246
62	31.7083	95.8596	NE	Mekong											44	-2.88	0.35	9.63	0.0245
63	31.0089	93.8679	N	Salween											51	0.35	0.71	7.51	0.0150
64	30.9253	93.8699	NE	Salween											53	-0.99	0.78	3.56	0.0158
65	30.6792	94.6483	E	Salween						58	-0.78	0.81	4.18	0.0250	66	-0.45	0.87	3.79	0.0285
66	30.7695	94.6702	E	Salween											39	-0.54	0.46	3.49	0.0118
67	35.2281	78.6456	N	Tarim Basin											54	-2.36	0.63	2.04	0.0134
68	35.3878	81.3971	N	Tarim Basin	575	-0.18	0.28	1.16	0.0075	633	-0.09	0.30	1.44	0.0082	656	-0.08	0.31	1.57	0.0085
69	35.4884	77.6894	N	Tarim Basin	162	-0.31	0.20	3.94	0.0269	185	-0.61	0.26	5.16	0.0307	199	-0.79	0.33	5.54	0.0330
70	35.5083	81.6237	N	Tarim Basin	341	0.38	0.25	1.45	0.0240	380	0.58	0.28	1.79	0.0267	404	0.43	0.31	2.02	0.0284
71	35.5157	82.1624	N	Tarim Basin						77	-1.02	0.43	5.07	0.0107	129	2.32	0.56	7.49	0.0179
72	35.5234	80.7134	N	Tarim Basin	1120	0.50	0.24	3.62	0.0076	1320	0.69	0.30	3.38	0.0090	1497	0.69	0.34	3.01	0.0102
73	35.6376	80.0381	N	Tarim Basin	308	0.54	0.20	2.16	0.0312	343	0.60	0.33	2.08	0.0348	373	0.89	0.41	2.90	0.0378
74	35.6398	77.1217	N	Tarim Basin	77	-0.91	0.27	2.33	0.0011	116	0.22	0.33	2.23	0.0016	190	-0.33	0.34	3.98	0.0027
75	35.7032	77.6240	N	Tarim Basin											76	-0.49	0.53	2.78	0.0157
76	35.7379	76.8019	N	Tarim Basin						59	-0.78	0.40	7.49	0.0012	73	-0.98	0.50	9.06	0.0015
77	35.7461	78.7394	N	Tarim Basin	70	0.45	0.42	3.12	0.0147	116	2.10	0.46	7.16	0.0244	145	1.97	0.64	4.31	0.0305
78	35.7896	93.3675	N	Tarim Basin											76	1.23	0.68	10.17	0.0364
79	35.8122	77.1481	N	Tarim Basin						47	0.19	0.57	3.16	0.0198	66	0.05	0.54	2.80	0.0278
80	35.9110	91.4375	N	Tarim Basin											59	-3.40	0.86	2.49	0.0166
81	35.9285	77.1800	N	Tarim Basin	143	0.46	0.29	1.32	0.0060	187	0.25	0.36	5.32	0.0079	236	-0.47	0.38	6.06	0.0099
82	35.9310	80.8954	N	Tarim Basin	45	-0.74	0.57	2.05	0.0126	69	-0.86	0.60	2.32	0.0194	88	0.09	0.54	2.98	0.0247
83	36.0723	79.3273	N	Tarim Basin						56	1.25	0.51	3.09	0.0070	80	2.56	0.75	5.19	0.0101

	Glacial area				S ≤ 15 deg and R ≤ 15 m					S ≤ 20 deg and R ≤ 15 m					S ≤ 25 deg and R ≤ 15 m				
No.	Lat.	Lon.	Orient.	Basin	N	V (m/yr)	s_{vv} (m/yr)	RMSE (m)	k	N	V (m/yr)	s_{vv} (m/yr)	RMSE (m)	k	N	V (m/yr)	s_{vv} (m/yr)	RMSE (m)	k
84	36.1386	75.9995	N	Tarim Basin	470	0.92	0.27	5.71	0.0028	528	0.99	0.28	6.69	0.0031	576	1.15	0.29	6.30	0.0034
85	36.4774	75.9075	N	Tarim Basin						52	0.00	0.63	2.98	0.0071	76	0.04	0.49	3.23	0.0103
86	36.5223	77.4777	N	Tarim Basin	93	-0.12	0.49	2.87	0.0070	106	-0.05	0.50	3.21	0.0079	129	0.30	0.49	3.36	0.0096
87	36.6339	91.1211	N	Tarim Basin						127	1.38	0.53	5.72	0.0087	204	1.13	0.54	6.73	0.0140
88	36.8127	84.8954	N	Tarim Basin						52	0.03	0.78	2.44	0.0164	70	-1.55	0.77	5.35	0.0221
89	36.9845	75.2616	N	Tarim Basin						62	-0.42	0.66	2.46	0.0117	66	-0.35	0.65	1.89	0.0125
90	37.0809	75.2591	N	Tarim Basin	49	-0.44	0.69	1.44	0.0104	67	-0.54	0.70	4.04	0.0143	103	0.46	1.00	5.47	0.0220
91	37.3722	87.7941	N	Tarim Basin	91	0.06	0.25	2.34	0.0477	92	0.07	0.25	2.34	0.0482	98	0.11	0.25	2.04	0.0514
92	37.3798	87.7196	N	Tarim Basin	49	0.63	0.29	1.05	0.0080	63	0.06	0.30	3.52	0.0102	70	0.17	0.31	2.51	0.0114
93	37.5106	87.8260	N	Tarim Basin						107	0.13	0.39	4.83	0.0466	137	0.57	0.56	5.02	0.0597
94	38.1895	96.3351	N	Tarim Basin	138	-0.57	0.31	3.04	0.0113	157	-0.33	0.31	2.36	0.0129	181	-0.68	0.35	3.12	0.0149
95	39.2061	73.5100	N	Tarim Basin	85	-1.03	0.50	4.29	0.0371	111	-0.47	0.50	4.91	0.0484	112	-0.47	0.50	5.00	0.0489
96	36.0925	80.1294	NE	Tarim Basin											52	0.49	0.42	6.64	0.0120
97	36.4999	91.3473	NE	Tarim Basin											85	-1.10	0.85	4.43	0.0229
98	36.5810	77.2859	NE	Tarim Basin											53	-0.25	0.52	5.22	0.0143
99	36.8056	76.6516	NE	Tarim Basin						73	0.75	0.34	3.43	0.0244	94	1.73	0.47	3.23	0.0314
100	37.7371	101.4823	NE	Tarim Basin						39	1.69	0.57	5.63	0.0173	57	1.12	0.54	5.25	0.0253
101	38.2362	89.2855	NE	Tarim Basin											60	0.90	0.52	6.36	0.0304
102	38.2380	95.9301	NE	Tarim Basin						65	0.81	0.70	6.49	0.0300	80	0.05	0.64	6.64	0.0370
103	35.9769	78.9192	E	Tarim Basin						49	1.10	0.61	7.50	0.0136	77	1.83	0.66	6.87	0.0214
104	36.7870	75.8619	E	Tarim Basin						96	1.09	0.50	4.84	0.0163	135	1.17	0.54	5.37	0.0229
105	37.6474	88.2015	E	Tarim Basin						52	0.21	0.44	3.22	0.0403	60	-0.13	0.60	4.74	0.0466
106	35.4097	81.6117	SE	Tarim Basin	301	-0.42	0.41	2.98	0.0296	338	-0.44	0.44	3.46	0.0332	360	-0.51	0.51	4.05	0.0354
107	38.8890	73.9813	SE	Tarim Basin											46	0.27	0.49	2.65	0.0430
108	39.3418	73.5386	SE	Tarim Basin	99	1.97	0.60	2.08	0.0140	135	1.34	0.84	2.64	0.0191	164	-0.85	0.86	4.64	0.0232
109	36.0236	90.9623	S	Tarim Basin	381	-0.66	0.36	3.07	0.0072	428	-0.80	0.38	7.03	0.0081	487	-1.12	0.47	7.59	0.0092
110	38.8333	74.9679	SW	Tarim Basin	142	0.06	0.38	2.27	0.0259	145	0.09	0.39	2.03	0.0265	146	-0.03	0.39	2.23	0.0267
111	35.7742	77.1298	W	Tarim Basin	65	0.98	0.34	2.12	0.0046	93	0.06	0.57	4.74	0.0066	138	0.11	0.68	7.20	0.0098
112	36.3990	78.8542	W	Tarim Basin	88	0.14	0.25	2.72	0.0287	116	-0.07	0.44	3.27	0.0378	139	-0.23	0.39	3.49	0.0453
113	38.2403	75.0779	W	Tarim Basin											107	-1.13	0.96	5.50	0.0048

	Glacial area				S ≤ 15 deg and R ≤ 15 m					S ≤ 20 deg and R ≤ 15 m					S ≤ 25 deg and R ≤ 15 m				
No.	Lat.	Lon.	Orient.	Basin	N	$\bar{V}$ (m/yr)	s_{vv} (m/yr)	RMSE (m)	k	N	$\bar{V}$ (m/yr)	s_{vv} (m/yr)	RMSE (m)	k	N	$\bar{V}$ (m/yr)	s_{vv} (m/yr)	RMSE (m)	k
114	39.0528	74.9451	W	Tarim Basin											43	2.05	1.42	5.01	0.0038
115	36.6042	77.4907	NW	Tarim Basin	96	1.24	0.27	2.64	0.0199	129	0.77	0.48	3.70	0.0267	156	-0.58	0.50	5.86	0.0323
116	38.7759	73.9556	NW	Tarim Basin						66	-1.96	0.51	2.38	0.0403	105	-0.41	0.94	7.20	0.0641
117	38.9077	73.9818	NW	Tarim Basin											58	0.56	0.62	6.39	0.0465
118	33.4012	91.3401	N	Yangtze	108	-0.61	0.54	3.41	0.0431	135	-1.67	0.48	3.91	0.0538	169	-0.96	0.48	3.95	0.0674
119	33.9536	90.6697	N	Yangtze	324	-0.48	0.29	3.19	0.0323	342	-0.60	0.30	3.23	0.0341	354	-0.61	0.32	3.55	0.0353
120	29.6724	101.9318	E	Yangtze	70	-0.39	0.59	4.23	0.0017	101	-0.45	0.48	5.14	0.0025	121	-0.67	0.54	7.19	0.0030
121	33.1281	92.1241	E	Yangtze	98	-1.19	0.53	2.25	0.0272	131	-1.37	0.55	2.92	0.0363	158	-0.59	0.56	4.30	0.0438
122	33.0758	92.1159	S	Yangtze	42	-0.98	0.77	3.64	0.0189	67	-1.63	0.49	4.54	0.0301	83	-0.46	0.59	6.37	0.0373

Appendix B

Table B1: Rates of individual lake level changes between 2003 and 2009 on the Tibetan Plateau

No.	Lat.	Lon.	Basin	Lake Name	Lake area [km^2]	Threshold = 15 [cm]		Threshold = 25 [cm]		Threshold = 35 [cm]	
						Rate [m a^{-1}]	RMSE [m]	Rate [m a^{-1}]	RMSE [m]	Rate [m a^{-1}]	RMSE [m]
1	30.0257	93.9973	Brahmaputra	Draksum Tso	25.973	-0.423	1.087	-0.436	1.091	-0.367	1.074
2	29.0117	90.4565	Brahmaputra	Gongmo Tso	39.791	0.020	0.179	0.025	0.188	-0.001	0.183
3	28.5596	90.3925	Brahmaputra	Phuma Tso	283.629	-0.039	0.241	0.005	0.426	0.005	0.427
4	29.8884	85.2471	Brahmaputra	Trengcham Tso	7.128	0.124	0.279	0.117	0.264	0.127	0.255
5	28.9790	90.7171	Brahmaputra	Yamdrok Tso	607.186	-0.380	0.568	-0.392	0.572	-0.398	0.538
6	28.3753	86.3064	Ganges	Lama Tso	3.721	-0.092	0.278	-0.088	0.290	-0.087	0.291
7	28.8982	85.5849	Ganges	Palku Tso	276.602	-0.118	0.259	-0.072	0.346	-0.071	0.345
8	34.1528	79.7836	Indus	Dyap Tso	113.923	0.135	0.373	0.132	0.365	0.140	0.352
9	30.6344	82.1228	Indus	Konggyu Tso	59.907	-0.087	0.272	-0.088	0.279	-0.088	0.275
10	30.6725	81.4876	Indus	Mapham Tso	412.796	-0.043	0.288	-0.045	0.293	-0.043	0.295
11	33.6060	79.7017	Indus	Pang Gong Tso	441.236	0.086	0.616	0.091	0.608	0.098	0.601
12	33.5384	78.8605	Indus	Pangur Tso	54.553	0.085	0.405	0.086	0.436	0.092	0.448
13	32.7559	81.7289	Indus		57.847	0.121	0.232	0.122	0.229	0.110	0.219
14	31.5787	80.9865	Indus		13.524	0.113	0.584	0.116	0.541	0.017	0.598

No.	Lat.	Lon.	Basin	Lake Name	Lake area [km^2]	**Threshold = 15 [cm]**		**Threshold = 25 [cm]**		**Threshold = 35 [cm]**	
						Rate [m a^{-1}]	RMSE [m]	Rate [m a^{-1}]	RMSE [m]	Rate [m a^{-1}]	RMSE [m]
15	33.3926	79.3600	Indus		5.053	0.099	0.561	0.100	0.572	0.098	0.552
16	33.4336	80.4694	Indus		3.865	-0.008	0.736	0.058	0.818	0.064	0.816
17	33.0985	80.1782	Indus		6.075	-0.142	0.414	-0.115	0.386	-0.111	0.377
18	33.0902	80.3916	Indus		13.629	-0.281	0.728	-0.278	0.726	-0.275	0.724
19	37.0671	88.4306	Inner plateau	Achik Kul	354.791	0.294	0.371	0.292	0.366	0.294	0.365
20	35.2084	79.8281	Inner plateau	Aksai Chin Kul	164.234	0.502	0.359	0.504	0.361	0.504	0.362
21	32.0229	91.4820	Inner plateau	Amdi Tsonak Tso	187.849	0.023	0.490	0.036	0.493	0.033	0.492
22	30.9801	82.2325	Inner plateau	Arkok Tso	58.428	-0.087	0.283	-0.090	0.293	-0.090	0.284
23	34.0106	82.3669	Inner plateau	Arku Tso	105.076	0.036	0.360	0.033	0.358	0.036	0.350
24	37.5462	89.3726	Inner plateau	Ayakum Kul	631.058	0.182	0.198	0.186	0.205	0.188	0.195
25	30.9367	89.6754	Inner plateau	Bul Tso	103.521	0.370	0.481	0.364	0.474	0.365	0.475
26	31.8236	88.2480	Inner plateau	Chagut Tso	87.861	-0.040	0.388	-0.046	0.370	-0.049	0.368
27	32.1953	87.7718	Inner plateau	Chanjun Tso	35.698	0.558	0.252	0.559	0.246	0.562	0.247
28	34.0141	81.5995	Inner plateau	Charol Tso	346.353	0.312	0.212	0.319	0.202	0.321	0.206
29	31.3774	87.8936	Inner plateau	Chikut Tso	73.069	-0.005	0.350	-0.004	0.350	0.000	0.470
30	31.9484	90.3365	Inner plateau	Chodjari Tso	29.200	0.293	0.312	0.295	0.307	0.295	0.301
31	31.2766	83.4299	Inner plateau	Chovo Tso	181.928	0.114	0.207	0.114	0.206	0.115	0.198
32	36.9781	95.2047	Inner plateau	Dabsan Nor	290.922	0.034	0.310	0.041	0.353	0.041	0.347

No.	Lat.	Lon.	Basin	Lake Name	Lake area [km^2]	Threshold = 15 [cm]		Threshold = 25 [cm]		Threshold = 35 [cm]	
						Rate [m a^{-1}]	RMSE [m]	Rate [m a^{-1}]	RMSE [m]	Rate [m a^{-1}]	RMSE [m]
33	31.0601	86.6010	Inner plateau	Dangra Tso	823.731	0.291	0.572	0.295	0.573	0.296	0.570
34	36.1895	88.1413	Inner plateau	Dekirpa Kul	24.414	0.189	0.434	0.192	0.429	0.192	0.427
35	34.9514	81.5643	Inner plateau	Echil Kul	106.581	0.727	0.378	0.728	0.367	0.737	0.375
36	38.1146	90.7815	Inner plateau	Gaekel Tso	124.335	0.002	0.409	0.044	0.369	0.028	0.370
37	31.8063	88.9496	Inner plateau	Garing Tso	1821.133	0.680	0.338	0.681	0.338	0.682	0.339
38	34.4334	82.3369	Inner plateau	Gore Tso	23.049	0.387	0.386	0.381	0.390	0.377	0.384
39	31.7128	88.0035	Inner plateau	Jagok Tso	346.132	-0.046	0.387	-0.048	0.386	-0.048	0.388
40	35.5810	91.1244	Inner plateau	Kekexili Tso	301.004	0.293	0.258	0.295	0.257	0.293	0.259
41	33.9487	80.9020	Inner plateau	Kenze Tso	105.528	0.303	0.144	0.302	0.144	0.305	0.148
42	38.3051	97.5962	Inner plateau	Khara Nor	586.663	0.158	0.163	0.160	0.165	0.161	0.170
43	31.1341	88.3068	Inner plateau	Kyaring Tso	476.197	-0.012	0.655	-0.013	0.653	-0.008	0.665
44	32.0298	84.1162	Inner plateau	Lakok Tso	94.482	0.202	0.160	0.205	0.151	0.202	0.149
45	35.7494	90.1903	Inner plateau	Lexiewuda Tso	224.935	0.394	0.169	0.388	0.169	0.390	0.176
46	30.9874	90.9674	Inner plateau	Long Gyok Tso	5.917	0.060	0.456	0.080	0.452	0.060	0.429
47	35.6927	87.2537	Inner plateau	Lotchuy Tso	43.388	0.007	0.377	0.010	0.379	0.010	0.356
48	34.1285	82.4155	Inner plateau	Memar Tsaka	17.622	0.430	0.394	0.427	0.396	0.429	0.403
49	30.7176	90.6461	Inner plateau	Nam Tso	1963.637	0.230	0.388	0.252	0.415	0.254	0.417
50	31.8585	89.7844	Inner plateau	Namka Tso	21.230	0.360	0.689	0.285	0.721	0.291	0.718

No.	Lat.	Lon.	Basin	Lake Name	Lake area [km^2]	**Threshold = 15 [cm]**		**Threshold = 25 [cm]**		**Threshold = 35 [cm]**	
						Rate [m a^{-1}]	RMSE [m]	Rate [m a^{-1}]	RMSE [m]	Rate [m a^{-1}]	RMSE [m]
51	32.0817	90.8458	Inner plateau	Namru Tso	207.865	0.347	0.309	0.349	0.307	0.349	0.307
52	36.7276	95.8222	Inner plateau	Nanhuoluxun Tso	4.108	0.003	0.468	0.015	0.469	0.011	0.464
53	31.5404	83.1013	Inner plateau	Nganglaring Tso	498.912	-0.002	0.369	0.015	0.431	0.016	0.430
54	31.0223	87.1541	Inner plateau	Ngangtse Tso	390.244	0.398	0.285	0.396	0.284	0.396	0.283
55	31.6226	82.3323	Inner plateau	Ruldan Tso	52.465	0.051	0.201	0.045	0.224	0.048	0.226
56	31.9977	88.2221	Inner plateau	Sibung Tso	60.121	0.353	0.120	0.361	0.133	0.360	0.125
57	35.2208	90.3428	Inner plateau	Sikin Ulan Nor	210.571	0.391	0.336	0.393	0.337	0.393	0.334
58	38.8685	93.8782	Inner plateau	Sukai Nor	102.235	-0.022	0.461	-0.017	0.454	-0.018	0.454
59	29.8530	85.7180	Inner plateau	Tak Kyel Tso	110.323	0.172	0.191	0.175	0.192	0.179	0.200
60	31.1302	84.1304	Inner plateau	Tarok Tso	473.976	0.294	0.322	0.302	0.325	0.300	0.329
61	30.9068	85.6178	Inner plateau	Terinam Tso	956.397	0.226	0.213	0.224	0.212	0.228	0.218
62	34.8141	90.3560	Inner plateau	Ulan Ula Nor	372.830	0.304	0.227	0.313	0.242	0.313	0.242
63	32.4582	89.9703	Inner plateau	Yrna Tso	149.804	0.475	0.352	0.474	0.357	0.474	0.355
64	33.9478	82.9648	Inner plateau		11.931	0.934	0.617	0.943	0.621	0.940	0.605
65	33.1693	89.0009	Inner plateau		29.477	0.791	0.807	0.858	0.892	0.858	0.887
66	33.2255	88.4025	Inner plateau		23.693	0.529	0.261	0.479	0.263	0.477	0.273
67	35.7376	86.6884	Inner plateau		50.534	0.495	0.387	0.497	0.388	0.499	0.387
68	36.0258	88.4931	Inner plateau		17.412	0.470	0.467	0.470	0.459	0.471	0.482

No.	Lat.	Lon.	Basin	Lake Name	Lake area [km^2]	**Threshold = 15 [cm]**		**Threshold = 25 [cm]**		**Threshold = 35 [cm]**	
						Rate [m a^{-1}]	RMSE [m]	Rate [m a^{-1}]	RMSE [m]	Rate [m a^{-1}]	RMSE [m]
69	33.7157	82.6703	Inner plateau		19.809	0.420	0.454	0.425	0.457	0.439	0.468
70	35.2087	90.1227	Inner plateau		60.047	0.411	0.300	0.434	0.300	0.428	0.311
71	31.5445	90.8160	Inner plateau		36.804	0.386	0.283	0.389	0.271	0.374	0.302
72	35.8049	89.4248	Inner plateau		87.783	0.365	0.189	0.362	0.191	0.358	0.193
73	31.9382	87.0315	Inner plateau		3.836	0.363	0.411	0.346	0.426	0.354	0.415
74	33.8625	88.3007	Inner plateau		44.946	0.363	0.167	0.356	0.163	0.362	0.166
75	34.4404	81.9419	Inner plateau		62.238	0.360	0.221	0.362	0.215	0.357	0.216
76	31.2360	84.9686	Inner plateau		105.690	0.352	0.398	0.362	0.407	0.362	0.392
77	31.5837	87.2801	Inner plateau		55.658	0.345	0.087	0.366	0.095	0.372	0.091
78	35.5630	90.1609	Inner plateau		1.623	0.332	0.344	0.337	0.353	0.341	0.326
79	34.5734	87.3068	Inner plateau		34.348	0.322	0.423	0.323	0.440	0.318	0.431
80	35.6087	90.3692	Inner plateau		20.329	0.310	0.283	0.315	0.283	0.310	0.290
81	35.5655	82.7259	Inner plateau		91.234	0.305	0.074	0.307	0.073	0.307	0.076
82	32.0245	83.9794	Inner plateau		8.668	0.293	0.106	0.294	0.096	0.300	0.087
83	34.0518	85.6026	Inner plateau		38.935	0.287	0.087	0.287	0.097	0.288	0.105
84	30.7517	85.9009	Inner plateau		3.529	0.265	0.471	0.255	0.465	0.248	0.484
85	32.4737	83.2152	Inner plateau		20.653	0.263	0.516	0.268	0.509	0.256	0.518
86	35.5097	88.0310	Inner plateau		1.715	0.259	0.214	0.261	0.202	0.262	0.199

No.	Lat.	Lon.	Basin	Lake Name	Lake area [km^2]	**Threshold = 15 [cm]**		**Threshold = 25 [cm]**		**Threshold = 35 [cm]**	
						Rate [m a^{-1}]	RMSE [m]	Rate [m a^{-1}]	RMSE [m]	Rate [m a^{-1}]	RMSE [m]
87	32.1696	86.2048	Inner plateau		9.042	0.256	0.524	0.267	0.509	0.271	0.512
88	32.5081	83.2244	Inner plateau		3.371	0.242	0.508	0.247	0.503	0.247	0.503
89	35.5438	90.1652	Inner plateau		1.692	0.236	0.146	0.255	0.179	0.245	0.162
90	34.6488	88.6904	Inner plateau		67.276	0.227	0.324	0.225	0.327	0.225	0.324
91	33.0117	89.7943	Inner plateau		108.270	0.190	0.408	0.185	0.424	0.192	0.411
92	33.3593	84.1909	Inner plateau		35.954	0.184	0.295	0.183	0.271	0.180	0.291
93	32.2507	83.2933	Inner plateau		9.399	0.174	0.364	0.190	0.366	0.179	0.331
94	34.8158	83.6308	Inner plateau		1.313	0.169	0.417	0.175	0.410	0.173	0.408
95	35.9872	90.1215	Inner plateau		34.590	0.169	0.266	0.171	0.271	0.173	0.266
96	35.7798	83.4635	Inner plateau		11.159	0.160	0.347	0.143	0.346	0.140	0.340
97	35.9931	88.1107	Inner plateau		17.412	0.154	0.304	0.162	0.282	0.161	0.289
98	34.6523	80.6606	Inner plateau		2.720	0.148	0.166	0.148	0.166	0.148	0.166
99	34.4326	83.5556	Inner plateau		11.307	0.123	0.321	0.125	0.314	0.130	0.320
100	31.4725	90.0344	Inner plateau		1.369	0.123	0.427	0.125	0.427	0.118	0.434
101	31.9315	82.7812	Inner plateau		12.939	0.113	0.153	0.112	0.309	0.136	0.495
102	31.8613	83.1596	Inner plateau		60.165	0.109	0.507	0.113	0.510	0.120	0.511
103	33.0216	83.9421	Inner plateau		2.623	0.094	0.118	0.120	0.220	0.101	0.106
104	35.4136	90.9595	Inner plateau		8.377	0.092	0.100	0.091	0.095	0.090	0.093

No.	Lat.	Lon.	Basin	Lake Name	Lake area [km^2]	**Threshold = 15 [cm]**		**Threshold = 25 [cm]**		**Threshold = 35 [cm]**	
						Rate [m a^{-1}]	RMSE [m]	Rate [m a^{-1}]	RMSE [m]	Rate [m a^{-1}]	RMSE [m]
105	33.5343	86.3397	Inner plateau		2.636	0.066	0.570	0.070	0.577	0.067	0.572
106	35.2199	83.6794	Inner plateau		6.839	0.060	0.568	0.060	0.568	0.060	0.568
107	35.1018	88.7404	Inner plateau		1.982	0.036	0.179	0.047	0.118	0.047	0.118
108	30.8356	88.0292	Inner plateau		2.565	0.035	0.373	0.035	0.370	0.026	0.382
109	34.0605	83.5017	Inner plateau		1.268	0.032	0.029	0.034	0.029	0.030	0.026
110	34.2040	87.7950	Inner plateau		14.310	0.022	0.374	0.022	0.365	0.021	0.369
111	35.2911	87.2596	Inner plateau		64.671	0.015	0.138	0.026	0.260	0.054	0.332
112	36.9035	95.9502	Inner plateau		92.946	0.012	0.136	0.010	0.140	0.049	0.294
113	31.5528	88.7754	Inner plateau		250.355	0.007	0.306	0.011	0.298	0.016	0.396
114	35.4390	95.4182	Inner plateau		7.991	0.005	0.510	0.003	0.532	0.005	0.508
115	33.0185	82.5075	Inner plateau		4.883	-0.002	0.043	0.011	0.062	0.011	0.062
116	33.9197	86.6872	Inner plateau		23.478	-0.003	0.473	-0.013	0.564	-0.017	0.571
117	37.0435	94.3903	Inner plateau		13.550	-0.008	0.059	-0.008	0.062	-0.008	0.062
118	31.3837	88.7237	Inner plateau		14.303	-0.013	0.405	-0.007	0.416	0.000	0.426
119	30.9071	86.4082	Inner plateau		3.231	-0.014	0.444	-0.011	0.442	-0.010	0.441
120	35.4827	83.7384	Inner plateau		4.145	-0.021	0.187	-0.026	0.273	-0.025	0.285
121	36.9747	90.7316	Inner plateau		18.195	-0.047	0.358	-0.037	0.368	-0.052	0.376
122	35.0350	84.4696	Inner plateau		2.597	-0.048	0.378	-0.035	0.502	-0.036	0.506

No.	Lat.	Lon.	Basin	Lake Name	Lake area [km^2]	Threshold = 15 [cm]		Threshold = 25 [cm]		Threshold = 35 [cm]	
						Rate [m a^{-1}]	RMSE [m]	Rate [m a^{-1}]	RMSE [m]	Rate [m a^{-1}]	RMSE [m]
123	30.6751	88.7936	Inner plateau		1.385	-0.074	0.124	-0.071	0.127	-0.076	0.130
124	35.0689	90.2730	Inner plateau		13.545	-0.090	0.362	0.034	0.408	0.052	0.361
125	34.3417	91.5602	Yangtze	Chamu Tso	67.916	0.080	0.458	0.079	0.434	0.084	0.432
126	33.3782	89.8233	Yangtze	Chibchang Tso	378.746	0.573	0.338	0.572	0.340	0.572	0.331
127	33.8862	91.1934	Yangtze	Dzurhen Nor	80.425	0.196	0.138	0.190	0.155	0.189	0.140
128	34.4211	91.0165	Yangtze	Hulu Tso	25.304	0.212	0.111	0.226	0.130	0.230	0.119
129	27.7052	100.7765	Yangtze	Lugu Tso	52.533	0.010	0.245	-0.003	0.265	0.001	0.272
130	33.4901	90.3625	Yangtze	Mitijiangzhanmu Tso	472.869	0.224	0.274	0.224	0.276	0.223	0.278
131	33.6337	89.7186	Yangtze		62.978	0.402	0.365	0.411	0.362	0.412	0.362
132	34.6517	94.0269	Yangtze		2.406	0.335	0.203	0.322	0.177	0.336	0.175
133	33.7381	90.6389	Yangtze		28.786	0.277	0.263	0.271	0.265	0.272	0.266
134	35.2416	90.9234	Yangtze		15.675	0.232	0.515	0.305	0.480	0.198	0.622
135	35.0347	91.5679	Yangtze		6.496	0.199	0.440	0.138	0.487	0.139	0.488
136	32.9570	93.5387	Yangtze		8.478	0.171	0.548	0.178	0.504	0.173	0.483
137	34.1934	91.6963	Yangtze		11.226	0.113	0.358	0.115	0.346	0.106	0.401
138	33.6687	90.8800	Yangtze		4.968	0.074	0.162	0.063	0.155	0.087	0.163
139	34.5987	92.4628	Yangtze		18.128	0.046	0.498	0.057	0.461	0.058	0.463
140	32.8897	92.0667	Yangtze		7.493	0.014	0.495	-0.004	0.496	-0.025	0.473

No.	Lat.	Lon.	Basin	Lake Name	Lake area [km^2]	**Threshold = 15 [cm]**		**Threshold = 25 [cm]**		**Threshold = 35 [cm]**	
						Rate [m a^{-1}]	RMSE [m]	Rate [m a^{-1}]	RMSE [m]	Rate [m a^{-1}]	RMSE [m]
141	34.3921	91.6983	Yangtze		4.124	-0.009	0.730	0.020	0.687	0.022	0.685
142	26.6221	100.6667	Yangtze		3.296	-0.289	0.543	-0.281	0.540	-0.275	0.564
143	34.7813	98.2852	Yellow River	Ayonggaima Tso	21.931	0.191	0.424	0.191	0.416	0.185	0.433
144	35.3069	99.1729	Yellow River	Karar Nor	47.884	-0.078	0.065	-0.082	0.066	-0.080	0.069
145	35.8123	103.1960	Yellow River	Luijiaxia Tso	113.179	0.149	1.073	0.155	1.070	0.152	1.071
146	36.8896	100.1817	Yellow River	Qinghai	4166.288	0.108	0.178	0.120	0.223	0.130	0.249
147	34.9140	97.2526	Yellow River	Tsaring Tso	525.092	0.177	0.291	0.179	0.291	0.177	0.289
148	35.3018	97.0055	Yellow River		5.385	0.456	0.423	0.458	0.422	0.460	0.422
149	34.9597	97.4744	Yellow River		10.218	0.437	0.427	0.432	0.431	0.434	0.402
150	36.8182	100.6835	Yellow River		98.050	0.189	0.295	0.194	0.285	0.195	0.287
151	33.8554	102.1424	Yellow River		0.973	0.018	0.496	0.015	0.630	0.023	0.608
152	34.8252	98.2572	Yellow River		1.272	-0.009	0.427	0.006	0.445	0.006	0.445
153	36.1402	101.7906	Yellow River		24.252	-0.012	0.848	-0.026	0.802	-0.089	0.953
154	36.1839	100.1529	Yellow River		3.809	-0.248	0.364	-0.238	0.372	-0.236	0.373

Table B2: The list of additional Tibetan observed lakes when the threshold value increases

No.	Lat.	Lon.	Basin	Lake name	Lake area [km^2]	Threshold = 15 [cm]		Threshold = 25 [cm]		Threshold = 35 [cm]	
						Rate [m a^{-1}]	RMSE [m]	Rate [m a^{-1}]	RMSE [m]	Rate [m a^{-1}]	RMSE [m]
1	35.9736	86.7766	Inner plateau		4.936					0.160	0.581
2	30.9061	90.4270	Inner plateau		2.341			-0.324	0.438	-0.322	0.450
3	28.7057	102.1891	Yangtze		17.280			3.614	12.544	3.600	12.510

Notes: Tibetan lake's names are collected from Google Earth, and lake areas are calculated in the Projected Coordinate System WGS84 UTM.

Appendix C

Table C: Lakes dominated by glaciers on the Tibetan Plateau

Note:

A_C: the area of the lake catchment (km^2)

A_{GD}: the total area of directly contributing glaciers (km^2)

A_{GU}: the total area of upstream glaciers (km^2)

R_D: the geometric dependency of the lake on directly contributing glaciers

R_U: the geometric dependency of the lake on upstream glaciers

No.	Lat.	Lon.	Basin	Lake Name	A_C	A_{GD}	A_{GU}	R_D	R_U
1	31.131	93.175	Brahmaputra		208.4	0.2	0.2	0.0010	0.0010
2	30.978	92.943	Brahmaputra		92.4	1.0	1.0	0.0113	0.0113
3	30.663	94.478	Brahmaputra		245.9	184.2	184.2	0.7492	0.7492
4	30.622	93.181	Brahmaputra		371.7	21.8	21.8	0.0586	0.0586
5	30.418	82.303	Brahmaputra		704.0	85.9	85.9	0.1221	0.1221
6	30.421	84.051	Brahmaputra		403.9	10.2	10.2	0.0253	0.0253
7	30.125	94.090	Brahmaputra		102.6	70.2	70.2	0.6845	0.6845
8	30.049	94.245	Brahmaputra		112.6	27.3	27.3	0.2424	0.2424
9	30.026	93.997	Brahmaputra	Draksum Tso	1721.9	307.2	404.7	0.1784	0.2350
10	29.957	94.288	Brahmaputra		30.1	0.5	0.5	0.0179	0.0179
11	29.842	82.784	Brahmaputra		69.6	19.2	19.2	0.2751	0.2751
12	29.888	85.247	Brahmaputra	Trengcham Tso	955.8	43.4	43.4	0.0454	0.0454
13	29.493	96.706	Brahmaputra	Rawok Tso	1836.3	57.0	555.2	0.0311	0.3024
14	29.467	96.787	Brahmaputra	Ngan Tso	1433.3	13.6	498.2	0.0095	0.3476
15	29.727	83.100	Brahmaputra		54.8	0.1	0.1	0.0015	0.0015
16	29.413	96.817	Brahmaputra	Ngagong Tso	1290.1	484.6	484.6	0.3756	0.3756
17	29.654	85.808	Brahmaputra		130.7	1.9	1.9	0.0147	0.0147
18	29.606	83.376	Brahmaputra		107.2	1.0	1.0	0.0090	0.0090
19	29.649	85.737	Brahmaputra		332.3	9.9	11.8	0.0298	0.0355
20	29.630	86.245	Brahmaputra		1570.7	28.1	28.1	0.0179	0.0179
21	29.558	86.264	Brahmaputra		1772.9	0.0	28.1	0.0000	0.0159

22	29.117	90.334	Brahmaputra		9999.3	0.0	255.1	0.0000	0.0255
23	29.118	85.402	Brahmaputra		376.9	0.4	0.4	0.0011	0.0011
24	29.012	90.457	Brahmaputra	Gongmo Tso	620.2	77.7	77.7	0.1252	0.1252
25	28.520	96.699	Brahmaputra		78.6	1.4	1.4	0.0172	0.0172
26	28.788	90.896	Brahmaputra		675.2	3.6	3.6	0.0053	0.0053
27	28.830	87.559	Brahmaputra		42.0	2.0	2.0	0.0483	0.0483
28	28.760	90.854	Brahmaputra		812.8	0.0	3.6	0.0000	0.0044
29	28.560	90.393	Brahmaputra	Phuma Tso	1815.4	152.6	152.6	0.0841	0.0841
30	28.275	90.733	Brahmaputra		24.7	11.5	11.5	0.4656	0.4656
31	28.278	89.340	Brahmaputra		2933.0	4.3	23.8	0.0014	0.0081
32	28.238	90.105	Brahmaputra		84.9	50.2	50.2	0.5909	0.5909
33	28.232	89.634	Brahmaputra		171.2	16.4	16.4	0.0960	0.0960
34	28.090	90.788	Brahmaputra		36.5	20.1	20.1	0.5507	0.5507
35	28.131	89.370	Brahmaputra		1788.2	19.5	19.5	0.0109	0.0109
36	28.979	90.717	Brahmaputra	Yamdrok Tso	9941.3	21.2	255.1	0.0021	0.0257
37	28.898	85.585	Ganges	Palku Tso	2380.2	113.4	146.1	0.0476	0.0614
38	28.721	85.878	Ganges		311.4	44.8	44.8	0.1438	0.1438
39	28.532	85.610	Ganges		29.4	10.3	10.3	0.3514	0.3514
40	28.497	85.639	Ganges		51.2	22.4	22.4	0.4375	0.4375
41	28.360	85.876	Ganges		33.6	19.9	19.9	0.5923	0.5923
42	28.375	86.306	Ganges	Lama Tso	67.3	40.1	40.1	0.5951	0.5951
43	28.329	85.871	Ganges		16.8	0.5	0.5	0.0286	0.0286
44	28.314	85.839	Ganges		48.2	22.4	22.9	0.4641	0.4741
45	28.292	88.126	Ganges		3990.2	77.4	77.4	0.0194	0.0194
46	28.115	87.653	Ganges		35.0	4.4	4.4	0.1266	0.1266
47	34.153	79.784	Indus	Dyap Tso	1784.6	170.5	170.5	0.0955	0.0955
48	33.538	78.860	Indus	Pangur Tso	1649.7	33.5	33.5	0.0203	0.0203
49	33.393	79.360	Indus		118.2	0.4	0.4	0.0033	0.0033
50	33.032	80.565	Indus		2401.7	1.2	1.2	0.0005	0.0005
51	32.756	81.729	Indus		3023.8	123.7	123.7	0.0409	0.0409
52	31.617	81.015	Indus		341.5	0.0	2.4	0.0000	0.0069
53	31.579	80.987	Indus		177.7	2.4	2.4	0.0133	0.0133
54	31.358	81.150	Indus		77.7	0.2	0.2	0.0026	0.0026
55	31.290	81.243	Indus		218.3	3.9	3.9	0.0179	0.0179
56	30.799	81.564	Indus		469.6	6.8	6.8	0.0145	0.0145
57	30.762	81.592	Indus		894.1	2.3	9.1	0.0025	0.0101

58	30.719	81.216	Indus		7288.0	50.8	173.7	0.0070	0.0238
59	30.634	82.123	Indus	Konggyu Tso	907.6	7.3	7.3	0.0080	0.0080
60	30.673	81.488	Indus	Mapham Tso	5329.8	106.5	122.9	0.0200	0.0231
61	33.606	79.702	Indus	Pang Gong Tso	23297.1	218.5	218.9	0.0094	0.0094
62	38.869	93.878	Inner plateau	Sukai Nor	20080.9	219.2	219.2	0.0109	0.0109
63	38.305	97.596	Inner plateau	Khara Nor	4737.5	92.4	92.4	0.0195	0.0195
64	38.237	94.307	Inner plateau		5517.4	136.3	136.3	0.0247	0.0247
65	38.115	90.782	Inner plateau	Gaekel Tso	24475.5	196.0	196.0	0.0080	0.0080
66	37.842	95.268	Inner plateau		1731.3	2.9	2.9	0.0017	0.0017
67	37.490	95.505	Inner plateau	Baga Tsaidam Nor	5813.5	194.5	194.5	0.0335	0.0335
68	37.288	96.899	Inner plateau		11994.3	10.0	10.0	0.0008	0.0008
69	37.496	93.935	Inner plateau	Dongtaiji'nai'er Lake	34148.0	691.5	822.0	0.0202	0.0241
70	37.546	89.373	Inner plateau	Ayakum Kul	24146.9	383.7	386.1	0.0159	0.0160
71	37.145	96.942	Inner plateau		15237.3	0.0	10.0	0.0000	0.0007
72	37.314	90.292	Inner plateau		1599.0	2.4	2.4	0.0015	0.0015
73	37.057	94.308	Inner plateau	Senie Lake	14727.1	2.7	2.7	0.0002	0.0002
74	36.978	95.205	Inner plateau	Dabsan Nor	109629.4	242.7	307.5	0.0022	0.0028
75	36.972	94.509	Inner plateau		19295.2	0.0	2.7	0.0000	0.0001
76	37.067	88.431	Inner plateau	Achik Kul	13263.3	280.8	280.8	0.0212	0.0212
77	36.342	89.439	Inner plateau		4842.8	79.4	79.4	0.0164	0.0164
78	36.110	82.677	Inner plateau		3182.3	19.8	36.9	0.0062	0.0116
79	35.867	78.568	Inner plateau		449.9	34.4	34.4	0.0764	0.0764
80	35.997	93.257	Inner plateau		1789.5	45.4	45.4	0.0254	0.0254
81	36.015	82.419	Inner plateau		315.5	17.1	17.1	0.0542	0.0542
82	36.035	87.881	Inner plateau		944.1	14.5	14.5	0.0154	0.0154
83	35.743	95.336	Inner plateau		9360.9	0.9	15.3	0.0001	0.0016
84	35.949	90.827	Inner plateau		1802.0	37.6	130.5	0.0209	0.0724
85	36.011	88.742	Inner plateau		2209.1	12.1	12.1	0.0055	0.0055
86	35.569	97.120	Inner plateau		1247.0	1.5	1.5	0.0012	0.0012
87	35.980	87.371	Inner plateau		1971.1	51.0	51.0	0.0259	0.0259
88	35.927	90.636	Inner plateau		1631.0	92.9	92.9	0.0569	0.0569
89	35.926	86.967	Inner plateau		3959.7	64.6	64.6	0.0163	0.0163
90	35.737	81.563	Inner plateau		962.8	17.6	17.6	0.0182	0.0182
91	35.636	79.353	Inner plateau		5372.7	22.9	22.9	0.0043	0.0043
92	35.735	92.838	Inner plateau		5829.4	50.2	78.1	0.0086	0.0134
93	35.805	89.425	Inner plateau		1264.5	6.4	6.4	0.0051	0.0051

94	35.671	81.615	Inner plateau		241.2	0.3	0.3	0.0011	0.0011
95	35.465	95.267	Inner plateau		993.7	0.0	14.4	0.0000	0.0144
96	35.749	90.190	Inner plateau	Lexiewuda Lake	2018.6	62.8	62.8	0.0311	0.0311
97	35.461	78.940	Inner plateau		607.5	13.7	13.7	0.0225	0.0225
98	35.738	86.688	Inner plateau		2277.2	66.6	66.6	0.0292	0.0292
99	35.531	93.406	Inner plateau		2731.1	22.1	22.1	0.0081	0.0081
100	35.415	95.121	Inner plateau		827.7	14.4	14.4	0.0173	0.0173
101	35.380	79.109	Inner plateau		123.1	1.1	1.1	0.0085	0.0085
102	35.565	82.726	Inner plateau		1853.8	148.0	148.0	0.0798	0.0798
103	35.581	91.124	Inner plateau	Kekexili Tso	2636.5	50.2	92.0	0.0190	0.0349
104	35.550	91.944	Inner plateau		1782.1	28.0	28.0	0.0157	0.0157
105	35.293	80.572	Inner plateau		117.7	96.0	96.0	0.8155	0.8155
106	35.426	84.655	Inner plateau		9497.6	40.7	40.7	0.0043	0.0043
107	35.382	88.761	Inner plateau		270.5	19.9	19.9	0.0736	0.0736
108	35.424	88.398	Inner plateau		5069.5	15.3	15.3	0.0030	0.0030
109	35.208	79.828	Inner plateau	Aksai Chin Kul	7992.5	672.8	768.7	0.0842	0.0962
110	35.294	83.105	Inner plateau		5557.5	58.8	58.8	0.0106	0.0106
111	35.300	89.238	Inner plateau		6170.0	108.6	128.6	0.0176	0.0208
112	35.251	89.941	Inner plateau		2348.9	39.8	39.8	0.0169	0.0169
113	35.204	90.545	Inner plateau		2135.8	0.7	0.7	0.0003	0.0003
114	35.221	90.343	Inner plateau	Sikin Ulan Nor	6651.7	39.7	80.2	0.0060	0.0121
115	35.028	81.082	Inner plateau	Ligmen Tso	2726.5	518.7	518.7	0.1902	0.1902
116	34.883	79.351	Inner plateau		2754.4	22.7	22.7	0.0082	0.0082
117	35.069	90.542	Inner plateau		1616.3	18.7	18.7	0.0116	0.0116
118	35.122	86.745	Inner plateau		4121.4	11.9	11.9	0.0029	0.0029
119	34.955	81.935	Inner plateau		2555.3	14.7	126.6	0.0057	0.0496
120	35.045	87.079	Inner plateau		3828.2	0.0	65.4	0.0000	0.0171
121	34.951	81.564	Inner plateau	Echil Kul	3613.9	13.8	132.5	0.0038	0.0367
122	34.845	80.233	Inner plateau		236.3	12.4	12.4	0.0526	0.0526
123	34.917	82.218	Inner plateau		856.8	31.0	31.0	0.0362	0.0362
124	34.765	80.172	Inner plateau		426.7	2.8	2.8	0.0066	0.0066
125	34.877	81.965	Inner plateau		1506.4	81.0	112.0	0.0537	0.0743
126	34.961	89.235	Inner plateau		672.7	3.9	3.9	0.0058	0.0058
127	34.681	79.691	Inner plateau		2218.8	26.6	26.6	0.0120	0.0120
128	34.652	80.661	Inner plateau		341.5	16.7	16.7	0.0489	0.0489
129	34.735	81.895	Inner plateau		2484.6	23.0	99.7	0.0092	0.0401

130	34.608	80.241	Inner plateau		1903.9	154.8	164.5	0.0813	0.0864
131	34.629	80.904	Inner plateau		147.2	6.6	6.6	0.0450	0.0450
132	34.814	90.356	Inner plateau	Ulan Ula Nor	6007.3	21.8	34.5	0.0036	0.0057
133	34.764	90.603	Inner plateau		2060.8	12.7	12.7	0.0062	0.0062
134	34.618	80.444	Inner plateau		957.2	3.2	19.9	0.0033	0.0208
135	34.713	89.031	Inner plateau		1308.2	3.3	3.3	0.0025	0.0025
136	34.706	86.393	Inner plateau		831.6	65.4	65.4	0.0786	0.0786
137	34.495	80.444	Inner plateau		401.5	1.0	1.0	0.0024	0.0024
138	34.529	81.036	Inner plateau		979.6	112.0	118.6	0.1143	0.1211
139	34.421	80.507	Inner plateau		343.0	3.3	3.3	0.0097	0.0097
140	34.573	87.307	Inner plateau		3793.7	73.1	73.1	0.0193	0.0193
141	34.482	81.800	Inner plateau		997.3	47.8	76.7	0.0479	0.0769
142	34.440	81.942	Inner plateau		425.7	29.0	29.0	0.0681	0.0681
143	34.570	89.035	Inner plateau	Dogai Coring Lake	7618.7	217.5	217.5	0.0286	0.0286
144	34.313	79.924	Inner plateau		32.6	9.8	9.8	0.2994	0.2994
145	34.277	81.052	Inner plateau		737.4	102.7	102.7	0.1393	0.1393
146	34.392	84.252	Inner plateau		2283.1	5.0	5.0	0.0022	0.0022
147	34.398	85.757	Inner plateau		651.8	88.6	88.6	0.1359	0.1359
148	34.280	85.072	Inner plateau		1816.3	36.4	36.4	0.0201	0.0201
149	34.228	82.287	Inner plateau		2315.1	129.9	228.6	0.0561	0.0987
150	34.261	85.718	Inner plateau		201.3	30.6	30.6	0.1518	0.1518
151	34.181	83.149	Inner plateau		2043.1	1.1	1.1	0.0006	0.0006
152	33.949	80.902	Inner plateau	Kenze Tso	2254.4	143.0	143.0	0.0634	0.0634
153	34.014	81.599	Inner plateau	Charol Tso	8365.2	189.1	291.8	0.0226	0.0349
154	33.948	82.965	Inner plateau		3178.6	0.0	1.1	0.0000	0.0004
155	34.011	82.367	Inner plateau	Arku Tso	928.1	98.7	98.7	0.1063	0.1063
156	33.920	86.687	Inner plateau		1083.0	9.2	9.2	0.0085	0.0085
157	33.860	87.019	Inner plateau		2671.7	16.4	16.4	0.0061	0.0061
158	33.851	88.584	Inner plateau		1835.0	163.5	163.5	0.0891	0.0891
159	33.716	82.670	Inner plateau		413.1	10.8	10.8	0.0261	0.0261
160	33.693	86.840	Inner plateau		1553.2	24.9	43.7	0.0161	0.0281
161	33.665	85.811	Inner plateau		6726.3	5.8	5.8	0.0009	0.0009
162	33.551	84.589	Inner plateau		4927.9	26.4	26.4	0.0054	0.0054
163	33.562	86.961	Inner plateau		450.9	18.7	18.7	0.0415	0.0415
164	33.452	88.725	Inner plateau		2739.7	12.0	12.0	0.0044	0.0044
165	33.388	82.975	Inner plateau		2434.3	7.0	7.0	0.0029	0.0029

166	33.320	85.581	Inner plateau		732.1	2.4	2.4	0.0033	0.0033
167	33.194	86.665	Inner plateau		609.1	10.1	10.1	0.0166	0.0166
168	33.155	89.080	Inner plateau		2994.1	23.7	23.7	0.0079	0.0079
169	33.169	89.001	Inner plateau		3210.9	0.0	23.7	0.0000	0.0074
170	33.007	85.370	Inner plateau		1759.0	4.8	4.8	0.0027	0.0027
171	32.924	82.080	Inner plateau		3698.5	20.0	20.0	0.0054	0.0054
172	32.983	88.698	Inner plateau		1316.5	24.4	24.4	0.0185	0.0185
173	32.903	88.191	Inner plateau		1681.7	0.7	0.7	0.0004	0.0004
174	32.828	82.198	Inner plateau		4313.1	0.0	20.0	0.0000	0.0046
175	32.920	86.700	Inner plateau		6912.4	20.1	20.1	0.0029	0.0029
176	32.796	87.838	Inner plateau		2233.3	11.3	11.3	0.0050	0.0050
177	32.436	82.933	Inner plateau		2256.1	2.2	2.2	0.0010	0.0010
178	32.385	88.041	Inner plateau		1392.9	13.2	16.6	0.0095	0.0119
179	32.344	87.303	Inner plateau		777.6	25.5	25.5	0.0328	0.0328
180	32.261	87.892	Inner plateau		193.0	3.4	3.4	0.0175	0.0175
181	32.173	84.734	Inner plateau		6003.2	12.9	12.9	0.0022	0.0022
182	32.110	83.542	Inner plateau		2725.0	120.4	120.4	0.0442	0.0442
183	32.025	87.761	Inner plateau		1151.0	9.6	9.6	0.0083	0.0083
184	32.030	84.116	Inner plateau	Lakok Tso	3667.0	34.7	34.7	0.0095	0.0095
185	31.927	82.132	Inner plateau		1329.4	13.7	13.7	0.0103	0.0103
186	31.998	88.222	Inner plateau	Sibung Tso	3481.9	0.0	9.6	0.0000	0.0028
187	31.954	87.000	Inner plateau		1429.8	2.9	2.9	0.0020	0.0020
188	31.916	87.198	Inner plateau		577.9	0.9	0.9	0.0016	0.0016
189	31.861	83.160	Inner plateau		2329.5	20.2	33.4	0.0087	0.0143
190	31.767	82.376	Inner plateau		200.3	2.7	2.7	0.0136	0.0136
191	31.898	87.526	Inner plateau		12848.7	39.3	71.8	0.0031	0.0056
192	31.721	82.378	Inner plateau		250.3	0.0	2.7	0.0000	0.0109
193	31.710	83.245	Inner plateau		204.2	13.1	13.1	0.0643	0.0643
194	31.714	86.977	Inner plateau		3134.7	26.5	31.6	0.0085	0.0101
195	31.623	82.332	Inner plateau	Ruldan Tso	1106.2	0.0	2.7	0.0000	0.0025
196	31.713	88.004	Inner plateau	Jagok Tso	15796.5	3.5	192.9	0.0002	0.0122
197	31.806	88.950	Inner plateau	Garing Tso	29077.2	197.2	199.0	0.0068	0.0068
198	31.584	87.280	Inner plateau		1440.6	2.9	5.1	0.0020	0.0035
199	31.570	86.744	Inner plateau		905.9	11.5	11.5	0.0127	0.0127
200	31.539	87.395	Inner plateau		910.8	2.2	2.2	0.0024	0.0024
201	31.540	83.101	Inner plateau	Nganglaring Tso	12463.8	291.2	296.5	0.0234	0.0238

202	31.512	90.967	Inner plateau		3321.2	0.0	39.8	0.0000	0.0120
203	31.553	88.775	Inner plateau		6139.4	1.8	1.8	0.0003	0.0003
204	31.445	84.054	Inner plateau		16767.8	1.3	285.9	0.0001	0.0170
205	31.380	83.659	Inner plateau		352.4	79.5	79.5	0.2257	0.2257
206	31.377	87.894	Inner plateau	Chikut Tso	13093.9	8.4	189.4	0.0006	0.0145
207	31.345	84.063	Inner plateau		12647.4	7.5	205.1	0.0006	0.0162
208	31.302	91.468	Inner plateau		1165.3	1.2	1.2	0.0010	0.0010
209	31.168	81.628	Inner plateau		92.1	3.0	3.0	0.0330	0.0330
210	31.277	83.430	Inner plateau	Chovo Tso	2575.9	186.8	186.8	0.0725	0.0725
211	31.221	91.150	Inner plateau		1546.2	39.8	39.8	0.0257	0.0257
212	31.236	84.969	Inner plateau		2457.7	38.6	38.6	0.0157	0.0157
213	31.130	84.130	Inner plateau	Tarok Tso	7892.4	197.6	197.6	0.0250	0.0250
214	30.980	82.232	Inner plateau	Arkok Tso	750.8	2.3	2.3	0.0030	0.0030
215	31.134	88.307	Inner plateau	Kyaring Tso	10842.0	62.9	181.0	0.0058	0.0167
216	31.022	87.154	Inner plateau	Ngangtse Tso	7132.4	10.1	10.1	0.0014	0.0014
217	30.884	83.585	Inner plateau		1734.2	131.3	131.3	0.0757	0.0757
218	31.060	86.601	Inner plateau	Dangra Tso	9031.7	151.1	151.1	0.0167	0.0167
219	30.907	85.618	Inner plateau	Terinam Tso	20080.1	131.2	131.6	0.0065	0.0066
220	30.693	88.746	Inner plateau		4739.0	40.8	118.2	0.0086	0.0249
221	30.641	86.258	Inner plateau		880.7	6.9	6.9	0.0078	0.0078
222	30.569	88.584	Inner plateau		284.2	37.2	37.2	0.1308	0.1308
223	30.718	90.646	Inner plateau	Nam Tso	10741.3	334.5	334.5	0.0311	0.0311
224	30.477	86.115	Inner plateau		229.3	0.3	0.3	0.0014	0.0014
225	30.467	88.612	Inner plateau		1435.9	36.2	37.4	0.0252	0.0261
226	30.370	89.379	Inner plateau		128.7	2.8	2.8	0.0214	0.0214
227	30.238	88.573	Inner plateau		406.6	1.2	1.2	0.0030	0.0030
228	30.278	86.413	Inner plateau		1933.0	76.2	76.2	0.0394	0.0394
229	30.225	84.784	Inner plateau		996.2	65.5	65.5	0.0657	0.0657
230	30.001	85.534	Inner plateau		261.4	28.5	28.5	0.1092	0.1092
231	29.853	85.718	Inner plateau	Tak Kyel Tso	763.6	15.1	15.1	0.0198	0.0198
232	35.604	90.638	Inner plateau	Yinma Tso	658.3	41.9	41.9	0.0636	0.0636
233	31.638	95.574	Mekong		99.9	8.9	8.9	0.0891	0.0891
234	31.620	95.663	Mekong		465.5	2.1	11.0	0.0046	0.0237
235	32.023	91.482	Salween	Amdi Tsonak Tso	4145.3	7.9	7.9	0.0019	0.0019
236	31.856	91.535	Salween		5377.6	0.0	7.9	0.0000	0.0015
237	31.420	92.334	Salween		13459.5	0.7	14.4	0.0000	0.0011

238	31.309	91.777	Salween		2021.4	5.9	5.9	0.0029	0.0029
239	30.967	93.790	Salween		69.8	39.0	39.0	0.5580	0.5580
240	35.414	93.631	Yangtze		672.1	6.9	6.9	0.0102	0.0102
241	34.378	89.209	Yangtze		937.4	0.9	2.0	0.0010	0.0022
242	34.231	89.508	Yangtze		400.8	0.0	1.1	0.0000	0.0028
243	34.117	89.566	Yangtze		57.4	1.1	1.1	0.0193	0.0193
244	34.014	89.955	Yangtze		1955.0	1.9	1.9	0.0009	0.0009
245	33.871	89.931	Yangtze		2569.4	0.0	1.9	0.0000	0.0007
246	33.812	90.516	Yangtze		277.0	11.2	11.2	0.0404	0.0404
247	33.794	90.359	Yangtze		492.5	29.0	29.0	0.0589	0.0589
248	33.721	90.868	Yangtze		516.7	7.8	7.8	0.0152	0.0152
249	33.729	90.005	Yangtze		3799.9	1.8	3.6	0.0005	0.0010
250	33.620	90.216	Yangtze		4042.4	0.0	3.6	0.0000	0.0009
251	33.634	89.719	Yangtze		1555.5	23.5	23.5	0.0151	0.0151
252	33.494	89.586	Yangtze		2234.4	110.8	110.8	0.0496	0.0496
253	33.093	93.224	Yangtze		1459.4	18.7	18.7	0.0128	0.0128
254	33.104	92.270	Yangtze		222.1	21.0	21.0	0.0946	0.0946
255	32.071	103.712	Yangtze		4876.3	1.2	1.2	0.0003	0.0003
256	32.916	91.978	Yangtze		111.2	9.0	9.0	0.0808	0.0808
257	32.890	92.067	Yangtze		37.8	0.3	0.3	0.0079	0.0079
258	31.849	99.113	Yangtze		220.6	47.2	47.2	0.2138	0.2138
259	30.188	99.549	Yangtze		118.2	9.2	9.2	0.0775	0.0775
260	33.378	89.823	Yangtze	Chibchang Tso	3628.1	0.0	110.8	0.0000	0.0305
261	33.490	90.362	Yangtze	Mitijiangzhanmu Tso	3628.1	218.7	251.3	0.0603	0.0693
262	36.890	100.182	Yellow River	Qinghai	29604.7	31.8	31.8	0.0011	0.0011
263	36.140	101.791	Yellow River		138248.5	0.0	135.4	0.0000	0.0010
264	35.812	103.196	Yellow River	Luijiaxia Lake	157962.6	0.0	135.4	0.0000	0.0009
265	36.022	100.709	Yellow River	Longyangxia Reservoir	132848.5	131.4	135.4	0.0010	0.0010
266	33.377	101.104	Yellow River		79.1	4.0	4.0	0.0506	0.0506